NEW TYLOPHORINE ANALOGS AS POTENTIAL ANTITUMOR AGENTS

Linyi Wei

A dissertation submitted to the faculty of the University of North Carolina at Chapel Hill in partial fulfillment of the requirements for the degree of Doctor of Philosophy in School of Pharmacy.

Chapel Hill
2006

Approved by:

Advisor: Dr. Kuo-Hsiung Lee
Reader: Dr. Kenneth F. Bastow
Reader: Dr. Arnold Brossi
Reader: Dr. Jian Liu
Reader: Dr.Qian Shi

ABSTRACT

LINYI WEI: Design, Synthesis and Biological Evaluation of New Tylophorine

Analogs as Potential Antitumor Agents

(Under the direction of Kenan Professor Kuo-Hsiung Lee)

Tylophorine and related phenanthroindolizidine alkaloids isolated principally from *Asclepiadaceae* have been targets of synthetic modification because of their profound cytotoxic antitumor activity. As part of our interest in plant-derived antitumor agents, novel water-soluble phenanthrene-based tylophorine derivatives (PBTs) were designed, synthesized and evaluated for anticancer activity.

Several PBTs showed superior activity profiles with EC_{50} values in the sub-micromolar range, which are comparable to those of currently used antitumor drugs. A structure-activity relationship (SAR) study was also explored to facilitate the further development of this new compound class.

Subsequently, C9-substituted PBTs were designed and synthesized using 2, 3 methylenedioxy-6-methoxyphenanthrene as a common skeleton based on our prior SAR findings. The C-9 site is an ideal position for introducing more polar, water-solubility-enhancing moieties. We also extended the *in vitro* antitumor screening to include additional significant tumor types [A549 (lung), DU-145 (prostate), ZR-751 (breast), KB (nasopharyngeal)] as well as a multi-drug resistant cancer cell subline [KB-Vin (multi-drug

resistant KB subline)]. Most of the compounds showed fairly uniform and potent cytotoxic activity with $EC_{50} \cong 10^{-7}$ M against both wild type and matched multi-drug resistant KB cell lines, and displayed notable selectivity toward DU-145 (prostate) and ZR-751 (breast) cancer cell lines.

A combination of QSAR modeling and database mining was used to facilitate further design and discovery of novel anticancer PBTs. MolConnZ 2D topological descriptors were applied to a dataset of 52 chemically diverse PBTs and variable selection models were generated using the κ nearest neighbor (κNN) method. The derived κNN QSAR models have high internal accuracy, with leave-one-out cross-validated R^2 (q^2) values ranging between 0.6 and 0.8. The original dataset was then divided into several training and test sets to provide highly predictive models with q^2 values greater than 0.5 for the training sets and R^2 values greater than 0.6 for the test sets. The ten best models were capable of mining the commercially available ChemDiv Database (450,000 compounds) and resulted in 34 consensus hits. Of these 34 compounds, 10 compounds were tested and 8 were confirmed to be active with a best EC_{50} of 1.8 μM. These models were further validated by predicting the activity of four new PBTs compounds with reasonable accuracy and 11 consensuses hits with R^2 of 0.52. These results indicate that this approach can be successfully applied to further design and discovery of anticancer drug candidates from this compound class.

ACKNOWLEDGEMENTS

This work is a result of several people's direct and indirect tireless contributions. My thesis would not have been successful without all of them. I would like to express my sincere appreciation and respect to the following:

To my advisor, Dr. Kuo-Hsiung Lee, for his encouragement, support, guidance and criticism as I fumbled my way through my Ph.D. study.

To my co-advisors Dr. Kenneth F. Bastow and Dr. Arnold Brossi, for their direct contribution and continuous support on organic synthesis and biological evaluation, without them, this project could not be completed.

To Dr. Jian Liu and Dr. Qian Shi, for their advice, criticism and encouragement.

To Dr. Susan Morris-Natschke for her tremendous time and patience on my publications and dissertation.

To Dana Deason for her cheering me up and Dr. Shuxing Zhang for his help on molecular modeling study.

I also would like to extend my thanks to all members and collaborators of the NPL for their help and friendship over the years.

Finally, my deepest grateful thanks are due to my parents, Ningzheng Wei and Youying Liang, for their love, support, understanding and encouragement of my life!

TABLE OF CONTENTS

Mode of Action Study

LIST OF TABLES

LIST OF FIGURES

LIST OF SCHEMES

LIST OF SYMBOLS AND ABBREVIATIONS

ADME	Absorption, Distribution, Metabolism, and Excretion
BBB	Blood Brain Barrier
BMS	Borane-Methyl Sulfide complex
$CDCl_3$	Deuterated chloroform
CNS	Central Nervous System
d	Doublet
dd	Double doublet
DCM	Dichloromethane
DIC	1,3-Diisopropylcarbodiimide
DHFR	Dihydrofolate reductase
DIEA	N,N`-Diisopropylethylamine
DMAP	4-(Dimethylamino) pyridine
DMF	Dimethyl formamide
DMSO	Dimethyl sulfoxide
EC_{50}	The concentration that reduced the cell number by 50%
EDC	*N*-(3-Dimethylaminopropyl)-*N'*-ethylcarbodiimide hydrochloride
FDA	Food and Drug Administration
HDP	Hypothetical Descriptor Pharmacophore
HEPES	*N*-2-Hydroxyethylpiperazine-*N'*-2-ethanesulfonic acid
HIA	Human Intestinal Absorption
HOBt	1-Hydroxybenzotriazole

IP	Intraperitoneal
IVCLSP	In Vitro Cell Line Screening Project
J	Coupling constant
kNN	k Nearest Neighbor
LOO	Leave-One-Out
m	Multiplet
MDR	Multi-Drug Resistant
MML	Molecular Modeling Laboratory
MS	Mass Spectrum
MTT	[3, (4,5-Dimethylthiazol-2-yl) 2,5-diphenyl tetrazolium bromide]
MZ	MolConnZ
NCE	New Chemical Entities
NF-kB	Nuclear Factor κB
NMR	Nuclear Magnetic Resonance
NMM	N-Methylmorpholine
NPL	Natural Products Laboratory
PBTs	Phenanthrene-Based Tylophorine derivatives
PPA	Polyphosphoric Acid
PPB	Plasma Protein Binding
q	Quartet
QSAR	Quantitative Structure-Activity Relationship
RRL	Rabbit Reticulocyte Lysates
s	Singlet

SAR	Structure-Activity Relationship
SCID	Severe Combined Immune Deficiency
SRB	Sulforhodamine B
t	Triplet
TCM	Traditional Chinese Medicine
THF	Tetrahydrofuran
TLC	Thin-Layer Chromatography
TMS	Tetramethyl Silane
TS	Thymidylate Synthase
δ	Chemical Shift

CHAPTER I. TYLOPHORINE AND ITS ANALOGS

1.1   ISOLATION OF TYLOPHORA

Figure 1-1. *Tylophora* (Asclepiadaceae)

Tylophorine (**1**) (Figure 1-2) and its analogs, phenanthroindolizidine alkaloids also referred to as *tylophora* alkaloids, have been isolated primarily from plants of the family *Asclepiadaceae*[1-4] (Figure 1-1), including members of the genus *Tylophora*, *Vincetoxicum, Pergularia*, *Cynanchum*, but also from *Hypoestes verticillaris* (Acanthaceae),[5] *Cryptocarya phyllostemmon* (Lauraceae),[6] *Ficus hispida*,[7] and *F. septica* (Moraceae).[8] The most important phenanthroindolizidine alkaloids are tylophorine (**1**), tylocrebrine (**2**), antofine (**3**) and tylophorinine (**4**) (Figure 1-2).
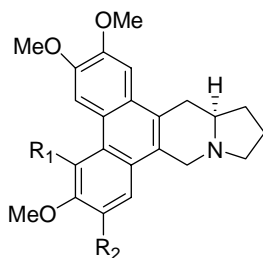
1. Tylophorine: R_1=H, R_2= OMe
2. Tylocrebrine: R_1=OMe, R_2= H
3. Antofine: R_1=H, R_2= H
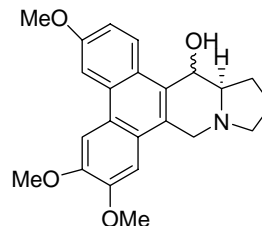
4. Tylophorinine

Figure 1-2. Chemical structures of tylophorine, tylocrebrine, antofine, and tylophorinine.

1.2   CHEMICAL SPECTRUM OF TYLOPHORA
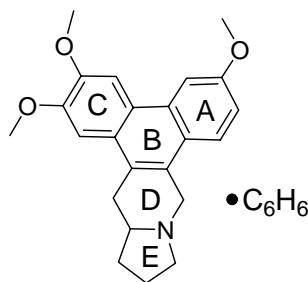
Figure 1-3. Tylophorine B benzene solvate.

Pure dried tylophorine is a yellow powder and crystallization in common solvents is difficult. Tylophorine B's (Figure 1-3) structure has conjoined phenanthrene and indolizidine moieties. The aromatic rings lie almost in the same plane with dihedral angles of 1.7^o (A/B), 2.8^o (B/C), 2.2^o (A/C), and 7.3^o (B/D). The E ring adopts an envelope conformation and makes a dihedral angle of $6.7(3)°$ with the D ring.[9]

1.3 TOTAL SYNTHESIS OF TYLOPHORINE-RELATED ALKALOIDS

The tylophorine (phenanthroindolizidine alkaloid) nucleus was first synthesized by Govindachari et al. in 1958[10] followed by the synthesis of cryptopleurine (phenanthroquinolizidine alkaloid) by Bradsher and Berger[11] as well as Marchini and Belleau.[12] Most naturally occurring tylophorine alkaloids (e.g., tylophorine, tylophorinine, and tylocrebine) have been synthesized, and the earlier routes before 1985 were well summarized in a comprehensive review by Suffness and Cordell.[13] The more recently reported synthetic approaches have been reviewed by Li et al.[14] and Michael.[15,16]

1.4 SAR OF TYLOPHORINE-RELATED ALKALOIDS
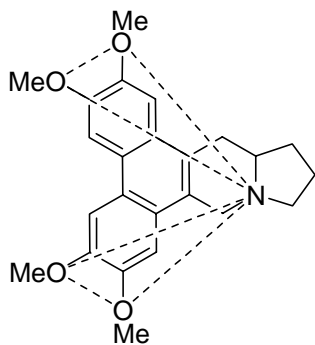
Figure 1-4. Triangulation of N-O-O in nonalkylating antileukemic agents.

In 1970, Zee-Cheng and Cheng[17] proposed a common structural feature among non-alkylating antileukemic agents, including emetine, camptothecin, tylocrebrine, tylophorine, vinblastine, and vincristine. This commonality involves a triangulation composed of one nitrogen and two oxygen atoms with relatively definite interatomic distances (Figure 1-4).
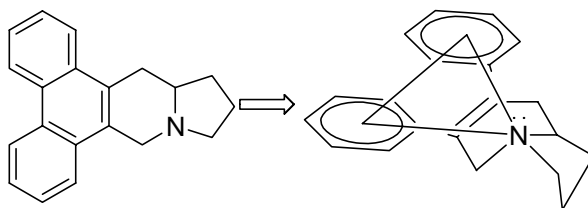
Figure 1-5. A model for the binding of emetine-type agonist to the hypothetical receptor site.

An extensive structure-activity by Gupta et al.[18, 19] regarding cross-resistance in two emetine-resistant CHO cell variants showed that phenanthroindolizidine alkaloids, phenanthroquinolizidines, and the emetine-related benzoquinolizidines may have the same site of action. The conformation of emetine was suggested to have a close spatial relationship to the other three compounds classes, and thus, they could bind to the same hypothetical binding site (Figure 1-5). Alkaloids that did not fit into this spatial hypothesis, including benzylisoquinilines and protoberberines, were not resistant to emetine-resistant cell lines. Therefore, the authors suggested that phenanthroindolizidine alkaloids, phenanthroquinolizidines, and emetine-related benzoquinolizidines possess common structural determinants responsible for their protein synthesis inhibitory activity. Similar results have been reported from studies on yeast.[20] Based on structural-activity comparisons, the required features are a planar molecule with two aromatic rings rendered slightly electronegative by methoxy or hydroxy groups and a free electron pair on nitrogen at a central distance from the aromatic rings.

Staerk et al.[21] assessed the cytotoxic activity of seven phenanthroindolizidine alkaloids, (-)-(R)-13aα-antofine (**5**), (-)-(R)-13aα-6-O-desmethylantofine (**6**), (-)-(R)-13aα-secoantofine (**7**), (-)-(R)-13aα-6-O-desmethylsecoantofine (**8**), (-)-(R)-13aα-tylophorine (**9**), (-)-(R)-13aα-7-O-desmethyltylophorine (**10**), and (+)-(S)-13aβ-isotylocrebrine (**11**) (Figure 1-6) against drug sensitive KB-3-1 and multidrug-resistant KB-V1 cancer cell lines. Compounds **7** and **8** showed remarkably decreased cytotoxicity compared with the five remaining compounds, suggesting that a rigid phenanthrene structure is a prerequisite for high cytotoxicity. In addition, compounds belonging to the 13aR series and having a free

phenolic function at C-6 or C-7 showed greater cytotoxic activity against the KB cancer cell lines. Although the S-configured **11** was less cytotoxic than the R series in this study, it still had quite high cytotoxicity against both cell lines (IC$_{50}$=50 nM). In contrast, previous studies showed equal or higher cytotoxicity with the 13aS series.[22]
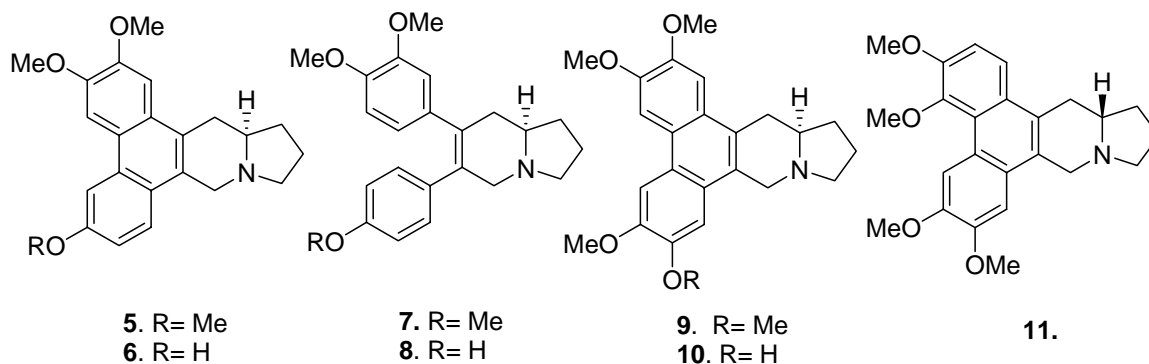
Figure 1-6. Chemical structures of phenanthroindolizidine alkaloids

Moreover, by using secophenanthroindolizidine septicine (**12**) as a template, a novel series of 6,7-diphenylindolizidinones (Figure 1-7) was synthesized and tested for in vitro anticancer activity against various human cancer cell lines.[23] Compounds with R = 3,4-difluoro, 3,4-dimethoxy, 4-methyl, 4-fluoro, 4-trifluoromethyl, and 4-methylthio (**13**) showed significant potency with GI$_{50}$ values in the range 2.1–8.1 μM. However, the reduced compound **14** and septicine (**12**) were inactive in this assay; thus, proving the importance of the lactam carbonyl in the central indolizidine ring to the cytotoxic activity. Substantial growth inhibitory activity was found when the 4-methylthio substituent was present in ring A, but substituents in ring B were less critical. Among all analogs, two compounds (R = 3, 4-dimethoxy and 4-methyl) exhibited encouraging pharmacokinetic properties in mice. However, further evaluation of *in vivo* efficacy in a modified hollow fiber assay (HFA) was disappointing, probably due to poor solubility.

Septicine (**12**)   **13**   **14**
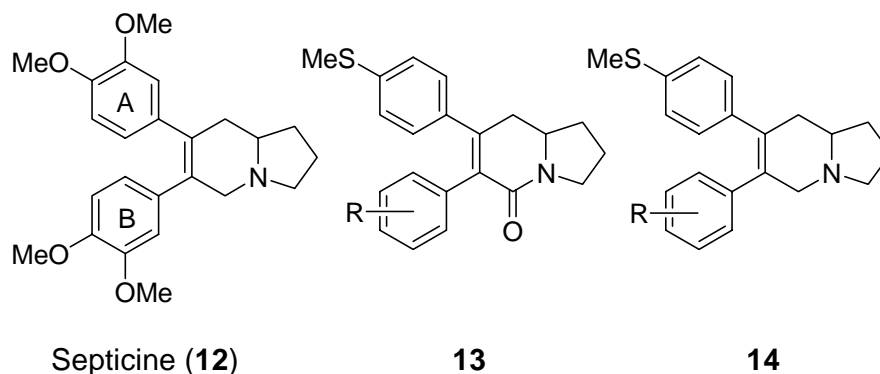
Figure 1-7. Structures of 6, 7-diphenylindolizidinones analogs.

1.5 ANTITUMOR ACTIVITY OF TYLOPHORA

Much of the current work on tylophorine alkloids was prompted by their profound antitumor activity. Evaluation of tylophorine (**1**) and its analogs in the National Cancer Institute's antitumor screen showed a uniform and potent growth inhibitory effect ($GI_{50} \cong 10^{-8}$ M) against all 60 cell lines, with notable selectivity toward several refractory cell lines, including melanoma and lung tumor cell lines.[24]

In 1964, Gellert and Rudzats[25] reported that administration of tylocrebrine (**2**), a phenanthrene alkaloid and positional isomer of tylophorine, caused approximately 50% increase in life span (ILS) in L1210 leukemia-bearing mice. Similarly to **2**, tylophorine (**1**) was active against L1210 leukemia but with lower efficacy (ILS ca. 30%). Based on the novel structure and superior antitumor activity against L1210 leukemia, tylocrebrine was selected as a drug candidate and successfully proceeded to Phase I clinical trials in the early 1960s. However, the trials were eventually terminated in 1966 due to central nervous system (CNS) toxicity, primarily ataxia and disorientation. Too few patients were treated to establish the efficacy of tylocrebrine.

1.6 MECHANISM OF ANTITUMOR ACTIVITY

A comprehensive evaluation of tylophorine's antitumor activities has not been reported, and its inhibition mechanisms on cell growth are largely unknown. However, significant advances in the field of molecular biology over the past decade have led to a new era in cancer therapeutics and should facilitate our understanding of the mode of actions (MOA) of this compound class.

1.6.1 Inhibition of DNA, RNA and Protein Synthesis

Early mechanistic studies in the 1960s demonstrated that tylophorine alkaloids irreversibly inhibit DNA synthesis and protein synthesis at the elongation stage of the translation cycle.[26] In HeLa cells, tylophorine reversibly inhibits RNA synthesis and irreversibly inhibits DNA synthesis, but its predominant effect is exerted on protein synthesis and elongation of peptide chains by preventing breakdown of polyribosomes and release of nascent peptides. Tylophorine and tylocrebrine were also found to inhibit protein synthesis in Ehrlich ascites cells and yeast cytoplasmic ribosomes but had no effect on *Escherichia coli (E. coli)* ribosomes even at high concentrations.[27]

Tylophorine, tylocrebrine, and cryptopleurine inhibit protein synthesis in eukaryotic cells. Cryptopleurine at low concentration blocks translocation of peptidyl tRNA from the 40S ribosomal A site to the P site, dependent on elongation factor EF-2 and GTP,[28-30] and inhibits peptide bond formation in the 60S ribosomal unit at higher concentration. In addition, tylophorine, tylocrebrine, tubulosine, and emetine compete with [14a-^{3}H] cryptopleurine for a binding site on 80-, 60-, and 40-S ribosomal units and also inhibit the peptide-bond formation at high concentrations, implying that these compounds have a similar mechanism of action on protein synthesis inhibition.[31]

1.6.2 Apoptosis Induction

Ganguly et al.[32] demonstrated that unspecified *tylophora* alkaloids could induce

apoptosis in a human erythroleukemic cell line (K562) with characteristic apoptotic features,

such as nuclear condensation apoptotic body formation, flipping of membrane

phosphatidylserine, activation of caspase 3 and release of mitochondrial cytochrome c.

These findings suggest that tylophora alkaloids, in addition to their antiproliferative activity,

also induce apoptosis in tumor cells.

1.6.3 Inhibition of Thymidylate Synthase (TS) and Dihydrofolate Reductase (DHFR)

In the 1990s, it was found that tylophorine alkaloids target several key targets for cancer

chemotherapy, including the metabolic enzymes thymidylate synthase (TS) and dihydrofolate

reductase.[33] TS catalyzes the reductive methylation of the substrate dUMP (2'-deoxyuridine

5'-monophosphate) to dTMP (2'-deoxythymidine 5'-monophosphate; thymidylate) with

concomitant conversion of the cofactor CH_2THF (5,10-methylenetetra-hydrofolate) to DHF

(7,8-dihydrofolate) (see Equation 1).

$$dUMP + CH_2THF \rightarrow dTMP + DHF \qquad \textbf{Equation 1}$$
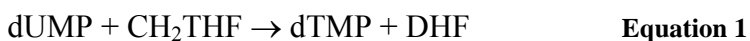
Thymidylate synthase (TS) and dihydrofolate reductase (DHFR) play a pivotal role in

the provision of precursors (thymidylate) for DNA biosynthesis through a de novo pathway.

In vitro studies of thymidylate synthase inhibition in human leukemic leukocytes showed that

pergularinine (PGL) and tylophorinidine (TPD) from the Indian medicinal plant *Pergularia*

pallida potently inhibited both chronic myelocytic leukemia (CML) and acute lymphocytic

leukemia (ALL) ($IC_{50} = 50$ µM). The authors indicated that 2 mol of PGL and TPD each

bound irreversibly and covalently to one mole of *L. leichmannii* TS (Narasimha Rao et al.,

unpublished data). In contrast, binding to DHFR was slow and reversible. Inhibition

kinetics showed that the Ki values for PGL and TDP were 9×10^{-6} and 7×10^{-6} M,

respectively.[33] TS is highly elevated in human leukemia and it is also a good tumor marker to

predict the progression of malignancy in leukemia and solid tumors such as breast and lung

cancers. Understanding of cancer biochemistry thus provides a good viewpoint for the

design of enzyme targeted anticancer chemotherapy with this compound class.

1.6.4 Inhibition of Activator Protein-1, CRE, and NF-kB

Activator protein-1, CRE, and NF-κB signaling pathways have been well studied and are

important players in the control of cell growth, differentiation, and survival.[34-36] Gao et al.[37]

found that NSC-717335, a stereoisomer of tylophorine, significantly inhibits activator

protein-1, CRE, and nuclear factor κB (NF-κB) mediated transcription. NSC-717335 and

NSC-716802 had significant inhibitory effects on NF-κB mediated transcription with IC_{50}

values of 30 nM and 100 nM, respectively. This result implied that tylophorine analogs may

alter the activity of the above transcription factors, subsequently modulating the expression

of their target genes involved in the control of cell growth, differentiation, and survival.

In addition, Gao et al demonstrated that tylophorine analogs are active against HepG2

tumor cells both in vitro and in vivo (HCC is refractory to chemotherapy because of tumor

heterogeneity, the development of multidrug resistance phenotypes, and recently reported

constitutive expression of NF-κB[38]). One of the major problems with current cancer

chemotherapy is drug resistance. Recently, NF-kB has been suggested as one mechanism of

drug resistance, because of its antiapoptotic role.[39,40] Tumors that have constitutive NF-kB

activity usually show increased resistance to chemotherapy.[41] Another explanation might be

that NF-kB is involved in regulation of p-glycoprotein, overexpression, which is a well

known mechanism of multidrug resistance to chemotherapy. Consistent with Gao's studies, Staerk et al.[21] also showed that phenanthroindolizidine alkaloids were cytotoxic to both drug sensitive KB-3-1 and multidrug-resistant KB-Vin-1 cell lines, with low IC_{50} values comparable to those of modern cytostatic drugs. This profile contrasts with those of many front-line antitumor drugs such as *Catharanthus* alkaloids and taxol, which are prone to multidrug-resistance based on glycoprotein transporter (MDR1) expressed in KB-Vin-1 cells.

1.6.5 Selective Interaction between Tylophorine B and Bulged DNA

Xi et al.[42] studied the interaction between tylophorine B and bulged DNA using fluorescence spectroscopy and thermal melting methods. Fluorescence quenched upon addition of the DNA, and the fluorescence intensity of tylophorine B tended to be constant at a high concentration of DNA, which suggests that the binding reaches saturation. The binding stoichiometry of the tylophorine B-DNA complex is ca. 1:1. The results indicate that oligonucleotides interact with tylophorine B at a submicromolar concentration, and the affinity for DNA bulge is optimal with Kd of 0.018 μM. In addition, as a planar molecule as mentioned previously, tylophorine interacts with DNA through an intercalative association in which a planar, heteroaromatic moiety slides between the DNA A-T and T-A base pairs.

1.7 CONCLUSION

Over the years, natural products have contributed enormously to the treatment of various human diseases. Recent findings demonstrate that tylophorines are cytotoxic to both drug sensitive and multidrug resistant cancer cells with a unique mode of action different from those of current known anticancer drugs. Therefore, although the phenanthroindolizidine alkaloid tylocrebrine previously failed in clinical trials due to CNS toxicity, tylophorine has a

high potential to be developed into a new anticancer drug class, based on the profound

cytotoxicity of these alkaloids, particularly to multidrug resistant cancer cells, and

emphasized by recent findings of tylophorine's mode of action in biological systems.

1.8 REFERENCES

1) Gellert, E. In *Alkaloids: Chemical and Biological Perspectives*. Pelletier, S. W., Ed; Academic Press: New York, 1987; pp 55-132.

2) Govindachari, T. R. In *The Alkaloids, Chemistry and Pharmacology.* Manske, R. H. F., Ed; Academic Press: New York, 1976; pp 517-528.

3) Bick, I. R. C.; Sinchai, W. In *The Alkaloids, Chemistry and Pharmacology*. Rodrigo, R. G. A., Ed; Academic Press: New York, 1981; pp 193-220.

4) Gellert, E. The indolizidine alkaloids. *J. Nat. Prod.* **1982***, 45*, 50-73.

5) Pettit, G. R.; Goswami, A.; Cragg, G. M.; Schmidt, J. M.; Zou, J.-C. Antineoplastic agents. 103. The isolation and structure of hypoestestatins 1 and 2 from the East African *Hypoestes verticillaris. J. Nat. Prod.* **1984***, 47*, 913-919.

6) a) Cave, A.; Leboeuf, M.; Moskowitz, H.; Ranaivo, A.; Bick, I. R. C.; Sinchai, W.; Nieto, M.; Sevenet, T.; Cabalion, P. Alkaloids of *Cryptocarya phyllostemon. Aust. J. Chem.* **1989***, 42*, 2243-2263. b) Mitra, S. N.; Rajan, S.; Govindachari, T.; Subramanian, E. Crystal structure of tylophorine methiodide monohydrate, C25H30NO4+I-.H2O. *J. Chem. Crystallogr.* **1996***, 26*, 223-226.

7) Venkatachalam, S. R.; Mulchandani, N. B. Isolation of phenathroindolizidine alkaloids and a novel biphenylhexahydroindolizine alkaloid from *Ficus hispida. Naturwissenschaften* **1982***, 69*, 287-288.

8) Baumgartner, B.; Erdelmeier, C. A. J.; Wright, A. D.; Rali, T.; Sticher, O. An antimicrobial alkaloid from *Ficus septica. Phytochemistry* **1990***, 29*, 3327-3330.

9) Wang, Q.; Xie, L.; Zhai, J. Tylophorine B benzene solvate. *Acta. Cryst.* **2000***, C56*, 197-198.

10) Govindachari, T.; Lakshmikantham, M. V.; Nagarajan, K.; Pai, B. R. Chemical examination of *Tylophora asthmatica*. II. *Tetrahedron* **1958***, 4*, 311-324.

11) Bradsher, C. K.; Berger, H. Synthesis of dl-cryptopleurine. *J. Am. Chem. Soc.* **1957***, 79*, 3287-3288.

12) Marchini, P.; Belleau, B. Synthesis of cryptopleurine and related phenanthroquinolizidines. *Can. J. Chem.* **1958***, 36*, 581-588.

13) Suffness, M.; Cordell, G. A. In *The Alkaloids, Chemistry and Pharmacology;* Brossi, A., Ed.; Academic Press: New York, 1985; Vol. 25, pp 156-163.

14) Li, Z., Jin, Z., Huang, R. Isolation, total synthesis and biological activity of phenanthroindolizidine and phenanthroquinolizidine alkaloids. *Synthesis* **2001**, *16*, 2365-2378

15) Michael, J. Indolizidine and quinolizidine alkaloids *Nat. Prod. Rep.*, **2004**, *21*, 625-649.

16) Michael, J, Indolizidine and quinolizidine alkaloids *Nat. Prod. Rep.*, **2005**, *22*, 603-626.

17) Zee-Cheng, K. Y.; Cheng, C. C. Common receptor-complement feature among some antileukemic compounds. *J. Pharm. Sc.* **1970**, *59*, 1630-1634.

18) Gupta, R. S.; Siminovitch, L. Mutants of CHO cells resistant to the protein synthesis inhibitors, cryptopleurine and tylocrebrine: genetic and biochemical evidence for common sit of action of emetine, cryptopleurine, tylocrebrine, and tubulosine. *Biochemistry* **1977**, *16*, 3209-3214.

19) Gupta, R. S.; Krepinsky, J. J.; Siminovitch, L. Structural determinants responsible of the biological activity of (-)-emetine, (-)-cryptopleurine, and (-)-tylocrebrine: structure-activity relationship among related compounds. *Mol. Pharmacol* **1980**, *18*, 136-143.

20) Sanchez, L.; Vazquez, D.; Jimenez, A. Genetics and biochemistry of cryptopleurine resistance in the yeast *Saccharomyces cerevisiae*. *Mol. Gen. Genet.* **1977**, *156*, 319-326.

21) Staerk, D.; Lykkeberg, A. K.; Christensen, J.; Budnik, B. A.; Abe, F.; Jaroszewski, J. W. In vitro cytotoxic activity of phenanthroindolizidine alkaloids from *Cynanchum vincetoxicum* and *Tylophora tanakae* against drug-sensitive and multidrug-resistant cancer cells. *J. Nat. Prod.* **2002**, *65*, 1299-1302.

22) Abe, F.; Hirokawa, M.; Yamauchi, T.; Honda, K.; Hayashi, N.; Ishii, M.; Imagawa, S.; Iwahana, M. Further investigation of phenanthroindolizidine alkaloids from *Tylophora tanakae*. *Chem. Pharm. Bull.* **1998**, *46*, 767-769.

23) Sharma, V. M.; Adi Seshu, K. V.; Vamsee Krishna, C.; Prasanna, P.; Chandra Sekhar, V.; Venkateswarlu, A.; Rajagopal, S.; Ajaykumar, R.; Deevi, D. S.; Rao Mamidi, N. V. S.; Rajagopalan, R. Novel 6,7-diphenyl-2,3,8,8a-tetrahydro-1H-indolizin-5-one analogues as cytotoxic agents. *Bioorg. Med. Chem. Lett.* **2003**, *13*, 1679-1682.

24) The 60-cell line NCI test data along with in vivo data can be accessed from the NSC numbers at the following Web site: http://dtp.nci.nih.gov/dtpstandard/dwindex/index.jsp

25) Gellert, E.; Rudzats, R. Antileukemia activity of tylocrebrine. *J. Med. Chem* **1964**, *7*, 361-362.

26) Huang, M.-T.; Grollman, A. P. Mode of action of tylocrebrine. Effects on protein and nucleic acid synthesis. *Mol. Pharmacol* **1972**, *8*, 538-550.

27) Donaldson, G. R.; Atkinson, M. R.; Murray, A. W. Inhibition of protein synthesis in Ehrlich ascites-tumour cells by the phenathrene alkaloids tylophorine, tylocrebrine and cryptopleurine. *Biochem. Biophys. Res. Commun.* **1968**, *31*, 104-109.

28) Barbacid, M.; Fresno, M.; Vazquez, D. Inhibitors of polypeptide elongation on yeast polysomes. *J. Antibiot* **1975**, *28*, 453-463.

29) Bucher, K.; Skogerson, L. Cryptopleurine – an inhibitor of translocation. *Biochemistry* **1976**, *15*, 4755-4759.

30) Carrasco, L.; Fernandez-Puente, C.; Vazquez, D. Antibiotics and compounds affecting translation by eukaryotic ribosomes. Specific enhancement of aminoacyl-tRNA binding by methylxanthines. *Mol. Cell Biochem.* **1976**, *10*, 97-122.

31) Dolz, H.; Vazquez, D.; Jimenez, A. Quantitation of the specific interaction of [14a-3H] cryptopleurine with 80S and 40S ribosomal species from the yeast *Saccharomyces cerevisiae. Biochemistry* **1982**, *21*, 3181-3187.

32) Ganguly, T.; Khar, A. Induction of apoptosis in a human erytholeukemic cell line K562 by Tylophora alkaloids involves release of cytochrome c and activation of caspase 3. *Phytomedicine* **2002**, *9*, 288-295.

33) Rao, K. N.; Bhattacharya, R. K.; Venkatachalam, S. R. Inhibition of thymidylate synthase and cell growth by the phenanthroindolizidine alkaloids pergularinine and tylophorinidine. *Chem. Biol. Interact* **1997**, *106*, 201-212.

34) Darnell, J. E., Jr. Transcription factors as targets for cancer therapy. *Nat. Rev. Cancer* **2002**, *2*, 740-749.

35) Shaulian, E.; Karin, M. AP-1 as a regulator of cell life and death. *Nature Cell Biol.* **2002**, *4*, E131-136.

36) Lin, A.; Karin, M. NF-κB in cancer: a marked target. *Seminars in Cancer Biology* **2003**, *13*, 107-114.

37) Gao, W.; Lam, W.; Zhong, S.; Kaczmarek, C.; Baker, D. C.; Chang, Y. C. Novel mode of action of tylophorine analogs as antitumor compounds.*Cancer Res.* **2004**, *64*, 678-688.

38) Tai, D. I.; Tsai, S. L.; Chang, Y. H.; Huang, S. N.; Chen, T. C.; Chang, K. S.S.; Liaw, Y. F. Constitutive activation of nuclear factor κB in hepatocellular carcinoma. *Cancer* **2000**, *89*, 2274-2281.

39) Wang, C. Y.; Cusack, J. C., Jr.; Liu, R.; Baldwin, A. S., Jr. Control of inducible chemoresistance: enhanced anti-tumor therapy through increased apoptosis by inhibition of NF-κB. *Nature Med.* **1999***, 5*, 412-417.

40) Cusack, J. C., Jr.; Liu, R.; Baldwin, A. S., Jr. Inducible chemoresistance to 7-ethyl-10-[4-(1-piperidino)-1-piperidino]-carbonyloxycamptothecin (CPT-11) in colorectal cancer cells and a xenograft model is overcome by inhibition of nuclear factor-κB. *Cancer Res.* **2000***, 60*, 2323-2330.

41) Bharti, A. C.; Aggarwal, B. B. Nuclear factor-kappa B: its role in prevention and therapy. *Biochemical Pharmacology* **2002***, 64*, 883-888.

42) Xi, Z.; Zhang, R.; Yu, Z.; Ouyang, D.; Huang, R. Selective interaction between tylophorine B and bulged DNA.. *Bioorg. Med. Chem. Lett.* **2005***, 15*, 2673-2677.

CHAPTER II. RESEARCH DESIGN

2.1   INTRODUCTION

Cancer is a group of more than 100 different diseases, characterized by uncontrolled cellular growth, local tissue invasion, and distant metastases. Cancer claims approximately 560,000 lives in the United States each year. It is second only to cardiovascular disease as a cause of mortality. The clinical use of chemotherapeutic agents against malignant tumors is successful in many cases but suffers from major drawbacks. One drawback is lack of selectivity, which leads to severe systemic side effects and limited efficacy. Another major problem is the emergence / selection of drug-resistance.

Natural products have been the major source of currently available anticancer drugs. According to a review of New Chemical Entities (NCE) from 1981 to 2002,[1] approximately 74% of anticancer drugs were either natural products, natural product-based, or mimicked them in one form or another. Therefore, as part of our studies in plant-derived antitumor agents, we have initiated the synthesis of new tylophorine (**1**) analogs. Our design template is TSWUCC1 (Antofine) (**2**), a tylophorine analog isolated from *Asclepiadaceae* by Dr. K.H. Lee's collaborator, Dr. T. S. Wu[2] in Taiwan. This compound showed both remarkable activity (EC$_{50}$ 10 ng/ml) and differential toxicity against different human cancer cell lines. The goal of this study is to generate and optimize phenanthrene derivatives as promising clinical trial candidates for treatment of cancer.

2.2 SIGNIFICANCE

Over the years, natural products have contributed enormously to the treatment of human diseases. Recent findings have demonstrated that tylophorine alkaloids are cytotoxic to both drug sensitive and mutidrug resistant cell lines with unique mode(s) of action different from those of other known antitumor drugs. These alkaloids possibly show an inhibitory effect on cyclic AMP response elements, activator protein-1 sites, or NF-κB binding site-mediated transcription, as well as potentiate retinoic acid differentiation to cause cancer cell apoptosis. Therefore, although the phenanthroindolizidine alkaloid tylocrebrine (**3**) previously failed in anticancer clinical trials due to CNS toxicity, this compound class merits further study in light of its profound cytotoxicity, particularly against multidrug resistant cancer cells. A better understanding of mode(s) of action, formulation of structural-activity relationships in targeting specific tissue receptors, and synthesis of more polar analogs that are unable to pass the blood-brain barrier should help to generate optimal clinical trial candidates and develop this new class of anticancer drugs that may overcome the current issue of chemotherapy resistance. [To date, bortezomib (**4**) (Figure 2-1), a proteasome inhibitor, is the only drug designed to target chemotherapy resistance by overcoming the anti-apoptosis mechanism of cancer cells through indirect inhibition of the NFκB pathway.]

2.3 SPECIFIC AIMS

Specific Aim 1:

To design and synthesize novel phenanthrene alkaloid derivatives structurally related to tylophorine as a new class of potent antitumor agents.

TSWUCC1 (Antofine) (**1**) (Figure 2-1), a tylophorine analog isolated from *Ficus septica* by Dr. T. S. Wu in Taiwan, will be used as the template to design and synthesize new antitumor phenanthrene-based tylophorine (PBT) derivatives:

1) Design and synthesis of phenanthroindolizidine alkaloid antofine.

2) Design and synthesis of water soluble phenanthrene-based tylophorine derivatives (PBTs).

3) Design and synthesis of 9-substituted PBTs.

Specific Aim 2:

To investigate the mode of action of this compound class.

Compounds synthesized from specific aim 1 will be evaluated for their inhibitory effects on cancer cell growth, as well as in other biological assays both in-house (Dr. K.F. Bastow's Laboratory, UNC) and at the National Cancer Institute (NCI), MD Anderson Cancer Center, as well as National Science and Techology Program for Bio- and Pharmaceuticals in Taiwan for in vivo activity. All compounds will also be tested for anti-telomerase related antitumor activity in Dr. M. Jasfer's laboratory, UNC. The results from these biological assays will facilitate our understanding of the specific targets for this new compound class.

Specific Aim 3:

To generate QSAR models and use the resulting database for new lead identification.

Based on the assumption that differences in structural properties account for differences in biological activities of compounds, validated predictive quantitative structure-activity relationship (QSAR) models will be generated using the chemical structures/activities of

compounds synthesized from Aim 1 and applied to database mining to assist further

development of this new compound class.

Specific Aim 4:

To evaluate the pharmacokinetic profiles of phenanthrene derivatives and explore their

potential for successful development into clinical trial candidates.

An ADME prediction program will be used to evaluate the pharmacokinetic profile of

the synthesized phenanthrene-based tylophorine (PBT) derivatives, including blood brain

barrier (BBB) permeability, protein binding, and human intestinal absorption (HIA), for each

promising analog in comparison to the parent tylophorine molecule.
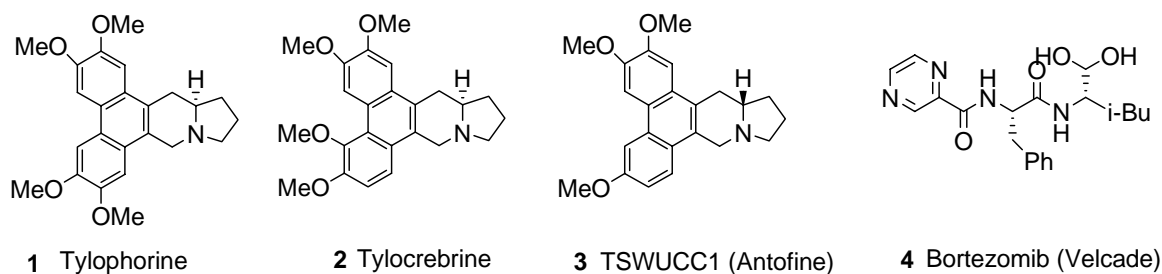
Figure 2-1. Structures of tylophorine (**1**) TSWUCC1 (antofine) (**2**), tylocrebrine (**3**) and bortezomib (**4**).

2.4   REFERENCES

1) Newman, D. J.; Cragg, G. M.; Snader, K. M. Natural products as sources of new drugs over the period 1981-2002. *J. Nat. Prod.* **2003**, *66*, 1022-1037.

2) Wu, P. L.; Rao K. V.; Su, C.-H.; Kuoh, C.-S.; Wu, T.-S. Phenanthroindolizidine alkaloids and their cytotoxicity from the leaves of *Ficus septica*. *Heterocycles* **2002**, *57*, 2401-2048.

CHAPTER III. DESIGN, SYNTHESIS AND BIOLOGICAL EVALUATION OF NEW PHENANTHRENE-BASED TYLOPHORINE DERIVATIVES (PBTS) (PART I)

3.1   INTRODUCTION
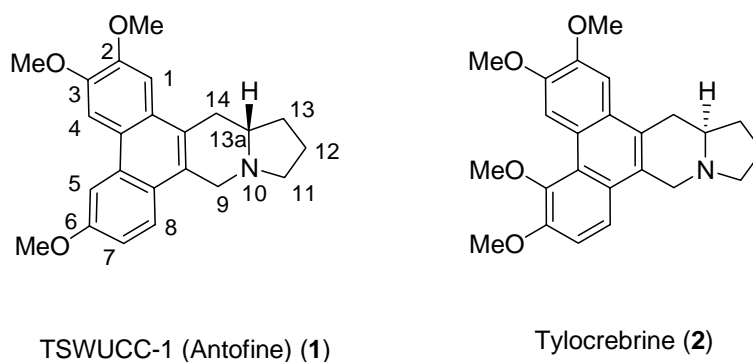
Figure 3-1. Structures of TSWUCC-1 (antofine) and tylocrebrine

The total synthesis of TSWUCC-1 (Antofine **1**) has been achieved by various groups.[1-4]
We designed the following alternate synthetic route based on high reported yields for each
step. Initially, two commercially available appropriately substituted phenyl acetic acid (**A**)
and *o*-nitrobenzaldehyde (**B**) compounds (Scheme 3-1) were condensed using a general
Perkin condensation procedure. After reduction of the nitro group to an amine, the key step
in the synthesis involves formation of the phenanthrene unit by an improved, reported free-
radical Pschorr cyclization[5] of the appropriately substituted stilbenic acid (**D**). The synthesis
of this highly condensed pentacyclic natural product should be completed in three addition
steps: amidation with proline methyl ester, carbonyl redution and a final polyphosphoric acid
(PPA)-catalyzed ring closure. However, the PPA catalyzed cyclisation (**f**) gave the unstable

ketone intermediate **H**, which is very sensitive to moisture and acid, and resulted in extensive

decomposition. The relative low yield (10%) could not be improved by conventional

Friedel-Crsfts acylation catalysis (acid chloride hydrochloride) or other dehydrogenation

reagent, such as Eaton's reagent, sulfuric acid and trifluoroacetic anhydride/acid. The

relative low yield of this ring closure halted the further development of this synthetic route to

the natural product or its derivatives.
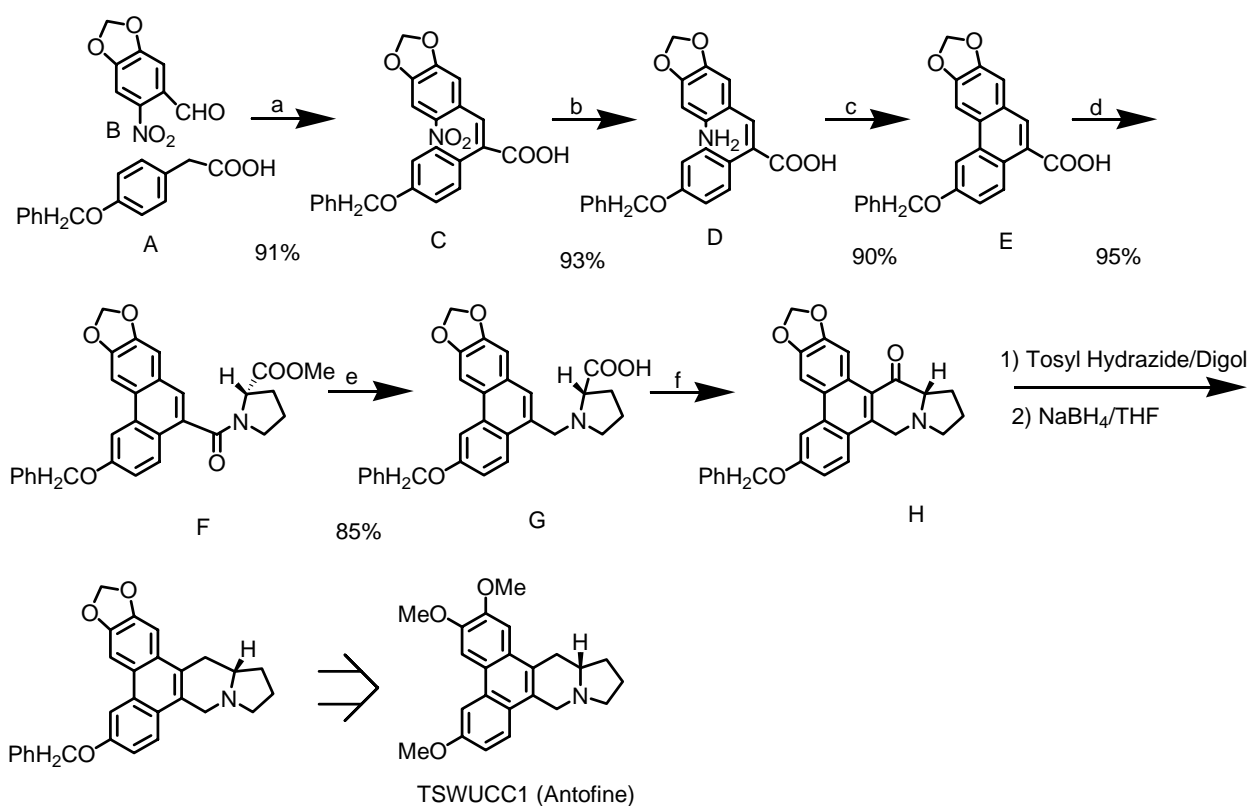
a: Ac$_2$O/Et$_3$N b: FeSO$_4$/NH$_4$OH c: NaNO$_2$/Fluoroboric acid; Ferrocene/acetone d; EDC/DMF e: BMS/THF f: PPA

Scheme 3-1. Attempted total synthesis of TSWUCC1

However, in a preliminary screen on all reaction intermediates, compound **G**, [N-(6-

benzyloxy-2,3-methylenedioxyphenanthr-9-ylmethyl)-L-proline] (Scheme 3-1), was

discovered serendipitously as a potent cytotoxic amino acid precursor of tylophorine. It

presents an unprecedented antitumor scaffold that led to our exploration of more polar

(water-soluble) tylophorine-related derivatives. Such phenanthrene-based tylophorine

derivative or PBTs could circumvent this prior obstacle learned from the drug development

failure of tylocrebrine (**2**) in the early 1960s due to its significant CNS toxicity, manifested as

disorientation and ataxia.[6] Increased polarity should diminish the CNS toxicity by

preventing compounds from penetrating across the blood brain barrier. Tylophorine

alkaloids are composed of a phenanthrene ring system and an indolizidine moiety – and the

rigid phenanthrene structure is a prerequisite for the antitumor activity.[7] However, by

opening the indolizidine ring, polar chemical moieties can easily be introduced into the

compound skeleton.

In addition, successful application of the Pschorr cyclization[5] and coupling reaction in

the presence of *N*-(3-dimethylaminopropyl)-*N'*-ethylcarbodiimide hydrochloride (EDC)

enabled efficient and concise access to these more polar and water soluble PBTs with overall

yields greater than 50% (Scheme 3-1). In comparison to the above reported total synthesis of

tylophorine, our PBT synthesis avoids the cyclization step (limiting synthetic factor) and

makes the parallel and large scale synthesis of PBTs feasible, which could potentially

enhance the development of these compounds into drugs.

Therefore, as part of our studies in plant-derived antitumor agents, this discovery led us

to explore a new series of novel PBTs. We have initiated the design, synthesis and structure-

activity relationship (SAR) study of this new anticancer compound class. The goal of this

study is to generate and optimize PBTs as promising clinical trial candidates for treating

cancer.

3.2 DESIGN OF SYNTHESIS

Compound **G** was used as the template to design and synthesize PBT derivatives. These compounds contain a core phenanthrene structure and can be synthesized efficiently in excellent yield as shown in Scheme3-2. The newly synthesized PBTs were evaluated for cytotoxic activity against the A549 human cancer cell line and both structures and activities are listed in Tables 3-1, -2 and -3.

Reagents and conditions: a: Ac_2O/Et_3N b: $FeSO_4/NH_4OH$ c: $NaNO_2$/fluoroboric acid; ferrocene/acetone d: EDC, DMAP, HOBt/DMF e: BMS/THF f: H_2, Pd/C/MeOH g: $LiAlH_4$/THF h: NaOH/MeOH (1:1)
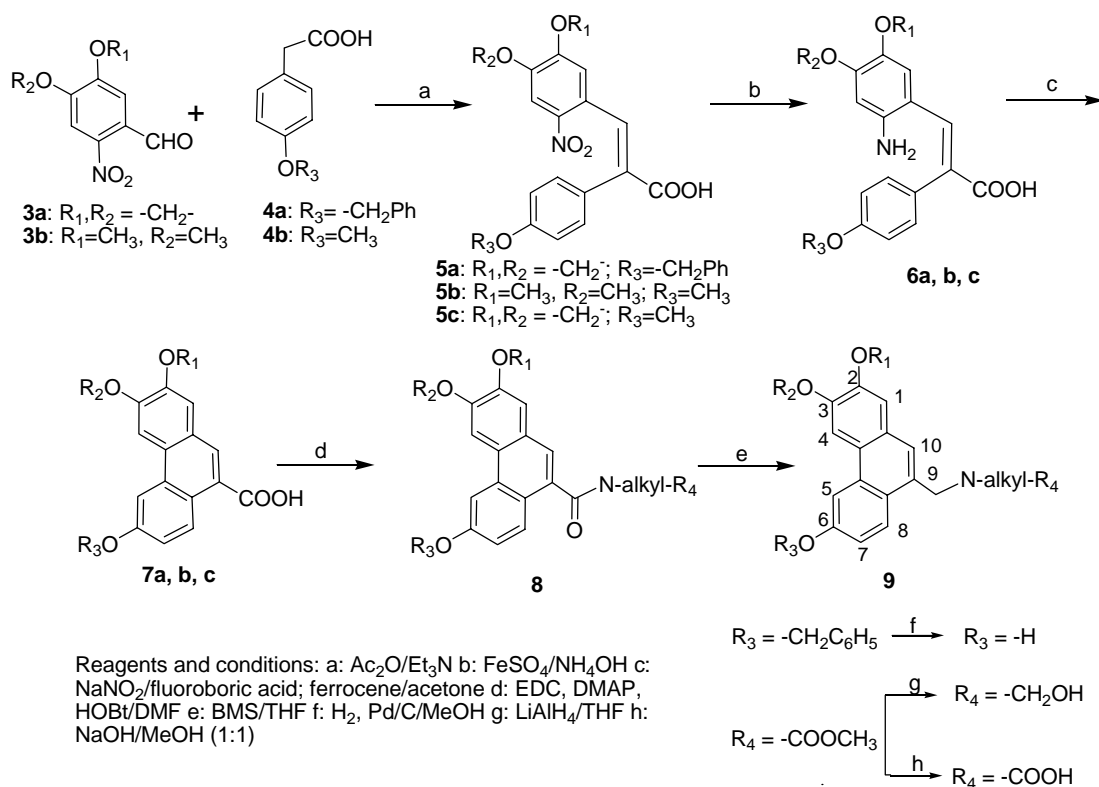
Structures of target compounds **10-42**, including R_1, R_2, R_3 and N-alkyl, are found in **Tables 1-3**.

For general structure **8** with R_4 = COOMe: **7a** $\xrightarrow{d}$ **10**

For general structure **8** with R_4 = COOH: **7a/b** $\xrightarrow{d+h}$ **11, 16, 25, 29**

For general structure **10** with R_4 = COOMe: **7a/b** $\xrightarrow{d+e}$ **14, 17, 26, 30**

For general structure **10** with R_4 = COOH: **7a/b/c** $\xrightarrow{d+e+h}$ **12, 15, 18, 20, 27, 31, 33, 35, 37**

For general structure **10** with R_4 = CH$_2$OH: **7a/b/c** $\xrightarrow{d+e+h+g}$ **13, 19, 21, 28, 32, 34, 36, 38**

For R_3 = OH, R_4 = COOH: **16, 18, 20** $\xrightarrow{f}$ **22, 23, 24**

For seco PBT analogs: **5c** $\xrightarrow{d+h}$ **39** $\xrightarrow{e}$ **40** $\xrightarrow{g}$ **41**

Scheme 3-2. Total synthesis of new phenanthrene-based tylophorine derivatives

3.3 CHEMISTRY

Compounds **10-49** were synthesized following the efficient reported procedure[5] outlined

in Scheme 3-2. A commercially available substituted *O*-nitrobenzaldehyde (**3a,b**) was

treated with 4-methoxy or -benzyloxyphenyl acetic acid (**4a,b**) in the presence of Ac_2O

(Perkin condensation) to yield an intermediate nitro-substituted cinnamic acid (**5a-c**). The

nitro group of **5** was converted to an amine using ammoniacal ferrous sulfate ($FeSO_4$) to

provide the amino-substituted cinnamic acid (**6a-c**). Phenanthrenes **7a-c**, which are the key

intermediates in our method, were formed by an improved free-radical Pschorr cyclization[5] in

high yield. Compound **6** was treated with sodium nitrite in 48% fluoroboric acid, and the

resulting diazonium tetrafluoroborate was then efficiently cyclized to the phenanthrene-9-

carboxylic acid (**7**) using catalytic ferrocene. Intermediates **7a-c** were then condensed with

the appropriate protected cyclic or acylic amino acid in the presence of *N*-(3-

dimethylaminopropyl)-*N*'-ethylcarbodiimide hydrochloride (EDC), 4-

(dimethylamino)pyridine (DMAP) and 1-hydroxybenzotriazole (HOBT) to give the amido-

substituted phenanthrene (**8**). These mild conditions avoid the production of degradation

products resulting from the acidic instability of the methylenedioxy group. Selective

reduction of the amide carbonyl group to a methylene was achieved by using borane-methyl

sulfide complex (BMS, 2.0M solution in THF) to provide **9**. The C-9 side chain methyl ester

was converted to carboxylic acid and hydroxymethyl groups by basic hydrolysis and lithium

aluminum hydride reduction, respectively. The 6-phenolic analogs were prepared by

hydrogenolysis (H_2, Pd/C) of the benzyloxy protecting group.

3.4 RESULTS AND DISCUSSION

Tables 3-1 – 3-3 summarize the structures of newly synthesized PBTs (**7a-c**, **10–42**) and their cytotoxic activity (EC_{50}) against the A549 lung cancer cell line. Etoposide (VP-16) was used as the reference compound.

Structure-Activity Relationship (SAR) Analysis

All three intermediate phenanthrene-9-carboxylic acids **7a-c** were inactive. Thus, the rigid, planar phenanthrene system is not sufficient for cytotoxic activity, and an appropriate C-9 side chain is crucial. However, the phenanthrene system is required for cytotoxic activity, as the *seco* analogues **39-42**, which contain an active proline side chain (see discussion below) but only a stilbene skeleton, were also inactive.

Active analogs contained both cyclic (pyrrole/proline, piperidine/pipecolinic acid) and acylic (aminopentanoic, aminohexanoic acids) nitrogen-containing side chains at the C-9 position of phenanthrene. However, the linkage between the nitrogen and the phenanthrene was very critical. Reduction of the amide carbonyl to methylene could dramatically increase the cytotoxic activity as shown in the comparison of **16** (L-proline amide, carbonyl linkage, EC_{50} 42.6 µM) and **18** (methylene linkage, EC_{50} 4.4 µM). This observation (carbonyl, unfavorable or less favorable; methylene, favorable) also could be seen in comparison of **11/12** and **25/27**. A simple explanation for this observation could possibly be the difference in configurational constraint. The carbonyl is conjugated with the phenanthrene ring and, thus, extends the coplanarity, while the methylene substituent can rotate freely around the C-C bond. The former geometric restriction appears to disfavor cytotoxic activity and may prevent the molecule from attaining the optimal conformation for binding to an assumed biological target.

26

On the phenanthrene skeleton, changing the benzyloxy moiety at the C-6 position to a hydroxy group was extremely detrimental to activity (cf. **18**/**23** and **20**/**24**). In addition, active compounds with a 6-benzyloxy moiety (**15** and **18-21**, EC_{50} 1.3 – 4.4 µM) were generally slightly less potent than corresponding analogs with a 6-methoxy group (**27** and **31-34**, EC_{50} 0.16 − 2.1 µM). Thus, the rank order of potency at the phenanthrene C-6 position was methoxy > benzyloxy >> hydroxyl, suggesting that this position cannot tolerate the introduction of a polar moiety. A hydrophilic moiety may be disfavored because a hydrophobic interaction occurs at this position between the compound and biological target that is essential for cytotoxic activity.

Interestingly, active compounds with a 2,3-methylenedioxy group (**33** and **34,** EC_{50} 0.5 and 0.16 µM) were up to 40 times more potent than the corresponding compounds with a 2,3-dimethoxy moiety (**37** and **38**, EC_{50} 9.7 and 6.3 µM). Thus, the five-membered methylenedioxy ring extension at the phenanthrene C2-C3 is quite favorable for cytotoxic activity.

In the amino side chain, when the terminal carboxylic acid group was masked as the methyl ester, the cytotoxic activity was diminished drastically or abolished (e.g., **14/15, 17/18, 26/27, 30/31**). However, reduction of the carboxylic acid to the hydroxymethyl generally increased activity, both in cyclic (**18/19**, **20/21**, **31/32**, **33/34**, **37/38**) and acyclic (**12/13, 27/28**, **35/36**) analogs. Thus, the rank order of potency of the terminal polar substituent was hydroxy > carboxylic acid >> methyl ester.

In summary, the favorable modification for these novel PBTs are as follows. 1) A planar phenanthrene system is required, but not sufficient for cytotoxic activity. 2) A *N*-hydrophilic substituent at the C-9 position is essential for the enhanced cytotoxicity and should be linked

through a methylene rather than a carbonyl group. 3) This C-9 *N*-hydrophilic substituent is ideal for the introduction of a polar moiety. Analogs containing terminal carboxylic acid or hydroxymethyl groups are more favorable than those with methyl esters. 4) On the phenanthrene skeleton, a methoxy substituent best fits both the steric and electronic requirements at the C-6 position and is preferred over benzyloxy and hydroxy groups. 5) Adding a methylenedioxy ring at the 2,3 position of the planar phenanthrene system can dramatically enhance the cytotoxic activity and led to the most potent derivatives.

3.5   CONCLUSION

In this study, a total of 33 novel phenanthrene-based tylophorine derivatives (PBTs) were synthesized and evaluated for cytotoxic activity against human A549 lung cancer cells. Among these compounds, N-(2,3-methylenedioxy-6-methoxy-phenanthr-9-ylmethyl)-L-2-piperidinemethanol (**34**) and N-(2,3-methylenedioxy-6-methoxy-phenanthr-9-ylmethyl)-5-aminopentanol (**28**) were the most potent compounds designed and synthesized to date with EC_{50} values of 0.16 and 0.27 μM, respectively. These two compounds incorporated all of the favorable modifications identified to date. They possess a novel structure and showed remarkable EC_{50} values in the sub-micromolar range, comparable with front-line antineoplastic drugs such as etoposide, suggesting that this new compound class is worthy of further development as potential antitumor clinical trials candidates

3.6   EXPERIMENTAL SECTION

3.6.1   Instruments and Chemicals

Melting points were measured using a Fisher Johns melting apparatus without correction. Proton nuclear magnetic resonance (^{1}H NMR) spectra were measured on a 300 MHz Varian

Gemini 2000 spectrometer using TMS as internal standard. The solvent used was CDCl$_3$

unless indicated. Mass spectra were recorded on a PE-Sciex API-3000 LC/MS/MS

instrument equipped with a Turbo IonsSpray ion source. Elemental analyses were performed

by Atlantic Microlab, Inc., Norcross, GA. All active target compounds were analyzed for C,

H, N and gave values within ±0.4% of the theoretical values. The purity of inactive target

compounds was verified by HPLC using three different solvent systems Thin-layer

chromatography (TLC) was performed on PLC silica gel 60 F$_{254}$ plates (0.5 mm, Merck).

Biotage Flash+ and Isco Companion systems were used as medium-pressure column

chromatography. Silica gel (200-400 mesh) from Aldrich, Inc. was used for column

chromatography. 4-Benzyloxyphenylacetic acid and 3, 4-methylenedioxy-6-

nitrobenzaldehyde were purchased from TCI. L-Pipecolinic acid and isonipecotic acid were

commercially available from Lancaster. All other chemicals were obtained from Aldrich, Inc.

and Fisher, Inc.

3.6.2 General Preparation

General procedure for the preparation of phenanthrene-9-carboxylic acids (**a,b,c**):

Phenanthrene-9-carboxylic acids **7a** and **7b** were synthesized following a reported

procedure.[4]

A solution of 3, 4-methylenedioxy-6-nitrobenzaldehyde (12 mmol), triethyl amine (12

mmol), and 4-benzyloxy- or 4-methoxy-phenylacetic acid (17 mmol) was refluxed with

stirring under Ar for 40 min. Water (30 ml) was added to the reaction mixture and the

temperature was maintained between 90 °C and 100 °C during the addition. The reaction

mixture was cooled to rt and the solid was collected by filtration and recrystallized from

EtOH.

To a solution of the nitrocinnamic acid (7 mmol) in 10% aqueous NH_4OH (100 ml) was added ferrous sulfate heptahydrate (15 g) dissolved in distilled water (100 mL) and concentrated aqueous NH_4OH (100 mL). The reaction mixture was refluxed for 1.5 h, cooled to 40 °C, filtered through Celite, and acidified with HOAc (100 mL). The resulting solid was collected by filtration and recrystallized from EtOH to yield the aminocinnamic acid.

A solution composed of the aminocinnamic acid (3 mmol), NaOH (33 mmol) and $NaNO_2$ in water (10 mL) was added dropwise over 30 min with stirring to 48% fluoroboric acid (43 mmol) at 0-5 °C. The mixture was stirred for 1 h, after which sulfamic acid was added until the mixture tested negative to starch-iodide paper. The crude solid was collected by filtration, dissolved in anhydrous acetone (10 mL) and then added dropwise with stirring over a 15 min period to ferrocene (0.056 g, 0.3 mmol) in acetone at rt. After an additional 15 min of stirring, the green reaction mixture was added to water (100 mL). A light-yellow precipitate was collected and the trace amount of ferrocene was removed in vacuo to afford the phenanthrene-9-carboxylic acid.

General procedure for the protection of cycloalkylamino acid:

To a solution of cycloalkylamino acid (4 mmol) in dry MeOH (4 mL) was added dropwise $SOCl_2$ (0.4 mL) at –30 °C. The reaction mixture was warmed to rt and refluxed for 1 h. Then the solvent was removed in vacuo and the product was used in the next reaction without further purification.

General procedure for the protection of acyclic alkylamino acid:

To a solution of dry MeOH (3 mL) was added dropwise acetyl chloride (0.45 mL) at 0 °C. After 10 min stirring, the amino acid was added to the solution in portions. The mixture

was warmed to rt and refluxed for 2 h, then the solvent was removed in vacuo and the product was used in the next reaction without further purification.

General procedure for the peptide bond condensation reaction (**d**):

To a solution of phenanthrene-9-carboxylic acid (4 mmol), 4-(dimethylamino) pyridine (DMAP) (2 mmol), 1-hydroxybenzotriazole (HOBT) (4 mmol) in 20 mL DMF was added NMM (1.028 mL). After the mixture was stirred at 0 °C for 15 min, *N*-(3-dimethylaminopropyl)-*N*'-ethylcarbodiimide hydrochloride (EDC) (4.4 mmol) was added in portions, then methyl protected amino acid (4.4 mmol) was added after 30 min stirring. The reaction mixture was stirred overnight at rt and partitioned between EtOAc and water. The organic layer was washed with brine, saturated NaHCO$_3$ and 1N HCl, dried over Na$_2$SO$_4$, and concentrated in vacuo. The crude product was chromatographed using Biotage Flash+ and Isco Companion systems using a 40g silica cartridge and EtOAc/hexane as eluant.

General Procedure for the carbonyl reduction reaction (**e**):

To a stirred solution of 9-amido-substituted phenanthrene (**8** in Scheme 3-2, 2 mmol) in THF (20 mL) was added dropwise borane-methyl sulfide (BMS) (4 mL, 2.0M solution in THF). The reaction mixture was stirred at rt overnight and quenched with 1N HCL. THF was removed in vacuo, and the residue was partitioned between CH$_2$Cl$_2$ and water. The organic layer was dried, filtered, and evaporated to afford the target product (**9** in Scheme 3-2). The crude product was chromatographed using Biotage Flash+ and Isco Companion systems using MeOH/CH$_2$Cl$_2$ as eluant.

General Procedure for the catalytic cleavage (**f**):

A solution of benzyoxy derivative (1mmol) and Pd/C (10%) was hydrogenated in a Parr apparatus (30 psi) for 2 h. The reaction mixture was filtrated through Celite, and filtrate was

concentrated in vacuo and was chromatographed using Biotage Flash+ and Isco Companion systems using MeOH/CH_2Cl_2 as eluant.

General Procedure for the LiAlH$_4$ reduction (**g**):

To a suspension of methyl ester (1mmol) in 15 ml dry THF was added LiAlH$_4$ (1g) in portions at 0 °C. After addition, the reaction mixture was refluxed for 4 h, and then cooled to 0 °C. The reaction mixture was quenched with methnol, and then 10% Rochelle salt was added. The reaction mixture was extracted with water and 10% MeOH/CH_2Cl_2. The organic layer was dried over Na_2SO_4, and the crude product was chromatographed using Biotage Flash+ and Isco Companion systems using MeOH/CH_2Cl_2 as eluant.

General Procedure for the basic hydrolysis reaction (**h**):

A solution of ester in a 1:1 mixture of 4N NaOH and MeOH was refluxed for 4 h. The reaction mixture was acidified and partitioned between 10% MeOH/CH_2Cl_2 and 1N HCl. The organic layer was dried over Na_2SO_4, filtered, and evaporated. The crude product was chromatographed using Biotage Flash+ and Isco Companion systems using MeOH/CH_2Cl_2 as eluant.

3.6.3 Chemistry

2,3-Methylenedioxy-6-benzyloxy-phenanthrene-9-carboxylic acid (7a)

75% yield over two steps; mp 263-265 °C; ^{1}H NMR (400.13 MHz) δ 8.40 (d, *J*=4Hz, 1H), 7.92 (d, *J*=2Hz, 1H), 7.88 (s, 1H), 7.52 (m, 2H), 7.38 (m, 5H), 7.26 (dd, *J*=4Hz, 2Hz, 1H), 6.14 (d, *J*= 4Hz, 2H), 5.35 (d, *J*=7Hz, 2H); MS (DCI/NH$_3$) *m/e*: 373 (M + H)$^+$.

2,3-Methylenedioxy-6-methoxy-phenanthrene-9-carboxylic acid (7b)

78% yield; white powder; mp 293-295 $^{\circ}$C; ^{1}H NMR (400.13 MHz) δ 7.67 (s, 1H), 7.60 (d, J= 4Hz, 1H), 7.22 (dd, J= 4Hz, 2Hz, 1H), 6.92 (s, 1H), 6.89 (d, J=2Hz, 1H), 6.70 (s, 1H), 5.98 (s, 2H), 3.79 (s,3H); MS (DCI/NH3) m/e: 297 (M + H)$^{+}$.

2,3,6-Trimethoxyphenanthrene-9-carboxylic acid (7c)

79% yield; white powder; mp 241-243 $^{\circ}$C; ^{1}H NMR (400.13 MHz) δ 8.93 (d, J=4Hz, 1H), 8.33 (s, 1H), 7.84 (d, J=2Hz, 1H), 7.82 (s, 1H), 7.23 (s, 1H), 7.22 (dd, J=4Hz, 2Hz, 1H), 4.07 (s, 3H), 3.98 (s,3H), 3.97 (s, 3H); MS (DCI/NH$_3$) m/e: 314 (M + H)$^{+}$.

Methyl N-(2,3-methylenedioxy-6-benzyloxy-phenanthr-9-ylcarbonyl)-6-aminohexanoate (10)

General procedure **d** from **7a** (92%); cololess syrup; ^{1}H NMR (400.13 MHz) δ 8.09 (d, J=4Hz, 1H), 7.81 (d, J=2Hz, 1H), 7.82 (s, 1H), 7.74 (d, J=4Hz , 2H), 7.45 (s, 1H), 7.33 (t, J=4Hz, 2H), 7.26 (m, 1H), 7.20 (dd, J= 4Hz, 2Hz, 1H), 7.09 (s, 1H), 6.03 (s, 2H), 5.18 (s, 2H), 3.41(s, 3H), 3.28 (m, 2H), 2.28 (t, J = 6Hz, 2H), 1.61 (m, 2H), 1.56 (m, 2H), 1.38 (m, 2H); MS (DCI/NH$_3$) m/e: 500 (M + H)$^{+}$.

N-(2,3-methylenedioxy-6-benzyloxy-phenanthr-9-ylcarbonyl)-6-aminohexanoic acid (11)

General procedure **h** from **10** (100%); white needles; mp 198-200 $^{\circ}$C; ^{1}H NMR (400.13 MHz) δ 8.06 (d, J=4Hz, 1H), 7.79 (d, J=2Hz, 1H), 7.75 (s, 1H), 7.48 (s, 1H), 7.40 (d, J=4Hz, 2H), 7.30 (t, J=4Hz, 2H), 7.23 (m, 1H), 7.16 (dd, J=4Hz, 2Hz, 1H), 7.09 (s, 1H), 6.00 (s, 2H), 5.15 (s, 2H), 3.23 (m, 2H), 2.23 (t, J = 6Hz, 2H), 1.58 (m, 4H), 1.36 (m, 2H); MS (DCI/NH$_3$) m/e: 486 (M + H)$^{+}$.

N-(2,3-Methylenedioxy-6-benzyloxy-phenanthr-9-ylmethyl)-6-aminohexanoic acid (12)

General procedure **e** from **11** (90%); white powder, recrytallized from EtOH to give white needles; mp 184-186 °C; ^{1}H NMR (400.13 MHz) δ 7.90 (d, *J*=4Hz, 1H), 7.87 (d, *J*=2Hz, 1H), 7.77 (s, 1H), 7.60 (s, 1H), 7.44 (d, *J*=4Hz, 2H), 7.34 (t, *J*=4Hz, 2H), 7.30 (dd, *J*=4Hz, 2Hz, 1H), 7.28 (m, 1H), 7.16 (s, 1H), 6.03 (s, 2H), 5.19 (s, 2H), 4.46 (s, 2H), 2.83 (m, 2H), 2.26 (t, *J* = 6Hz, 2H), 1.90 (m,2H), 1.68 (m, 2H), 1.28 (m, 2H); MS (DCI/NH$_3$) *m/e*: 472 (M + H)$^+$.

_N_-(2,3-Methylenedioxy-6-benzyloxy-phenanthr-9-ylmethyl)-5-aminohexanol (13)

General procedure **g** from **10** (95%); white powder; mp 175-177 °C; ^{1}H NMR (400.13 MHz) δ 7.90 (d, *J*=4Hz, 1H), 7.86 (d, *J*=2Hz, 1H), 7.76 (s, 1H), 7.45 (s, 1H), 7.44 (d, *J*=4Hz, 2H), 7.32 (t, *J*=4Hz, 2H), 7.26 (m, 1H), 7.24 (dd, *J*=4Hz, 2Hz, 1H), 7.14 (s, 1H), 6.03 (s, 2H), 5.22 (s, 2H), 4.24 (s, 2H), 3.53 (t, *J*=6Hz, 2H), 2.72 (t, *J*=6Hz, 2H), 1.58 (m, 2H), 1.47 (m, 2H), 1.29 (m, 4H); MS (DCI/NH$_3$) *m/e*: 458 (M + H)$^+$.

Methyl N-(2,3-methylenedioxy-6-benzyloxy-phenanthr-9-ylmethyl)-5-aminopentanoate (14)

General procedures **d** and **e** from **7a** (93%); colorless syrup; ^{1}H NMR (400.13 MHz) δ 7.97 (d, *J*=4Hz, 1H), 7.83 (d, *J*=2Hz, 1H), 7.77 (s, 1H), 7.46 (s, 1H), 7.45 (d, *J*=4Hz, 2H), 7.35 (t, *J*=4Hz, 2H), 7.27 (m, 1H), 7.20 (dd, *J*=4Hz, 2Hz, 1H),7.07 (s, 1H), 6.01 (s, 2H), 5.17 (s, 2H), 4.95 (s, 2H), 3.50(s, 3H), 3.01 (m, 2H), 2.42 (t, *J*=6Hz, 2H), 1.67 (m, 2H), 1.59 (m, 2H); MS (DCI/NH$_3$) *m/e*: 472 (M + H)$^+$.

_N_-(2,3-Methylenedioxy-6-benzyloxy-phenanthr-9-ylmethyl)-5-aminopentanoic acid (15)

General procedure **h** from **14** (93%); white powder, recrystallized from EtOH to give white needles; mp 197-199 °C; ^{1}H NMR (400.13 MHz) δ 7.89 (d, *J*=4Hz, 1H), 7.88 (d, *J*=2Hz, 1H), 7.77 (s, 1H), 7.46 (s, 1H), 7.45 (d, *J*=4Hz , 2H), 7.34 (t, *J*=4Hz, 2H), 7.29 (dd, *J*= 4Hz, 2Hz,

1H), 7.27 (m, 1H), 7.16 (s, 1H), 6.05 (s, 2H), 5.21 (s, 2H), 4.42 (s, 2H), 2.89 (m, 2H), 2.27 (t, J=6Hz, 2H), 1.89 (m, 2H), 1.68 (m, 2H); MS (DCI/NH$_3$) m/e: 458 (M + H)$^+$.

N-(2,3-Methylenedioxy-6-benzyloxy-phenanthr-9-ylcarbonyl)-L-proline (16)

General procedures **d** & **h** from **7a** (95%); white powder; mp 221-223 $^{\circ}$C; ^{1}H NMR (400.13 MHz) δ 8.00 (d, J=4Hz, 1H), 7.85 (d, J=2Hz, 1H), 7.81 (s, 1H), 7.46 (s, 1H), 7.45 (d, J=4Hz , 2H), 7.36 (t, J=4Hz, 2H), 7.30 (m, 1H), 7.23 (dd, J= 4Hz, 2Hz, 1H), 7.13 (s, 1H), 6.04 (s, 2H), 5.19 (s, 2H), 4.71 (t, J=7Hz, 1H), 3.62 (m, 2H), 2.21 (m, 2H), 1.83 (m, 2H); MS (DCI/NH$_3$) m/e: 470 (M + H)$^+$.

N-(2,3-Methylenedioxy-6-benzyloxy-phenanthr-9-ylmethyl)-L-proline methyl ester (17)

General procedures **d** & **e** from **7a** (85%); brown syrup; ^{1}H NMR (400.13 MHz) δ 7.97 (d, J=4Hz, 1H), 7.83 (d, J=2Hz, 1H), 7.80 (s, 1H), 7.71 (s, 1H), 7.59 (d, J=4Hz, 2H), 7.47 (t, J=4Hz, 2H), 7.36 (m, 1H), 7.22 (dd, J= 4Hz, 2Hz, 1H), 7.11 (s, 1H), 6.06 (s, 2H), 5.20 (s, 2H), 4.75 (s, 2H), 3.67 (s, 3H), 3.26 (d, J=17Hz, 1H), 2.45 (m, 2H), 1.96 (m, 2H), 1.68 (m, 2H); MS (DCI/NH$_3$) m/e: 470 (M + H)$^+$.

N-(2,3-Methylenedioxy-6-benzyloxy-phenanthr-9-ylmethyl)-L-proline (18)

General procedure **h** from **17** (100%); white powder; mp 147-149 $^{\circ}$C; ^{1}H NMR (400.13 MHz) δ 8.11 (d, J=4Hz, 1H), 7.84 (d, J=2Hz, 1H), 7.75 (s, 1H), 7.42 (s, 1H), 7.40 (d, J=4Hz , 2H), 7.30 (t, J=4Hz, 2H), 7.27 (m, 1H), 7.23 (dd, J= 4Hz, 2Hz, 1H), 7.14 (s, 1H), 6.01 (s, 2H), 5.16 (s, 2H), 4.30 (s, 2H), 3.24 (m, 1H), 2.48 (m, 2H), 2.0 (m, 2H), 1.68 (m, 2H); MS (DCI/NH$_3$) m/e: 456 (M + H)$^+$. Anal. (C$_{28}$H$_{25}$O$_5$N·1.0H$_2$O) C, H, N.

N-(2,3-Methylenedioxy-6-benzyloxy-phenanthr-9-ylmethyl)-L-prolinol (19)

General procedure **g** from **17** (95%); colorless oil, recrystallization from EtOH gave white powder; mp 122-124 $^{\circ}$C; ^{1}H NMR (400.13 MHz) δ 8.13 (d, J=4Hz, 1H), 7.90 (d, J=2Hz, 1H),

7.84 (s, 1H), 7.51 (d, *J*=4Hz , 2H), 7.42 (s, 1H), 7.41 (t, *J*=4Hz, 2H), 7.34 (m, 1H), 7.29 (dd,

J=4Hz, 2Hz, 1H), 7.14 (s, 1H), 6.06 (s, 2H), 5.24 (s, 2H), 4.36 (d, *J*=7Hz, 2H), 3.78 (d,

J=17Hz, 2H), 3.41 (m, 1H), 2.42 (m, 2H), 1.83 (m, 2H), 1.66 (m, 6H); MS (DCI/NH3) m/e:

442 (M + H)+.

N-(2,3-Methylenedioxy-6-benzyloxy-phenanthr-9-ylmethyl)-L-2-piperidinecarboxylic acid (20)

General procedures **d**, **e** & **h** from **7a** (83%); white powder; mp 168-170 ^{o}C; ^{1}H NMR

(400.13 MHz) δ 8.26 (d, *J*=4Hz, 1H), 7.85 (d, *J*=2Hz, 1H), 7.77 (s, 1H), 7.56 (s, 1H), 7.45 (d,

J=4Hz, 2H), 7.35 (t, *J*=4Hz, 2H), 7.30 (m, 1H), 7.26 (dd, *J*= 4Hz, 2Hz, 1H), 7.12 (s, 1H),

6.05 (s, 2H), 5.20 (s, 2H), 4.24 (s, 2H), 3.16 (m, 1H), 2.26 (m, 2H), 1.80 (m, 2H), 1.64 (m,

4H); MS (DCI/NH$_3$) *m*/*e*: 470 (M + H)$^{+}$.

N-(2,3-Methylenedioxy-6-benzyloxy-phenanthr-9-ylmethyl)-L-piperidinemethanol (21)

General procedure **g** from **20** (95%); light brown oil, recrystallization from EtOH to gave

white powder; mp 151-152 ^{o}C ; ^{1}H NMR (400.13 MHz) δ 8.17 (d, *J*=4Hz, 1H), 7.89 (d,

J=2Hz, 1H), 7.83 (s, 1H), 7.51 (d, *J*=4Hz, 2H), 7.43 (s, 1H), 7.40 (t, *J*=4Hz, 2H), 7.34 (m,

1H), 7.27 (dd, *J*=4Hz, 2Hz, 1H), 7.14 (s, 1H), 6.06 (s, 2H), 5.23 (s, 2H), 4.45 (d, *J*=7Hz, 2H),

3.46 (d, *J*=17Hz, 2H), 2.85 (m, 1H), 2.37 (m, 2H), 1.69 (m, 6H); MS (DCI/NH$_3$) *m*/*e*: 456 (M

+ H)$^{+}$.

N-(2,3-Methylenedioxy-6-hydroxy-phenanthr-9-ylcarbonyl)-L-proline (22)

General procedure **f** from **16** (92%); white powder; mp 230-231 ^{o}C; ^{1}H NMR (400.13 MHz)

δ 7.73 (d, *J*=4Hz, 1H), 7.67 (s, 1H), 7.50 (d, *J*=2Hz, 1H), 7.35 (s, 1H), 7.21 (dd, *J*=4Hz, 2Hz,

1H), 7.06 (m, 1H), 6.01 (s, 2H), 4.67 (t, *J*=7Hz, 1H), 3.22 (m, 2H), 2.38 (m, 2H), 2.18 (m,

2H), 1.86 (m, 2H); MS (DCI/NH$_3$) *m*/*e*: 380 (M + H)$^{+}$.

N-(2,3-Methylenedioxy-6-hydroxy-phenanthr-9-ylmethyl)-L-proline (23)

General procedure **f** from **18** (95%); white powder; mp 205-206 $^{\circ}$C; ^{1}H NMR (400.13 MHz) δ 8.07 (d, *J*=4Hz, 1H), 7.82 (s, 1H), 7.80 (d, *J*=2Hz, 1H), 7.42 (s, 1H), 7.21 (dd, *J*=4Hz, 2Hz, 1H), 7.10 (s, 1H), 6.04 (s, 2H), 4.09 (s, 2H), 3.16 (m, 1H), 2.38 (m, 2H), 2.23 (m, 2H), 1.95 (m, 2H); MS (DCI/NH$_3$) *m/e*: 366 (M + H)$^+$.

N-(2,3-Methylenedioxy-6-hydroxy-phenanthr-9-ylmethyl)-L-2-piperidinecarboxylic acid (24)

General procedure **f** from **20** (95%); white powder; mp 211-213 $^{\circ}$C; ^{1}H NMR (400.13 MHz) δ 8.07 (d, *J*=4Hz, 1H), 7.80 (s, 1H), 7.76 (d, *J*=2Hz, 1H), 7.50 (s, 1H), 7.22 (dd, *J*= 4Hz, 2Hz, 1H), 7.12 (s, 1H), 6.05 (s, 2H), 4.06 (s, 2H), 3.12 (m, 1H), 2.38 (m, 2H), 1.88 (m, 2H), 1.64 (m, 4H); MS (DCI/NH$_3$) *m/e*: 380 (M + H)$^+$.

N-(2,3-Methylenedioxy-6-methoxy-phenanthr-9-ylcarbonyl)-5-aminopentanoic acid (25)

General procedures **d & h** from **7b** (100%); white powder; mp 137-138 $^{\circ}$C; ^{1}H NMR (400.13 MHz) δ 7.92 (d, *J*= 4Hz, 1H), 7.82 (s, 1H), 7.75 (s, 1H), 7.71 (d, *J*=2Hz, 1H), 7.13 (dd, *J*=4Hz, 2Hz, 1H), 7.09 (s, 1H), 6.00 (s, 2H), 3.89 (s, 3H), 3.23 (m, 2H), 2.23 (t, *J*=6Hz, 2H), 1.58 (m, 4H); MS (DCI/NH$_3$) *m/e*: 412 (M + H)$^+$.

Methyl N-(2,3-Methylenedioxy-6-methoxy-phenanthr-9-ylmethyl)-5-aminopentanoate (26)

General procedures **d & e** from **7b** (90%); colorless syrup; ^{1}H NMR (400.13 MHz) δ 8.10 (d, *J*= 4Hz, 1H), 7.82 (s, 1H), 7.70 (d, *J*=2Hz, 1H), 7.52 (s, 1H), 7.12 (dd, *J*= 4Hz, 2Hz, 1H), 7.08 (s, 1H), 6.04 (s, 2H), 3.89 (s, 3H), 3.80 (s, 2H), 3.56 (s, 3H), 2.80 (m, 2H), 2.33 (t, *J*=6Hz, 2H), 1.64 (m, 4H); MS (DCI/NH$_3$) *m/e*: 396 (M + H)$^+$.

N-(2,3-Methylenedioxy-6-methoxy-phenanthr-9-ylmethyl)-5-aminopentanoic acid (27)

General procedure **h** from **26** (99%); white powder; mp 145-146 °C; ^{1}H NMR (400.13 MHz) δ 8.06 (d, *J*=4Hz, 1H), 7.79 (s, 1H), 7.75 (d, *J*=2Hz, 1H), 7.48 (s, 1H), 7.22 (dd, *J*=4Hz, 2Hz, 1H), 7.10 (s, 1H), 6.03 (s, 2H), 4.02 (s, 2H), 3.82 (s, 3H), 2.75 (m, 2H), 2.23 (t, *J*=6Hz, 2H), 1.53 (m, 2H), 1.44 (m, 2H); MS (DCI/NH3) m/e: 382 (M + H)$^+$.

N-(2,3-Methylenedioxy-6-methoxy-phenanthr-9-ylmethyl)-5-aminopentanol (28)

General procedure **g** from **27** (97%); colorless oil, recrystallization from EtOH gave white powder; mp 125-126°C; ^{1}H NMR (400.13 MHz) δ 8.00 (d, *J*=4Hz, 1H), 7.76 (s, 1H), 7.72 (d, *J*=2Hz, 1H), 7.44 (s, 1H), 7.13 (dd, *J*= 4Hz, 2Hz, 1H), 7.05 (s, 1H), 6.04 (s, 2H), 3.95 (s, 2H), 3.93 (s, 3H), 3.58 (t, *J*=6Hz, 2H), 2.75 (m, 2H), 1.55 (m, 2H), 1.44 (m, 2H), 1.30 (m, 2H); MS (DCI/NH$_3$) *m*/*e*: 368(M + H)$^+$.

N-(2,3-Methylenedioxy-6-methoxy-phenanthr-9-ylcarbonyl)-L-proline (29)

General procedures **d & h** from **7b** (93%); white powder; mp 207-208 °C; ^{1}H NMR (400.13 MHz) δ 7.78(d, *J*= 4Hz, 1H), 7.70 (s, 1H), 7.54 (d, *J*=2Hz, 1H), 7.35 (s, 1H), 7.20 (dd, *J*=4Hz, 2Hz, 1H), 7.14 (m, 1H), 6.01 (s, 2H), 4.67 (m, 1H), 3.90 (s, 3H), 3.22 (m, 2H), 2.38 (m, 2H), 1.86 (m, 2H); MS (DCI/NH$_3$) *m*/*e*: 394 (M + H)$^+$.

N-(2,3-Methylenedioxy-6-methoxy-phenanthr-9-ylmethyl)-L-proline methyl ester (30)

General procedures **d & e** from **7a** (85%); white syrup; ^{1}H NMR (400.13 MHz) δ 8.20(d, *J*=4Hz, 1H), 7.80(s, 1H), 7.70 (d, *J*=2Hz, 1H), 7.52 (s, 1H), 7.21 (dd, *J*=4Hz, 2Hz, 1H), 7.13 (s, 1H), 6.05 (s, 2H), 4.02 (s, 2H), 3.89 (s, 3H), 3.67 (s, 3H), 3.14 (m, 1H), 2.32 (m, 2H), 2.14 (m, 2H), 1.86 (m, 2H); MS (DCI/NH$_3$) *m*/*e*: 394 (M + H)$^+$.

N-(2,3-Methylenedioxy-6-methoxy-phenanthr-9-ylmethyl)-L-proline (31)

General procedure **h** from **30** (100%); white powder; mp 145-146 °C; ^{1}H NMR (400.13 MHz) δ 8.21 (d, *J*=4Hz, 1H), 7.77 (s, 1H), 7.72 (d, *J*=2Hz, 1H), 7.56 (s, 1H), 7.23 (dd,

J=4Hz, 2Hz, 1H), 7.10 (s, 1H), 6.04 (s, 2H), 4.05 (s, 2H), 3.96 (s, 3H), 3.16 (m, 1H), 2.36 (m, 2H), 2.14 (m, 2H), 1.81 (m, 2H); MS (DCI/NH$_3$) *m/e*: 380 (M + H)$^+$.

N-(2,3-Methylenedioxy-6-methoxy-phenanthr-9-ylmethyl)-L-prolinol (32)

General procedure **g** from **31** (95%); white powder; mp 138-139 ^{o}C; ^{1}H NMR (400.13 MHz) δ 8.16 (d, *J*=4Hz, 1H), 7.88(s, 1H), 7.80 (d, *J*=2Hz, 1H), 7.46 (s, 1H), 7.23 (dd, *J*=4Hz, 2Hz, 1H), 7.14 (s, 1H), 6.07 (s, 2H), 4.03 (s, 2H), 3.94 (s, 3H), 3.70 (d, *J*=17Hz, 2H), 3.16 (m, 1H), 2.38 (m, 2H), 2.23 (m, 2H), 1.95 (m, 2H); MS (DCI/NH$_3$) *m/e*: 366 (M + H)$^+$.

N-(2,3-Methylenedioxy-6-methoxy-phenanthr-9-ylmethyl)-L-2-piperidinecarboxylic acid (33)

General procedures **d**, **e** & **h** from **7b** (80%); white powder; mp 171-172 ^{o}C; ^{1}H NMR (400.13 MHz) δ 8.21 (d, *J*=4Hz, 1H), 7.77 (s, 1H), 7.72 (d, *J*=2Hz, 1H), 7.56 (s, 1H), 7.23 (dd, *J*=4Hz, 2Hz, 1H), 7.10 (s, 1H), 6.04 (s, 2H), 4.08 (s, 2H), 3.96 (s, 3H), 3.08 (m, 1H), 2.38 (m, 2H), 1.84 (m, 2H), 1.60 (m, 4H); MS (DCI/NH$_3$) *m/e*: 394 (M + H)$^+$. Anal. (C$_{23}$H$_{23}$O$_5$N·2.0H$_2$O) C, H, N

N-(2,3-Methylenedioxy-6-methoxy-phenanthr-9-ylmethyl)-L-2-piperidinemethanol (34)

General procedure **g** from **33** (98%); white powder; mp 155-157 ^{o}C; ^{1}H NMR (400.13 MHz) δ 8.16 (d, *J* = 4Hz, 1H), 7.88 (s, 1H), 7.80 (d, *J*=2Hz, 1H), 7.47 (s, 1H), 7.22 (dd, *J*=4Hz, 2Hz, 1H), 7.15 (s, 1H), 6.07 (s, 2H), 4.06 (s, 2H), 3.98 (s, 3H), 3.68 (d, *J*=7Hz, 2H), 2.87 (m, 1H), 2.40 (m, 2H), 1.64 (m, 6H); MS (DCI/NH$_3$) *m/e*: 380 (M + H)$^+$.

N-(2,3,6-Trimethoxyphenanthr-9-ylmethyl)-6-aminohexanoic acid (35)

General procedures **d**, **e** & **h** from **7b** (77%); brown powder; mp 133-134 ^{o}C; ^{1}H NMR (400.13 MHz) δ 7.90 (d, *J*=4Hz, 1H), 7.78 (s, 1H), 7.72 (d, *J*=2Hz, 1H), 7.52 (s, 1H), 7.20

(dd, *J*=4Hz, 2Hz, 1H), 7.08 (s, 1H), 3.92 (s, 9H), 3.71 (s, 2H), 2.87 (m, 2H), 2.23 (m, 2H), 1.55 (m, 2H), 1.46 (m, 2H), 1.28 (m, 2H); MS (DCI/NH₃) *m/e*: 412 (M + H)⁺.

N-(2,3,6-Trimethoxyphenanthr-9-ylmethyl)-5-aminohexanol (36)

General procedure **g** from **35** (92%); yellow oil; ¹H NMR (400.13 MHz) δ 7.88 (d, *J*=4Hz, 1H), 7.76 (s, 1H), 7.71 (d, *J*=2Hz, 1H), 7.44 (s, 1H), 7.13 (dd, *J*=4Hz, 2Hz, 1H), 7.05 (s, 1H), 5.99 (s, 2H), 3.94 (s, 9H), 3.80 (s, 2H), 3.73 (t, *J*=6Hz, 2H), 2.75 (m, 2H), 1.50 (m, 4H), 1.28 (m, 4H); MS (DCI/NH₃) *m/e*: 398 (M + H)⁺.

N-(2,3,6-Trimethoxyphenanthr-9-ylmethyl)-L-2-piperidinecarboxylic acid (37)

General procedures **d**, **e** & **h** from **7c** (75%); light yellow powder; mp 187-188 °C; ¹H NMR (400.13 MHz) δ 8.21 (d, *J*=4Hz, 1H), 7.78 (s, 1H), 7.71 (d, *J*=2Hz, 1H), 7.56 (s, 1H), 7.23 (dd, *J*=4Hz, 2Hz, 1H), 7.10 (s, 1H), 4.10 (s, 2H), 3.98 (s, 9H), 3.12 (m, 1H), 2.42 (m, 2H), 1.80 (m, 2H), 1.60 (m, 4H); MS (DCI/NH₃) *m/e*: 410 (M + H)⁺.

N-(2,3,6-Trimethoxyphenanthr-9-ylmethyl)-L-2-piperidinemethanol (38)

General procedure **g** from **37** (95%); brown oil, recrystallization from EtOH gave yellow powder; mp135-137 °C; ¹H NMR (400.13 MHz) δ 8.21 (d, *J*=4Hz, 1H), 7.78 (s, 1H), 7.72 (d, *J*=2Hz, 1H), 7.50 (s, 1H), 7.20 (dd, *J*=4Hz, 2Hz, 1H), 7.14 (s, 1H), 6.07 (s, 2H), 4.10 (s, 2H), 3.96 (s, 9H), 3.74 (d, *J*=17Hz, 2H), 2.87 (m, 1H), 2.41 (m, 2H), 1.66 (m, 6H); MS (DCI/NH₃) *m/e*: 396 (M + H)⁺.

1-[3-(4,5-Dimethoxy-2-nitrophenyl)-2-(4-methoxyphenyl)-acryloyl]-pyrrolidine-2-carboxylic acid (39)

General procedures **d** & **h** from **5b** (90%); brown powder; mp 120-122 °C; ¹H NMR (400.13 MHz) δ7.67 (s, 1H), 7.26(d, *J*=4Hz, 2H), 7.08 (s, 1H), 6.73 (d, *J*=4Hz, 2H), 6.44 (s, 1H),

4.63 (t, J=7Hz, 1H), 3.92 (s, 6H), 3.73 (s, 3H), 3.41(t, J=7Hz, 2H), 2.22 (m, 2H), 1.92 (m, 2H); MS (DCI/NH$_3$) m/e: 443 (M + H)$^+$.

1-[3-(4,5-Dimethoxy-2-nitrophenyl)-2-(4-methoxyphenyl)-allyl]-pyrrolidine-2-carboxylic acid (40)

General procedure **e** from **39** (90%); brown syrup; ^{1}H NMR (400.13 MHz) δ 7.61 (s, 1H), 7.24 (d, J=4Hz, 2H), 7.01(s, 1H), 6.77 (d, J=4Hz, 2H), 6.64 (s, 1H), 4.36 (d, J=7Hz, 2H), 3.89 (s, 3H), 3.72 (t, J=7Hz, 1H), 3.69 (s, 3H), 3.42 (s, 3H), 3.24 (m, 2H), 2.18 (m, 2H), 1.84 (m, 2H); MS (DCI/NH$_3$) m/e: 429 (M + H)$^+$.

{1-[3-(4,5-Dimethoxy-2-nitrophenyl)-2-(4-methoxyphenyl)-allyl]-pyrrolidin-2-yl}-methanol (41)

General procedure **g** from **40** (90%); dark oil; ^{1}H NMR (400.13 MHz) δ 7.59 (s, 1H), 7.23 (d, J=4Hz, 2H), 7.00 (s, 1H), 6.71 (d, J=4Hz, 2H), 6.23 (s, 1H), 4.17 (d, J=7Hz, 2H), 3.89 (s, 3H), 3.78 (d, J=7Hz, 2H), 3.69 (s, 3H), 3.58 (m, 1H), 3.41 (s, 3H), 3.16 (m, 2H), 1.91 (m, 2H), 1.80 (m, 2H); MS (DCI/NH$_3$) m/e: 415 (M + H)$^+$.

{1-[3-(3,4-Dimethoxyphenyl)-2-(4-methoxyphenyl)allyl]-pyrrolidin-2-yl}-methanol (42)

Silmilar procedure as **40** (77% for two steps); yellow syrup; ^{1}H NMR (400.13 MHz) δ 7.11 (d, J=5Hz, 2H), 6.89 (d, J=5Hz, 2H), 6.63 (s, 1H), 6.58 (d, J=3Hz, 2H), 6.39 (s, 1H), 4.06 (d, J=7Hz, 2H), 3.90 (d, J=6Hz, 2H), 3.71 (s, 3H), 3.69 (s, 3H), 3.65 (m, 1H), 3.39 (s, 3H), 3.27 (m, 2H), 1.84 (m, 2H), 1.70 (m, 2H); MS (DCI/NH$_3$) m/e: 370 (M + H)$^+$.
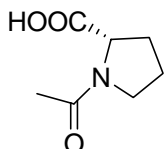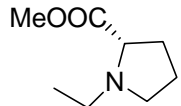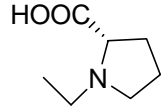
3.6.4 Cell Growth Inhibition Assay
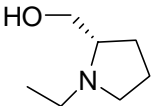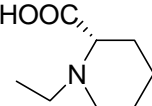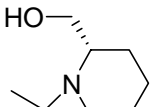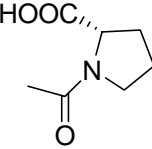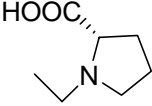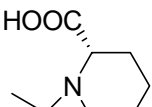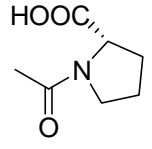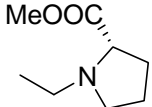
The human A549 lung cancer cell line was used for the cytotoxicity screening of PBT derivatives using the cell-based sulforhodamine B (SRB) microtitre plate assay.[8] Compound stock solutions were prepared in DMSO with the final solvent concentration ≤2% DMSO
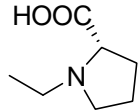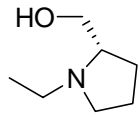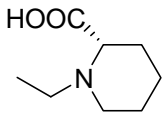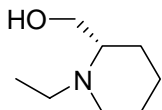
(v/v), a concentration without effect on cell replication. The cells were cultured at 37 $^{\circ}$C in RPMI-1640 supplemented with 25 mM N-2-hydroxyethylpiperazine-N'-2-ethanesulfonic acid (HEPES), 2% (w/v) sodium bicarbonate, 10% (v/v) fetal bovine serum, and 100 µg/mL kanamycin in a humidified atmosphere containing 5% CO_2. Duration of compound exposure was 3 days. The ED_{50} value (the concentration that reduced the cell number by 50%) was interpolated from dose-response data. Each test was performed in triplicate with variation less than 5%. The EC_{50} values determined in each independent test varied less than 10%.

Table 3-1. Cytotoxicity of 2,3-Methylenedioxy-6-alkyloxy-9-substituted PBT Analogs
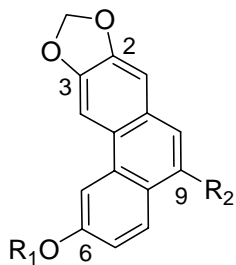
Compound	R_1	R_2	EC_{50} $(\mu M)^{a,b}$
7a	$-CH_2C_6H_5$	$-COOH$	NA
7b	$-CH_3$	$-COOH$	NA
10	$-CH_2C_6H_5$	$-CONH(CH_2)_5COOMe$	41.2
11	$-CH_2C_6H_5$	$-CONH(CH_2)_5COOH$	41.2
12	$-CH_2C_6H_5$	$-CH_2NH(CH_2)_5COOH$	1.6
13	$-CH_2C_6H_5$	$-CH_2NH(CH_2)_5CH_2OH$	1.1
14	$-CH_2C_6H_5$	$-CH_2NH(CH_2)_4COOMe$	17.0
15	$-CH_2C_6H_5$	$-CH_2NH(CH_2)_4COOH$	2.2
16	$-CH_2C_6H_5$		42.6
17	$-CH_2C_6H_5$		32.1
18	$-CH_2C_6H_5$		4.4

19	-CH$_2$C$_6$H$_5$		1.8
20	-CH$_2$C$_6$H$_5$		3.2
21	-CH$_2$C$_6$H$_5$		1.3
22	-H		39.7
23	-H		41.2
24	-H		39.7
25	CH$_3$	-CONH(CH$_2$)$_4$COOH	73.3
26	CH$_3$	-CH$_2$NH(CH$_2$)$_4$COOMe	25.3
27	CH$_3$	-CH$_2$NH(CH$_2$)$_4$COOH	1.3
28	CH$_3$	-CH$_2$NH(CH$_2$)$_4$CH$_2$OH	0.27
29	CH$_3$		5.3
30	CH$_3$		73.8

31	CH$_3$		2.1
32	CH$_3$		0.7
33	CH$_3$		0.5
34	CH$_3$		0.16

[a]Etoposide (VP-16) used as positive control, EC$_{50}$ = 1.4 µM. [b]NA = Not Active
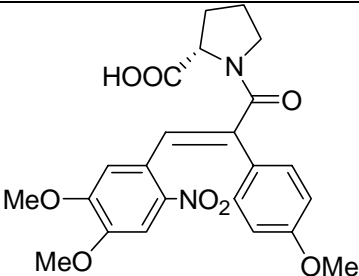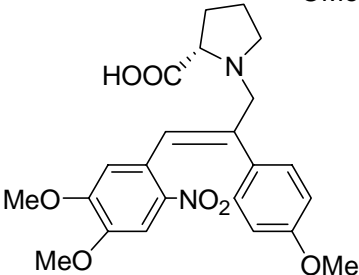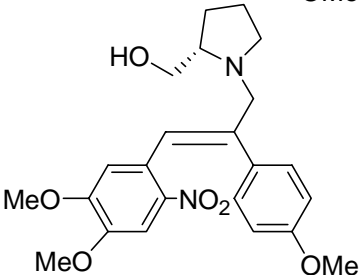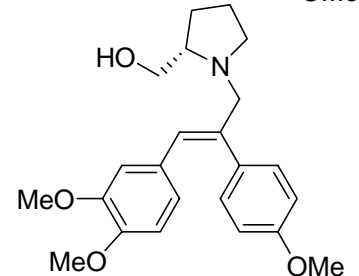
Table 3-2. Cytotoxicity of 2,3,6-Trimethyoxy-9-substituted PBT Analogs
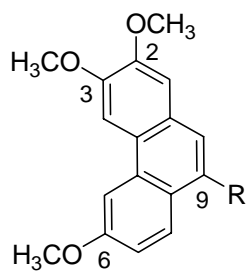
Compound	R	EC_{50} (μM)
7c	-COOH	NA
35	-CH$_2$NH(CH$_2$)$_5$COOH	9.7
36	-CH$_2$NH(CH$_2$)$_5$CH$_2$OH	2.7
37		9.7
38		6.3

[a]Etoposide (VP-16) used as positive control, EC_{50} = 1.4 μM. [b]NA = Not Active

Table 3-3. Cytotoxicity of seco-PBT Analogs

Compound	Structure	EC$_{50}$ (μM)
39		80
40		45.2
41		11.7
42		52.2

Etoposide (VP-16) used as positive control, EC$_{50}$ = 1.4 μM

3.7 REFERENCES

1) Ciufolini, M. A.; Roschangar, F. A unified strategy for the synthesis of phenanthroizidine alkaloids: preparation of sterically congested pyridines. *J. Am. Chem. Soc.* **1996***, 118*, 12082-12089.

2) Lebrun, S.; Couture, A.; Deniau, E.; Grandclaudon, P. Total synthesis of (±)-cryptopleurine, (±)-antofine and (±)-deoxypergularinine. *Tetrahedron* **1999***, 55*, 2659-2670.

3) Kim, S.; Lee, J.; Lee, T.; Park, H.; Kim, D. First asymmetric total synthesis of (-)-antofine by using an enantioselective catalytic phase transfer alkylation. *Org. Lett.* **2003***, 5*, 2703-2706.

4) Kim, S.; Lee, T.; Lee, E.; Lee, J.; Fan, G. J.; Lee, S. K.; Kim, D. Asymmetric total syntheses of (-)-antofine and (-)-cryptopleurine using (R)-(E)-4-(tributylstannyl)but-3-en-2-ol. *J. Org. Chem.* **2004***, 69*, 3144-3149.

5) Wassmundt, F. W.; Kiesman, W. F.; Soluble catalysts for improved Pschorr cyclizations. *J Org. Chem*. **1995***, 60*, 196-201

6) Suffness, M.; Cordell, G. A. In *The Alkaloids, Chemistry and Pharmacology*, Brossi, A., Ed.; Academic Press: New York, 1985; Vol. 25, pp 3-355.

7) Stark, D.; Lykkeberg, A. K.; Christensen, J.; Budnik, B. A.; Abe, F.; Jaroszewski, J. W. In vitro cytotoxic activity of phenanthroindolizidine alkaloids from *Cynanchum vincetoxicum* and *Tylophora tanakae* against drug-sensitive and multidrug-resistant cancer cells. *J. Nat. Prod.* **2002**, *65*, 1299-1302.

8) Rubinstein, L. V.; Shoemaker, R. H.; Paull, K. D.; Simon, R. M.; Tosini, S.; Skehan, P.; Scudiero, D. A.; Monks, M. R. Comparison of in vitro anticancer-drug-screening data generated with a tetrazolium assay versus a protein assay against a diverse panel of human tumor cell lines. *J. Natl. Cancer Inst*. **1990**, *82*, 1113-1118.

CHAPTER IV. DESIGN, SYNTHESIS AND CYTOTOXIC EVALUATION OF 9-SUBSTITUTED PHENANTHRENE-BASED TYLOPHORINE DERIVATIVES (PBTS) (PART II)

4.1 INTRODUCTION

Chapter III reported the design, synthesis and cytotoxicity evaluation of a series of novel polar water-soluble phenanthrene-based tylophorine derivatives (PBTs) with $EC_{50} \cong 10^{-7}$ M against the A549 human lung cancer cell line. These compounds could possibly have lower or no CNS toxicity because the increased polarity should prevent them from penetrating the blood-brain barrier. Preliminary structure-activity relationship (SAR) studies revealed that 2,3-methylenedioxy-6-methoxyphenanthrene was an optimized core structural unit that incorporated all of the favorable modifications identified at the C-2, C-3 and C-6 positions. A *N*-containing substituent at the C-9 position is also required for cytotoxic activity, and this site presents an ideal position for introducing more polar, water-solubility-enhancing moieties, such as a terminal hydroxyl or carboxylic acid. These critical SAR clues prompted us to explore additional C-9 substituents to better understand the SAR of the PBT compound class. Most importantly, we wanted to extend the in vitro anticancer spectra to include additional significant tumor types as well as investigate whether target PBTs exhibit cross-resistance in a multi-drug resistant cancer cell subline.

In this Chapter, we describe new developments toward the design and synthesis of novel C-9 substituted PBTs. Several *N*-containing cyclic and acyclic terminal-hydoxyl moieties

were introduced at the C9 position in order to explore and optimize the activity profiles of novel C-9 substituted PBTs. All compounds were evaluated as in vitro anticancer agents against the human A549 lung cancer cell line. Several C9-substituted PBTs showed superior cytotoxic activity profiles with EC_{50} values in the sub-micromolar range, indicating that rational C-9 modification was an effective approach to optimize the activity profile of this compound class. The active compounds were further examined against DU-145 (prostate), ZR-751 (breast), KB (nasopharyngeal), and KB-Vin (multi-drug resistant KB subline) human cancer cell lines. Finally, the SAR is discussed relative to the current issues of chemotherapy-induced toxicity and resistance.

4.2 DESIGN AND SYNTHESIS
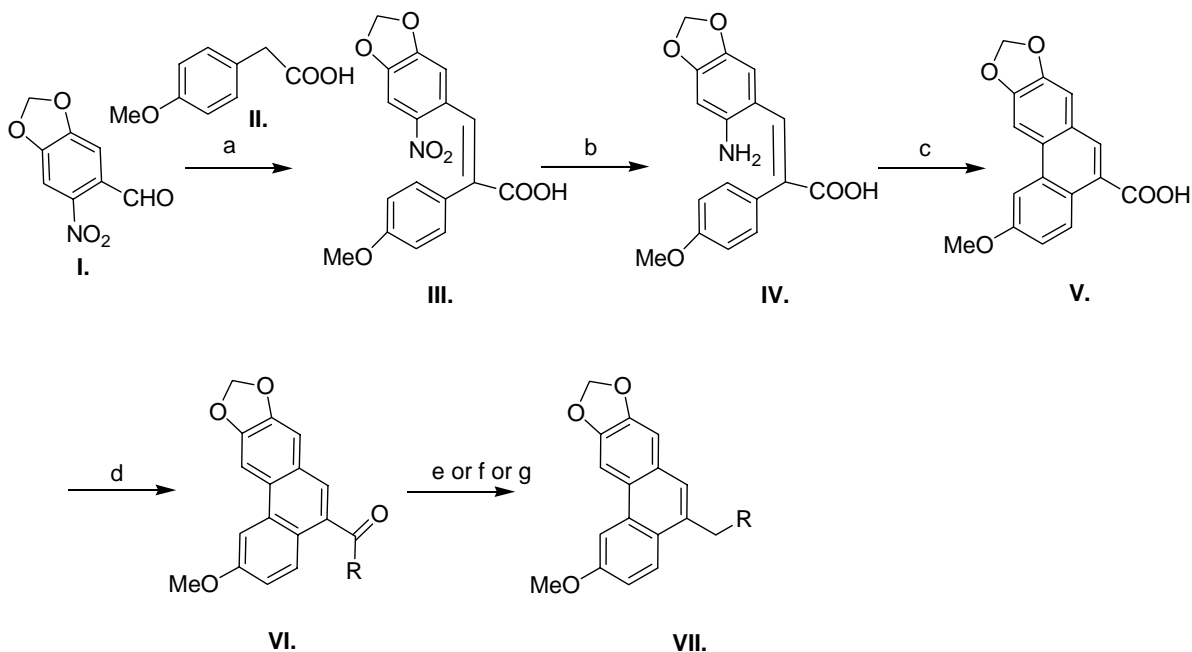
Reagents and conditions: a: Ac_2O/Et_3N b: $FeSO_4/NH_4OH$ c: $NaNO_2$/Fluoroboric acid; Ferrocene/acetone d; EDC,DMAP,HOBt/DMF e: BMS/THF f: NaOH/MeOH (1:1) g: $LiAlH_4$/THF

Scheme 4-1. Synthesis of 6-methoxy-9-substituted PBTs.

4.3 CHEMISTRY

Compounds **43-56** were synthesized from commercially available 3,4-methylenedioxy-6-nitrobenzaldehyde and 4-methoxyphenylacetic acid according to the methods we described in Chapter III (compounds **57** and **58** were synthesized using similar procedures). Briefly, 2,3-methylenedioxy-6-methoxy-phenanthrene-9-carboxylic acid (**V**) was obtained through a Perkin reaction and an improved free-radical Pschorr cyclization (Scheme 4-1)[1-2] in a satisfactory overall yield of 78%. Compound **V** was then condensed with the appropriate amines in the presence of *N*-(3-dimethylaminopropyl)-*N'*-ethylcarbodiimide hydrochloride (EDC), 4-(dimethylamino) pyridine (DMAP) and 1-hydroxybenzotriazole (HOBT) (Scheme 4-1). The carbonyl bond of the amide was reduced with borane-methyl sulfide complex (BMS) to give the methylene amines and then the target carboxylic acid and hydroxymethyl analogs were produced by basic hydrolysis and lithium aluminum hydride (LiAlH$_4$) reduction, respectively.

4.4 RESULTS AND DISCUSSION

The new target compounds (**43-58**), together with **20**, **21**, **27**, **28**, **31-34** from the previous chapter, were first evaluated for in vitro anticancer activity against the human A549 lung cancer cell line using the cell-based sulforhodamine B (SRB) microtitre plate assay.[3] Compound structures and cytotoxic activity data are shown in Tables 4-1 and -2. Twelve active compounds were further evaluated against three additional cancer cell lines (KB, DU145 and ZR-751) and one resistant subline (KB-Vin) (Table 4-3). Antofine, emetine, doxorubicin and etoposide (VP-16) were used as reference compounds.

4.4.1 Structure-Activity Relationship (SAR) Studies

Interestingly, changing the stereochemistry of the 2'-substituent on the pyrrole ring altered the potency. Compounds **31** and **32** were more potent that their stereoisomers **43** and **44**. These findings are consistent with those from earlier studies of tylophorine alkaloids that showed equal or higher cytotoxicity of the 13a*S* series as compared with the 13a*R* series,[4] suggesting a well-defined regioselective interaction of these compounds with the putative biological target.

For target compounds with varied acyclic N-containing side chains, the distance between the nitrogen and terminal substituent affected the potency. The aminoundecanoic acid analog was significantly less active than the corresponding aminopentanoic acid, which in turn was slightly less active than the aminohexanoic acid (**49** < **27** < **45**). A similar rank order of potency was found when the terminal carboxylic acid was reduced to a hydroxymethyl group (**50** < **28** < **46**). The shorter spacing was definitely preferable to the longer spacing.

Based on the significant biological activity of the acylic amines, the position of the piperidine substituent was changed from 2' (ortho) to 4' (para), which resulted in increased potency (**33** vs **47**; **34** vs **48**), demonstrating that a terminal hydroxyl/carboxylic acid in a para position could favorably affect the activity. This conclusion was confirmed for compounds where the C-6 methoxy group was replaced with a benzyloxy ether (Table 4-2; **57** > **20** and **58** > **21**).

To investigate the relationship between activity and nitrogen content in the C-9 side chain, both piperidine (one nitrogen) and piperazine (two nitrogens) analogs were prepared and tested. Although the second nitrogen was tolerated, its presence slightly decreased

activity [compare the EC_{50} values between the piperazine-ethanol (**54**) and piperidine-ethanol (**56**) analogs].

Additional SAR observations relative to the C-9 N-containing side chain were also noted in the course of our study. 4'-Hydroxymethyl and 4'hydroxyethylpiperidine analogs (**48** and **56**, respectively) were both quite potent, but the former was more active than the latter. While the piperazine-ethanol analog (**54**) was quite active, the piperazine-ethoxyethanol analog (**55**) lost all activity. In contrast, potency was increased when the hydroxylethyl of **54** was replaced with a phenol in **53**. These results corroborate the conclusion that an appropriate side chain length is important for maximal activity.

Since compound **53** was quite potent, while both ortho- and para-chlorophenyl substituted piperazine analogs (**51**, **52**) were inactive, the presence of a hydrogen bond acceptor/donor group at C-9 chain terminus appears essential for cytotoxic activity. It could be that a hydrogen bonding interaction between the terminal group and a biological target plays an important role in binding the hypothetical target, and the spacing between this group and the remainder of the molecule needs to be well optimized.

4.4.2 Drug-Resistance Study

Twelve active compounds [including four hydrochloride salts (**34-HCl**, **46-HCl**, **48-HCl**, **56-HCl**) of corresponding active free bases (**34**, **46**, **48**, **56**)] were further screened against an extended panel of human tumor cell lines including DU-145 (prostate), ZR-751 (breast), KB (nasopharyngeal), and KB-VIN (multidug-resistant KB subline) in order to explore their antitumor spectra and drug-resistance profiles. Four compounds were used as reference compounds. Antofine is a positional isomer of tylophorine isolated from *Asclepiadaceae* by Dr. T. S. Wu[5] in Taiwan. Emetine is a protein synthesis inhibitor, which exhibits cross-

resistance with tylocrebine in mutant CHO cells.[3] Doxorubicin (adriamycin), vincristine, and etoposide (VP-16, Vepesid®) are widely used anticancer agents for treating a range of solid tumors. The results are illustrated in Table 4-3. In general, all new compounds exhibited potent activity against KB (EC_{50}: 0.07-0.50 μM), DU-145 (EC_{50}: 0.03-0.67 μM), and ZR-751 (EC_{50}: 0.02-0.54 μM) cell lines, as well as KB-Vin (EC_{50}: 0.09-0.38 μM) cells. The corresponding salts showed similar selectivity pattern and slightly better potency than the free bases, possibly due to improved water solubility. Compared to the reference compounds emetine, doxorubicin, etoposide and vincristine, neither the C-9 substituted PBTs nor antofine showed any cross-resistance with the KB-Vin resistant cell line, suggesting that their mode may be distinctly different from that of other cancer chemotherapeutic compounds. All PBTs exhibited cytotoxic activity in the sub-micromolar range against the limited set of representative human cancer cell lines. Compound **46-HCl** was most active against DU-145 (prostate) and ZR-751 (breast) cancer cell lines, and compound **48-HCl** exhibited a fairly uniform and potent cytotoxic activity with ED_{50} values less than 100 nM against the tumor cell line panel. Compound **56** and its HCl salt (**56-HCl**) were most active against ZR-751 breast cancer cell replication, suggesting that further exploration of this compound as a selective breast cancer drug lead will be worthwhile.

In summary, a series of novel 9-substituted 2, 3-methylenedioxy-6-methoxy-PBTs were synthesized and exhibited potent cytotoxic activity against a limited but diverse panel of human tumor cell lines, including a multidrug-resistant variant. The EC_{50} values were in the sub-micromolar range, comparable with the activity of the two front-line antineoplastic drugs used as positive controls, and the new compounds had a superior drug-resistance profile. Combination of a 2, 3-methylenedioxy-6-methoxyphenanthrene skeleton with a C-9 cyclic

piperidine ring and para terminal hydroxyl side chain generated the most potent PBTs. N-(2,3-Methylenedioxy-6-methoxy-phenanthr-9-ylmethyl)-L-4-piperidinemethanol (**48**) exhibited a fairly uniform and potent cytotoxic activity with EC_{50} values less than 100 nM against the cell line panel. The activity was maintained and the water solubility increased by formation of the hydrochloride salt. These PBT salts are the first reported water soluble tylophorine derivatives with significant cytotoxic activity, in particular to multidrug-resistant cells. They represent well-qualified and promising clinical trial candidates for cancer (especially refractory cancer) treatment.

4.5 CONCLUSIONS

More than 70 PBTs were designed and synthesized. All compounds were screened against human cancer cell lines. The most active compounds which incorporated all of the favorable modifications identified to date possess novel structures and showed remarkable EC_{50} values in the sub-micromolar range, and displayed notable selectivity. These derivatives are the first reported water soluble tylophorine derivatives with remarkable cytotoxic activity, in particular to multidrug-resistant cells. They represent well-qualified and promising clinical trial candidates for cancer (especially refractory cancer) treatment.

4.6 EXPERIMENTAL SECTION

4.6.1 Instruments and Chemicals

Melting points were measured using Fisher Johns melting apparatus without correction. The proton nuclear magnetic resonance (^{1}H NMR) spectra were measured on a 300 MHz Varian Gemini 2000 spectrometer using TMS as internal standard. Mass spectra were recorded on a PE-Sciex API-3000 LC/MS/MS instrument equipped with a Turbo IonsSpray

ion source. The solvent used was CDCl₃ unless indicated. Elemental analyses were performed by Atlantic Microlab, Inc., Norcross, GA. All active target compounds were analyzed for C, H, N and gave values within $\pm 0.4\%$ of the theoretical values. The purity of inactive target compounds was verified by HPLC using three different solvent systems. Thin-layer chromatography (TLC) was performed on PLC silica gel 60 F_{254} plates (0.5 mm, Merck). Biotage Flash+ and Isco Companion systems were used as medium-pressure column chromatography. Silica gel (200-400 mesh) from Aldrich, Inc., was used for column chromatography. 4-benzyloxyphenylacetic acid and 3,4-Methylenedioxy-6-nitrobenzaldehyde were purchased from TCI. Isonipecotic acid and L-pipecolinic acid were commercially available from Lancaster. All other chemicals were obtained from Aldrich, Inc. and Fisher, Inc.

4.6.2 Chemistry

4,5-Methylenedioxy-(4-methoxyphenyl)-2-nitrocinnamic acid (III in Scheme 4-1)

A solution of 3,4-methylenedioxy-6-nitrobenzaldehyde (12 mmol), NEt₃ (12 mmol), 4-methoxyphenylacetic acid (17 mmol) was refluxed with stirring under Ar for 40 min.[20] Water (30 ml) was added to the reaction mixture and during the addition the temperature was maintained between 90 °C and 100 °C. The reaction mixture was cooled to ambient temperature and solid was collected by filtration and recrystallized from EtOH.

91% yield; yellow powder; mp 184-185 °C; ¹H NMR (400.13 MHz) δ 7.92 (s, 1H), 7.53 (s, 1H), 7.01 (d, $J = 2$ Hz, 2H), 6.73 (d, $J = 2$ Hz, 2H), 6.22 (s, 1H), 5.96 (s, 2H), 3.74 (s, 3H); MS (DCI/NH₃) m/e: 344 $(M + H)^+$.

4,5-Methylenedioxy-(4-methoxyphenyl)-2-aminocinnamic acid (IV in Schem 4-1)

56

To a solution of the acid (**III**) (7 mmol) in 10% aqueous NH_4OH (100 ml) was added ferrous sulfate heptahydrate (15 g) dissolved in distilled water (100 ml) and concentrated aqueous NH_4OH (100 ml). The reaction mixture was refluxed for 1.5 h, cool to 40 °C and filtrate on Celite and acidified with acetic acid (100 ml), the solid was collected by filtration and recrystallization from EtOH yielded the aminostilbenic acid.

95% yield; yellow powder; mp 165-166 °C; ^{1}H NMR (400.13 MHz) δ 7.74(s, 1H), 7.08 (d, *J* = 2Hz, 2H), 6.80 (d, *J* = 2 Hz, 2H), 6.17 (s, 1H), 6.06 (s, 1H), 5.70 (s, 2H), 3.80 (s, 2H), 3.73 (s, 3H); MS (DCI/NH_3) *m/e*: 314 (M + H)[+].

2,3-Methylenedioxy-6-methoxy-phenanthrene-9-carboxylic acid (V in Scheme 4-1)

A solution composed of the aminostilbenic acid (**IV**) (3 mmol), NaOH (33 mmol) and $NaNO_2$ in water (10 ml) was added dropwise over 30 min with stirring to 48% fluoroboric acid (43 mmol) at 0-5 °C. The mixture was stirred for 1 h after which sulfamic acid was added until the mixture tested negative to starch-iodide paper. The crude solid was collected by filtration, dissolved in anhydrous acetone (10 ml) and then added dropwise with stirring over a 15 min period to ferrocene (0.056 g, 0.3 mmol) in acetone at ambient temperature. After an additional 15 min of stirring the green reaction mixture was added to water (100 ml). A light-yellow precipitate was collected and the trace amount of ferrocene was removed in vacuo to afford the phenanthroic acid.

92% yield; white powder; mp 293-295 °C; ^{1}H NMR (400.13 MHz) δ 7.67 (s, 1H), 7.60 (d, *J*= 4Hz, 1H), 7.22 (dd, *J*= 4Hz, 2Hz, 1H), 6.92 (s, 1H), 6.89 (d, *J*=2Hz, 1H), 6.70 (s, 1H), 5.98 (s, 2H), 3.79 (s,3H); MS (DCI/NH3) m/e: 297 (M + H)[+].

4.6.3 General Procedures

General Procedure for the protection of cycloalkylamino acid:

To a solution of cycloalkylamino acid (4 mmol) in dry MeOH (4 ml) was added dropwise $SOCl_2$ (0.4 ml) at -30 °C. The reaction mixture was warmed to room temperature and refluxed for 1 h. Then the solvent was removed in vacuo and the product was used in the next reaction without any further purification.

General Procedure for the protection of acyclic alkylamino acid:

To a solution of dry MeOH (3 ml) was added dropwise AcCl (0.45 ml) at 0 °C. After 10 min stirring, the amino acid was added to the solution in portions. The mixture was warmed to room temperature and refluxed for 2 h, then the solvent was removed in vacuo and the product was used in the next reaction without any further purification.

General Procedure for the peptide bond condensation reaction (d):

To a solution of phenanthroic acid (4 mmol), 4-(dimethylamino) pyridine (DMAP) (2 mmol), 1-hydroxybenzotriazole (HOBT) (4 mmol) and methyl protected amino acid (4.4 mmol) in 20 ml DMF was added NMM (1.03 ml). The mixture was stirring at 0 °C for 15 min, *N*-(3-dimethylaminopropyl)-*N'*- ethylcarbodiimide hydrochloride (EDC) (4.4 mmol) was added by portion. The reaction mixture was stirred overnight at room temperature and partitioned between EtOAc and water. The organic layer was washed with brine, saturated $NaHCO_3$ and1N HCl, dried over Na_2SO_4, and concentrated in vacuo. The crude product was chromatographed using Biotage Flash+ and Isco Companion systems using a 40g silica cartridge and EtOAc/hexane as eluant.

General Procedure for the carbonyl reduction reaction (e):

To a stirred solution of 9-ylcarbonyl compound (2 mmol) in THF (20 ml) was added dropwise borane-methyl sulfide (BMS)(4 ml, 2.0M solution in THF), the reaction was stirred at room temperature overnight and quenched with 1N HCl. THF was removed in vacuo. The residue was partitioned between CH_2Cl_2 and water. The organic layer was dried, filtered and evaporated to afford 9-ylmethyl ester. The crude product was chromatographed using Biotage Flash+ and Isco Companion systems using $MeOH/CH_2Cl_2$ as eluant.

General Procedure for the basic hydrolysis reaction (f):

A solution of ester, 4N NaOH and MeOH (1:1) was refluxed for 4 h. The reaction mixture was acidified and partitioned between 10% $MeOH/CH_2Cl_2$ and 1N HCl, The organic layer was dried over Na_2SO_4, filtered and evaporated. The crude product was chromatographed using Biotage Flash+ and Isco Companion systems using $MeOH/CH_2Cl_2$ as eluant.

General Procedure for the LiAlH$_4$ reduction (g):

To a suspension of methyl ester (1 mmol) in 15 ml dry THF was added LiAlH$_4$ (1 g) in portions at 0 °C. After addition, the reaction mixture was refluxed for 4 h, and then cooled to 0 °C. The reaction mixture was quenched with MeOH, and then 10% Rochelle salt was added. The reaction mixture was extracted with water and 10% $MeOH/CH_2Cl_2$. The organic layer was dried over Na_2SO_4, and the crude product was chromatographed using Biotage Flash+ and Isco Companion systems using $MeOH/CH_2Cl_2$ as eluant. The product was partitioned between water and 10% $MeOH/CH_2Cl_2$. Organic layer was dried over Na_2SO_4, and the crude product was chromatographed using Biotage Flash+ and Isco Companion systems using $MeOH/CH_2Cl_2$ as eluant.

General Procedure for making hydrochloride salts:

To a suspension of the free base (3 mmol) in EtOH (15 ml) was added dropwise an equivalent of 6N HCl. After the free base was well dissolved, the solvent was removed in vacuo and the remaining hydrochloride salt was dried over phosphorus pentoxide.

The physical and spectral data for **20**, **21**, **27**, **28**, and **31-34** were reported in Chapter III.

4.6.4 Chemistry

N-(2,3-Methylenedioxy-6-methoxy-phenanthr-9-ylmethyl)-L-2-piperidinemethanol hydrochloride (34-HCl)

mp 193-194 °C; ^{1}H NMR (400.13 MHz) δ 8.14 (d, J=4Hz, 1H), 8.00 (s, 1H), 7.78 (d, J=2Hz, 1H), 7.49 (s, 1H), 7.20 (dd, J=4Hz, 2Hz, 1H), 7.15 (s, 1H), 6.04 (s, 2H), 4.20 (s, 2H), 3.90 (s, 3H), 3.72 (d, J=17Hz, 2H), 3.04 (m, 1H), 2.68 (m, 2H), 1.83 (m, 6H); MS (DCI/NH$_3$) m/e: 380 (M + H)$^+$. Anal. (C$_{23}$H$_{25}$O$_4$N·1.0HCl·2.0H$_2$O) C, H, N,

N-(2,3-Methylenedioxy-6-methoxy-phenanthr-9-ylmethyl)-D-proline (43)

General procedures **d, e** & **f** from **V** (81%); white powder; p 152-153 °C; ^{1}H NMR (400.13 MHz) δ 8.21 (d, J=4Hz, 1H), 7.77 (s, 1H), 7.72 (d, J=2Hz, 1H), 7.56 (s, 1H), 7.23 (dd, J=4Hz, 2Hz, 1H), 7.10 (s, 1H), 6.04 (s, 2H), 4.05 (s, 2H), 3.96 (s, 3H), 3.16 (m, 1H), 2.36 (m, 2H), 2.14 (m, 2H), 1.81 (m, 2H); MS (DCI/NH$_3$) m/e: 380 (M + H)$^+$.

N-(2,3-Methylenedioxy-6-methoxy-phenanthr-9-ylmethyl)-D-prolinol (44)

General procedure **g** from **43** (95%); yellow syrup, recrystalization from EtOH gave white powder; mp 130-132 °C; ^{1}H NMR (400.13 MHz) δ 8.16 (d, J=4Hz, 1H), 7.88(s, 1H), 7.80 (d, J=2Hz, 1H), 7.46 (s, 1H), 7.23 (dd, J=4Hz, 2Hz, 1H), 7.14 (s, 1H), 6.07 (s, 2H), 4.03 (s, 2H), 3.94 (s, 3H), 3.70 (d, J= 17Hz, 2H), 3.16 (m, 1H), 2.38 (m, 2H), 2.23 (m, 2H), 1.95 (m, 2H); MS (DCI/NH$_3$) m/e: 366 (M + H)$^+$.

N-(2,3-Methylenedioxy-6-methoxy-phenanthr-9-ylmethyl)-6-aminohexanoic acid (45)

General procedures **d, e & f** from **V** (78%); white powder; mp 167-169 °C; ^{1}H NMR (400.13 MHz) δ 7.88 (d, *J*=4Hz, 1H), 7.76 (s, 1H), 7.71 (d, *J*=2Hz, 1H), 7.44 (s, 1H), 7.13 (dd, *J*=4Hz, 2Hz, 1H), 7.05 (s, 1H), 5.99 (s, 2H), 3.87 (s, 2H), 3.82 (s, 3H), 2.75 (m, 2H), 2.23 (t, *J*=6Hz, 2H), 1.53 (m, 2H), 1.44 (m, 2H), 1.28 (m, 2H); MS (DCI/NH$_3$) *m/e*: 396 (M + H)$^+$.

N-(2,3-Methylenedioxy-6-methoxy-phenanthr-9-ylmethyl)-6-aminohexanol (46)

General procedure **g** from **45** (90%); light green syrup, recrystalization from EtOH gave pale green powder; mp 145-147 °C; ^{1}H NMR (400.13 MHz) δ 7.90 (d, *J* =4Hz, 1H), 7.84 (s, 1H), 7.78 (d, *J*=2Hz, 1H), 7.51 (s, 1H), 7.21 (dd, *J*=4Hz, 2Hz, 1H), 7.14 (s, 1H), 6.03 (s, 2H), 4.34 (s, 2H), 3.94 (s, 3H), 3.48 (t, *J*=6Hz, 2H), 2.76 (m, 2H), 1.58 (m, 2H), 1.45 (m, 2H, 1.26 (m, 2H), 1.20(m, 2H); MS (DCI/NH$_3$) *m/e*: 382 (M + H)$^+$.

N-(2,3-Methylenedioxy-6-methoxy-phenanthr-9-ylmethyl)-6-aminohexanol hydrochloride (46-HCl)

White powder; mp 187-188°C; ^{1}H NMR (400.13 MHz) δ δ 8.14 (d, *J*=4Hz, 1H), 7.82 (s, 1H), 7.76 (d, *J*=2Hz, 1H), 7.50 (s, 1H), 7.18 (dd, *J*=4Hz, 2Hz, 1H), 7.13 (s, 1H), 6.08 (s, 2H), 4.67 (s, 2H), 3.98 (s, 3H), 3.60 (t, *J*=6Hz, 2H), 3.44 (m, 2H), 1.66(m, 2H), 1.59 (m, 2H), 1.40 (m, 2H), 1.33 (m, 2H), ; MS (DCI/NH$_3$) *m/e*: 382 (M + H)$^+$. Anal. (C$_{23}$H$_{27}$O$_4$N·1.0HCl·1.5H$_2$O) C, H, N.

N-(2,3-Methylenedioxy-6-methoxy-phenanthr-9-ylmethyl)-L-4-piperidinecarboxylic acid (47)

General procedures **d, e & f** from **V** (85%); light yellow powder; mp 238-240 °C; ^{1}H NMR (400.13 MHz) δ 8.30 (d, *J*=4Hz, 1H), 7.92 (s, 1H), 7.83 (d, *J*=1Hz, 1H), 7.42 (s, 1H), 7.22

(dd, *J*=4Hz, 2,4Hz, 1H), 7.17 (s, 1H), 6.09 (s, 2H), 4.04 (s, 2H), 3.66 (s, 3H), 2.98 (m, 1H),

2.58 (m, 4H), 1.75 (m, 4H); MS (DCI/NH$_3$) *m/e*: 394 (M + H)$^+$.

N-(2,3-Methylenedioxy-6-methoxy-phenanthr-9-ylmethyl)-L-4-piperidinemethanol (48)

General procedure **g** from **47** (92%); light green syrup, recrystallization from EtOH gave

white powder; mp 130-132 °C; ^{1}H NMR (400.13 MHz) δ 8.26 (d, *J*=4Hz, 1H), 7.87 (s, 1H),

7.78 (d, *J*=2Hz, 1H), 7.38 (s, 1H), 7.19 (dd, *J*=4Hz, 2Hz, 1H), 7.14 (s, 1H), 6.05 (s, 2H), 3.97

(s, 3H), 3.81(s, 2H), 3.43 (d, *J*=7Hz, 2H), 2.97 (m, 2H), 2.02 (m, 2H), 1.65 (m, 2H), 1.48 (m,

1H), 1.26 (m, 2H); MS (DCI/NH$_3$) *m/e*: 380 (M + H)$^+$.

N-(2,3-Methylenedioxy-6-methoxy-phenanthr-9-ylmethyl)-L-4-piperidinemethanol

hydrochloride (48-HCl)

White powder; mp 256-258 °C; ^{1}H NMR (400.13 MHz) δ 8.00 (d, *J*=4Hz, 1H), 7.85 (s, 1H),

7.82 (s, 1H), 7.77 (d, *J*=2Hz, 1H), 7.22 (dd, *J*=4Hz, 2Hz, 1H), 7.20 (s, 1H), 6.03 (d, *J*=4Hz,

2H), 4.59 (s, 2H), 3.92 (s, 3H), 3.46 (d, *J*=4Hz, 2H), 3.31 (m, 2H), 2.77 (m, 2H), 1.76 (m,

4H), 1.68 (m, 1H); MS (DCI/NH$_3$) *m/e*:380 (M + H)$^+$. Anal. (C$_{23}$H$_{25}$O$_4$N·1.0HCl·1.0H$_2$O) C,

H, N.

N-(2,3-Methylenedioxy-6-methoxy-phenanthr-9-ylmethyl)-11-aminoundecanoic acid

(49)

General procedures **d, e** & **f** from **V** (75%); white powder; mp 146-148 °C; ^{1}H NMR (400.13

MHz) δ 7.98 (d, *J*=4Hz, 1H), 7.80 (s, 1H), 7.72 (d, *J*=2Hz, 1H), 7.50 (s, 1H), 7.11 (dd,

J=4Hz, 2Hz, 1H), 7.06 (s, 1H), 6.05 (s, 2H), 4.02 (s, 3H), 3.86 (s, 2H), 2.93 (m, 2H), 2.2 (m,

2H), 1.67 (m, 2H), 1.53 (m, 2H), 1.21 (m, 12H); MS (DCI/NH$_3$) *m/e*: 466 (M + H)$^+$.

N-(2,3-Methylenedioxy-6-methoxy-phenanthr-9-ylmethyl)-6-aminoundecanol (50)

General procedure **g** from **49** (90%); light green syrup, recrystalization from EtOH gave pale green powder; mp 122-124 °C; ^{1}H NMR (400.13 MHz) δ 7.86 (d, *J*=4Hz, 1H), 7.67 (s, 1H), 7.40 (d, *J*=2Hz, 1H), 7.43 (s, 1H), 7.18 (dd, *J*=4Hz, 2Hz, 1H), 7.08 (s, 1H), 6.01 (s, 2H), 4.32 (s, 2H), 3.88 (s, 3H), 3.68 (t, *J*=6Hz, 2H), 2.86 (m, 2H), 1.68 (m, 2H), 1.58 (m, 2H), 1.26 (m, 14H); MS (DCI/NH₃) *m*/*e*: 452 (M + H)⁺.

N-(2,3-Methylenedioxy-6-methoxy-phenanthr-9-ylmethyl)-(2-chlorophenyl)-piperazine (51)

General procedures **d** & **e** from **V** (87%); white powder; mp 196-198 °C; ^{1}H NMR (400.13 MHz) δ 8.32 (d, *J*=4Hz, 1H), 7.91 (s, 1H), 7.81 (d, *J*=2Hz, 1H), 7.44 (s, 1H), 7.32 (dd, *J*=4Hz, 2 Hz, 1H), 7.22 (d, *J*=9Hz, 1H), 7.18 (s, 1H), 7.16 (d, *J*=9Hz, 1H), 7.00 (m, 1H), 6.93 (m, 1H), 6.08 (s, 2H), 4.30 (s, 2H), 3.94 (s, 3H), 3.68 (t, *J*=6Hz, 4H), 3.05 (m, 4H); MS (DCI/NH₃) *m*/*e*: 461.5 (M + H)⁺.

N-(2,3-Methylenedioxy-6-methoxy-phenanthr-9-ylmethyl)-(4-chlorophenyl)-piperazine (52)

General procedures **d** & **e** from **V** (80%); white powder; mp 222-223 °C; ^{1}H NMR (400.13 MHz) δ 8.30 (d, *J*=4Hz, 1H), 7.90 (s, 1H), 7.81 (d, *J*=2Hz, 1H), 7.50 (s, 1H), 7.22 (dd, *J*=4Hz, 2Hz, 1H), 7.19 (s, 1H), 7.17 (d, *J*=9Hz, 2H), 6.89 (d, *J*=9Hz, 2H), 6.09 (s, 2H), 4.68 (s, 2H), 3.90 (s, 3H), 3.65 (t, *J*=8Hz, 4H), 3.14 (m, 4H); MS (DCI/NH₃) *m*/*e*: 461.5 (M + H)⁺.

N-(2,3-Methylenedioxy-6-methoxy-phenanthr-9-ylmethyl)-(4-hydroxyphenyl)-piperazine (53)

General procedures **d** & **e** from **V** (82%); white powder; mp 225-227 °C; ^{1}H NMR (400.13 MHz) δ 8.10 (d, *J*=4Hz, 1H), 7.90 (s, 1H), 7.82 (d, *J*= 2Hz, 1H), 7.49 (s, 1H), 7.22 (dd,

J=4Hz, 2Hz, 1H), 7.14 (s, 1H), 6.76 (d, J=9Hz, 2H), 6.61 (d, J=9Hz, 2H), 6.12 (s, 2H), 4.43 (s, 2H), 3.85 (s, 3H), 3.21 (t, J=8Hz, 4H), 2.83 (m, 4H); MS (DCI/NH$_3$) m/e: 443 (M + H)$^+$.

N-(2,3-Methylenedioxy-6-methoxy-phenanthr-9-ylmethyl)-N-(2-hydroxyethyl)-piperazine (54)

General procedures **d** & **e** from **V** (86%); white powder; mp 142-144 °C; ^{1}H NMR (400.13 MHz) δ 8.18 (d, J=4Hz, 1H), 7.85 (s, 1H), 7.76 (d, J=2Hz, 1H), 7.32(s, 1H), 7.16 (dd, J=4Hz, 2Hz, 1H), 7.10 (s, 1H), 6.05 (s, 2H), 3.96 (s, 3H), 3.82 (s,2H), 3.70 (t, J=6Hz, 2H), 2.70 (m, 8H), 2.61 (m, 2H); MS (DCI/NH$_3$) m/e: 395 (M + H)$^+$.

N-(2,3-Methylenedioxy-6-methoxy-phenanthr-9-ylmethyl)-(2-hydroxyethylethoxy)-piperazine (55)

General procedures **d** & **e** from **V** (78%); white powder; mp 145-147 °C; ^{1}H NMR (400.13 MHz) δ 8.10 (d, J=4Hz, 1H), 7.80 (s, 1H), 7.75 (d, J=2Hz, 1H), 7.46(s, 1H), 7.14 (dd, J=4Hz, 2Hz, 1H), 7.09 (s, 1H), 6.05 (s, 2H), 3.96 (s, 3H), 3.89 (s,2H), 3.79 (t, J=6Hz, 2H), 3.61 (t, J=6Hz, 2H), 3.49 (t, J=6Hz, 2H), 3.12 (m, 8H), 2.87 (m, 2H); MS (DCI/NH$_3$) m/e: 439 (M + H)$^+$.

N-(2,3-Methylenedioxy-6-methoxy-phenanthr-9-ylmethyl)-4-piperidineethanol (56)

General procedures **d** & **e** from **V** (88%); white powder; mp 148-149 °C; ^{1}H NMR (400.13 MHz) δ 8.08 (d, J=4Hz, 1H), 7.90 (s, 1H), 7.81 (d, J=2Hz, 1H), 7.45 (s, 1H), 7.22 (dd, J=4Hz, 2Hz, 1H), 7.17 (s, 1H), 6.09 (s, 2H), 4.14 (s, 2H), 3.98 (s, 3H), 3.52 (t, J=6Hz, 2H), 3.00 (m, 2H), 2.58 (m, 2H), 1.65 (m, 4H), 1.55 (m, 1H), 1.43 (m, 2H); MS (DCI/NH$_3$) m/e: 394 (M + H)$^+$.

N-(2,3-Methylenedioxy-6-methoxy-phenanthr-9-ylmethyl)-4-piperidineethanol hydrochloride (56-HCl)

White powder; mp 153-155 °C; ^{1}H NMR (400.13 MHz) δ δ 8.07 (d, *J*=4Hz, 1H), 7.94 (s, 1H), 7.83 (d, *J*=2Hz, 1H), 7.50 (s, 1H), 7.22 (dd, *J*= 4Hz, 2Hz, 1H), 7.15 (s, 1H), 6.10 (s, 2H), 4.56 (s,2H), 3.98 (s, 3H), 3.56 (t, *J*=6Hz, 2H), 3.44 (m, 2H), 2.84 (m, 2H), 1.85 (m, 4H), 1.73 (m, 1H), 1.45 (m, 2H); MS (DCI/NH$_3$) *m/e*: 394 (M + H)$^+$. Anal. (C$_{24}$H$_{27}$O$_4$N·1.0HCl·2.0H$_2$O) C, H, N,

***N*-(2,3-Methylenedioxy-6-benzyloxy-phenanthr-9-ylmethyl)-L-4-piperidinecarboxylic acid (57)**

Similar procedure as **47** (77% for **d**, **e** & **f**); white powder; mp 183-185 °C; ^{1}H NMR (400.13 MHz) δ 8.05 (d, *J*=4Hz, 1H), 7.89 (d, *J*=2Hz, 1H), 7.81 (s, 1H), 7.52 (d, *J*=4Hz , 2H), 7.43 (s, 1H), 7.40 (t, *J*=4Hz, 2H), 7.33 (m, 1H), 7.26 (dd, *J*=4Hz, 2Hz, 1H), 7.15 (s, 1H), 6.08 (s, 2H), 5.26 (s, 2H), 3.92 (s, 2H), 2.89 (m, 1H), 2.36 (m, 4H), 1.83 (m, 4H); MS (DCI/NH$_3$) *m/e*: 470 (M + H)$^+$.

***N*-(2,3-Methylenedioxy-6-benzyloxy-phenanthr-9-ylmethyl)-L-4-piperidinemethanol (58)**

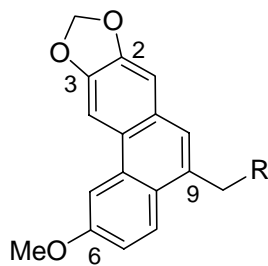General procedure **g** from **57** (93%); white powder; mp 120-122 °C; ^{1}H NMR (400.13 MHz) δ 8.25 (d, *J*=4Hz, 1H), 7.89 (d, *J*=2Hz, 1H), 7.84 (s, 1H), 7.51 (d, *J*=4Hz, 2H), 7.44 (t, *J*=4Hz, 2H), 7.33 (m, 1H), 7.26 (dd, *J*=4Hz, 2Hz, 1H), 7.15 (s, 1H), 6.07 (s, 2H), 5.28 (s, 2H), 3.95 (s, 2H), 3.47 (d, *J*=3Hz, 2H), 2.12 (m, 4H), 1.69 (m, 1H), 1.48 (m, 4H); MS (DCI/NH$_3$) *m/e*: 456 (M + H)$^+$.

4.6.5 Cell Growth Inhibition Assay
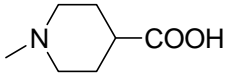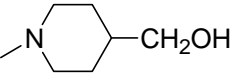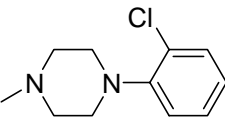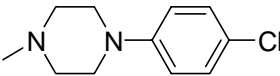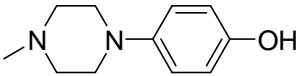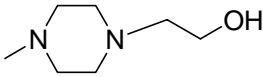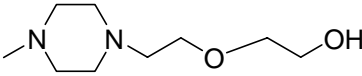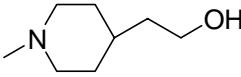
The sulforhodamine B assay was used according to the procedures developed and validated at NCI.[6] The in vitro anticancer activities are expressed as EC_{50} values, which is the test compound concentration (μM) that reduced the cell number by 50% after 72-h of continuous treatment. The values were interpolated from dose-response data. Each test was performed in triplicate with variation less than 5%. The ED_{50} values determined in each of independent tests varied less than 10%. Compound stock solutions were prepared in DMSO with the final solvent concentration ≤1% DMSO (v/v), a concentration without effect on cell replication. The cells were cultured at 37 °C in RPMI-1640 supplemented with 25 mM *N*-2-hydroxyethylpiperazine-*N'*-2-ethanesulfonic acid (HEPES), 2% (w/v) sodium bicarbonate, 10% (v/v) fetal bovine serum, and 100 μg/mL kanamycin in a humidified atmosphere containing 5% CO_2.

Table 4-1. Cytotoxicity of 6-Methoxy-9-Substituted PTBs.

Compound	R	EC$_{50}$ (µM) A549
27*	-NH(CH$_2$)$_4$COOH	1.3
28*	-NH(CH$_2$)$_4$CH$_2$OH	0.27
31*	HOOC pyrrolidine (N-methyl)	2.1
32*	HOH$_2$C pyrrolidine (N-methyl)	0.7
33*	HOOC piperidine (N-methyl)	0.5
34*	HOH$_2$C piperidine (N-methyl)	0.16
43	HOOC pyrrolidine (N-methyl)	5.2
44	HOH$_2$C pyrrolidine (N-methyl)	1.1
45	-NH(CH$_2$)$_5$COOH	0.8
46	-NH(CH$_2$)$_5$CH$_2$OH	0.2

47	N–CH₃ piperidine–COOH	0.23
48	N–CH₃ piperidine–CH$_2$OH	0.08
49	-NH(CH$_2$)$_{10}$COOH	3.2
50	-NH(CH$_2$)$_{10}$CH$_2$OH	2.6
51	methylpiperazine–(2-Cl-phenyl)	NA
52	methylpiperazine–(4-Cl-phenyl)	65.2
53	methylpiperazine–(4-OH-phenyl)	0.22
54	methylpiperazine–CH$_2$CH$_2$OH	0.63
55	methylpiperazine–CH$_2$CH$_2$–O–CH$_2$CH$_2$OH	57.1
56	methylpiperidine–CH$_2$CH$_2$OH	0.15
Emetine		0.04
Doxorubicin		0.18
Etoposide(VP-16)		1.4
Antofine		0.008
Vincristine		0.04

* From Chapter III.

Table 4-2. Cytotoxicity of 6-Benzyloxy-9-Substituted PBTs.
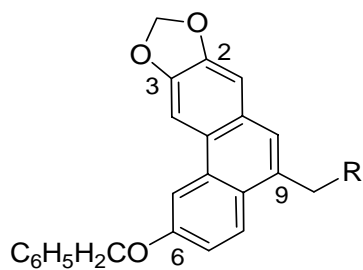
Compound	R	EC$_{50}$ (μM) A549
20*	HOOC— N-methyl piperidine	3.2
21*	HOH$_2$C— N-methyl piperidine	1.3
57	N-methyl piperidine —COOH	2.1
58	N-methyl piperidine —CH$_2$OH	0.7

* From Chapter III.

Table 4-3. Cytotoxicity of PBTs in different cancer cell lines.

Compound	EC$_{50}$ (µM)				
	A549	KB	DU-145	ZR-751	KB-VIN
34	0.2	0.12	0.21	0.1	0.16
34-HCl	0.16	0.12	0.09	0.08	0.09
45	0.5	0.33	0.67	0.54	0.83
46	0.16	0.25	0.04	0.13	0.35
46-HCl	0.13	0.23	0.07	0.08	0.16
47	0.23	0.15	0.31	0.25	0.38
48	0.08	0.24	0.03	0.03	0.09
48-HCl	0.07	0.07	0.05	0.04	0.04
53	0.22	0.13	0.15	0.18	0.34
54	0.63	0.50	0.25	0.23	0.51
56	0.15	0.42	0.15	0.03	0.50
56-HCl	0.09	0.20	0.1	0.02	0.20
Antofine	0.008	0.013	0.009	0.008	0.009
Emetine	0.04	0.04	0.06	0.1	>2
Doxorubicin	0.18	0.18	0.13	0.04	>4
Etoposide (VP-16)	1.4	4.8	2.4	3.1	>10
Vincristine	0.04	0.006	0.085	0.04	5.3

4.7 REFERENCES

1) Wassmundt, F. W.; Kiesman, W. F. Soluble catalysts for improved Pschorr cyclizations. *J Org. Chem.* **1995**, *60*, 196-201.

2) Lebrun, S.; Couture, A.; Deniau, E.; Grandclaudon, P. Total syntheses of (±)-cryptopleurine, (±)-antofine and (±)-deoxypergularinine. *Tetrahedron* **1999**, *55*, 2659-2670.

3) Rubinstein, L. V.; Shoemaker, R. H.; Paull, K. D.; Simon, R. M.; Tosini, S.; Skehan, P.; Scudiero, D. A.; Monks, M. R. Comparison of in vitro anticancer-drug-screening data generated with a tetrazolium assay versus a protein assay against a diverse panel of human tumor cell lines. *J. Natl. Cancer Inst.* **1990**, *82*, 1113-1118.

4) Abe, F.; Hirokawa, M.; Yamauchi, T.; Honda, K.; Hayashi, N.; Ishii, M.; Imagawa, S.; Iwahana, M. Further investigation of phenanthroindolizidine alkaloids from *Tylophora tanakae*. *Chem. Pharm. Bull.* **1998**, *46*, 767-769.

5) Wu, P. L.; Rao K. V.; Su, C.-H.; Kuoh, C.-S.; Wu, T.-S. Phenanthroindolizidine alkaloids and their cytotoxicity from the leaves of *Ficus septica*. **Heterocycles 2002**, *57*, 2401-2408.

6) Rubinstein, L. V.; Shoemaker, R. H.; Paull, K. D.; Simon, R. M.; Tosini, S.; Skehan, P.; Scudiero, D. A.; Monks, M. R. Comparison of in vitro anticancer-drug-screening data generated with a tetrazolium assay versus a protein assay against a diverse panel of human tumor cell lines. *J. Natl. Cancer Inst.* **1990**, *82*, 1113-1118.

CHAPTER V. QUANTITATIVE STRUCTURE-ACTIVITY RELATIONSHIP ANALYSIS OF PHENANTHRINE-BASED TYLOPHORINE DERIVATIVES (PBTS) USING *K*-NEAREST NEIGHBOR AND DATABASE MINING

5.1   INTRODUCTION

In Chapters III and IV, we described a novel series of polar water-soluble phenanthrene-based tylophorine derivatives (PBTs) with $EC_{50} \cong 10^{-7}$ M against the A549 human lung cancer cell line. These compounds could possibly have lower or no CNS toxicity because the increased polarity should prevent them from penetrating the blood-brain barrier. The target(s) of PBTs function has not been identified; however, several structure-activity trends have been observed: 1) A planar phenanthrene system is required, but not sufficient for cytotoxic activity. 2) A *N*-hydrophilic substituent at the C-9 position is essential for the enhanced cytotoxicity and should be linked through a methylene rather than a carbonyl group. 3) This C-9 *N*-hydrophilic substituent is ideal for the introduction of a polar moiety. Analogs containing terminal carboxylic acid or hydroxymethyl groups are more favorable than those with methyl esters. 4) On the phenanthrene skeleton, a methoxy substituent best fits both the steric and electronic requirements at the C-6 position and is preferred over benzyloxy and hydroxy groups. 5) Adding a methylenedioxy ring at the 2, 3 position of the planar phenanthrene system can dramatically enhance the cytotoxic activity and led to the most potent derivatives. The new PBT derivatives possess a novel structure and showed remarkable EC_{50} values in the sub-micromolar range, comparable those of with front-line

antineoplastic drugs, suggesting that this new compound class is of great potential to be developed into antitumor drugs. Useful and powerful quantitative structure-activity relationship (SAR) would greatly facilitate such further development.

Many different QSAR approaches, including both two-dimensional (2D) and three-dimensional (3D) methods, have been developed during the past few decades.[1-9] The major differences among these methods can be analyzed from two viewpoints: (i) structural parameters (descriptors) that are used to characterize molecules; (ii) the mathematical approach used to establish a correlation between biological activity and descriptor values. In recent years, we have been motivated to explore possible alternatives that would use alignment-free descriptors derived from 2D molecular topology, which can alleviate the frequent ambiguity of structural alignment typical for 3D QSAR methods. Consequently, our molecular modeling laboratory has developed a variable selection approach, k nearest neighbor (kNN) QSAR[10], which employs topological descriptors of chemical structures. Variable selection techniques choose the most informative variables and eliminate irrelevant variables to improve the signal-to-noise ratio in the resulting models. Additionally, these techniques are not computationally intensive and are practically automated. The validated 2D_kNN models with high predictive power can be easily adapted to conduct a database search or virtual screening.[11] This strategy was recently applied successfully to the discovery of novel anticonvulsant agents[12-13] and D_1 dopaminergic antagonists.[14]

In this chapter, we discuss the application of a kNN method on an experimental dataset including 52 PBTs with known EC_{50} values (Tables 5-1, 5-2, and 5-3). Their structures were characterized with MolConnZ[15] (MZ) descriptors. The models developed herein have been extensively validated using several criteria of robustness and accuracy.[16] The robustness of

the models was evaluated from the values of the internal leave-one-out cross-validated R^2 (q^2) for the training sets and external R^2 (predictive R^2) for the test sets, as well as other criteria. The developed models with high predictive power were adapted to mining the publicly available commercial ChemDiv[17] database, and resulted in 34 consensus hits with moderate to high activities. Ten structurally diverse hits were experimentally tested and eight compounds were confirmed active, with the most potent compound having an EC_{50} value of 1.8 μM. The predictive power of the models was further confirmed by the high correlation coefficient between the predicted and actual cytotoxic activity for an external set including four new PBTs and the eight active ChemDiv hits, which not included in the original 52 PBTs dataset. The correlation coefficient (R^2) was as high as 0.52. This result demonstrated a successful application of modern QSAR to traditional medicinal chemistry research.

5.2   DATASET AND BIOLOGICAL ACTIVITY

All PBTs used in this study were synthesized and evaluated (Tables 5-1, 5-2, 5-3) as described in Chapters III and IV. The general synthetic procedures and the biological, physical and spectral data were reported therein. The identified hits via database mining hits were purchased from Chem.Div, Inc with physical and spectral data. The human A549 lung cancer cell line was used for the cytotoxicity screening of PBTs and ChemDiv consensus hits using the cell-based sulforhodamine B (SRB) microtitre plate assay[18],which has been reported in detail elsewhere.

5.3   COMPUTATIONAL METHODS

5.3.1   Generation of Molecular Descriptors

All chemical structures were generated using SYBYL 7.0.[19] Molecular descriptors[20] were calculated for each compound with the MolConnZ (MZ) software version 4.05.[15] Overall, MolConnZ produces over 400 descriptors. In our study, only 244 chemically relevant descriptors were used after removing those with zero values or zero variance prior to model generation. MZ descriptors were range-scaled prior to distance calculations because the absolute scales for MZ descriptors can differ by orders of magnitude. Using range scaling could avoid disproportional weightings upon distance calculations in multidimensional MZ descriptor space.

5.3.2   Dataset Division into Training and Test Sets

It is generally accepted that the internal validation of the QSAR models built for the training set is sufficient to establish their predictive power.[21-30] However, our previous studies as well as those conducted by other groups have demonstrated that no correlation exists between leave-one-out (LOO) cross-validated R^2 (q^2) for the training set and the correlation coefficient R^2 between the predicted and observed activities for the test set.[16,31] We have developed a rational approach to dividing the dataset into multiple training and test sets for internal and external validations.[32]

The dataset of 52 compounds was divided into multiple chemically diverse training and test sets with the algorithm based on Sphere Exclusion (SE) developed in our group.[32] SE is a general procedure that is typically applied to databases of organic molecules characterized by

multiple descriptors of their chemical structure such that each compound is represented as a point (or vector) in multidimensional descriptor space. The goal of the SE method is to divide a dataset (i.e., a collection of points in multidimensional chemometric space) into two subsets (training and test set) using a diversity sampling procedure as follows. SE starts with the calculation of the distance matrix D between representative points in the descriptor space. Let Dmin and Dmax be the minimum and maximum elements of D, respectively. N probe sphere radii are defined by the following formulas. Rmin=R1=Dmin, Rmax=RN=Dmax/4, Ri=R1+(i-1)*(RN-R1)/(N-1), where i=2,…,N-1. Each probe sphere radius corresponds to one division into the training and test set.

In this study, each compound was characterized with multiple MolConnZ descriptors. The entire dataset was then treated as a collection of points (each corresponding to an individual compound) in the MolConnZ descriptor space. Thus, the SE algorithm used in this study consisted of the following steps. (i) Select randomly a point in the MolConnZ descriptor space. (ii) Include it in the training set. (iii) Construct a probe sphere around this point. (iv) Select points from this sphere and include them alternatively into test and training sets. (v) Exclude all points within this sphere from further consideration. (vi) If no more compounds left, stop. Otherwise let m be the number of probe spheres constructed and n be the number of remaining points. Let dij (i=1,…,m; j=1,…,n) be the distances between the remaining points and probe sphere centers. Select a point corresponding to the lowest dij value and go to step (ii). The training sets were used to build models and the test sets were used for validation.

5.3.3 kNN QSAR Method

Our kNN QSAR method[10] employs the kNN pattern recognition principle[33] and a variable selection procedure. Briefly, a subset of nvar (number of selected variables) descriptors between 1 and the total number of the original descriptors is selected randomly as a hypothetical descriptor pharmacophore (HDP). The model is built using this random descriptor selection with leave-one-out (LOO) cross-validation, where each compound is eliminated from the training set and its biological activity is predicted as the average activity of k most similar molecules (k = 1-5). The value k is optimized during the model building process to give the best prediction of the training set. The similarity is characterized by the Euclidean distance between compounds in multidimensional descriptor space. A method of simulated annealing with the Metropolis-like acceptance criterion is used to sample the entire descriptor space to converge on the subset of the same size that affords the highest value of LOO R^2 (q^2). The descriptor subsets of different sizes are optimized using this procedure to arrive at a variety of models with acceptable q^2 greater than a certain threshold (we chose 0.6 as the default threshold). The training set models with acceptable q^2 are then validated on external test sets to select predictive models as discussed above. Further details of the kNN method implementation, including the description of the simulated annealing procedure used for stochastic sampling of the descriptor space, are given elsewhere.[10]

The original kNN method[10] was enhanced in this study by using weighted molecular similarity. Estimated activities $\hat{y}_i$ of compounds excluded by LOO procedure are calculated using the following formulas.

$$\hat{y}_i = \frac{\sum\limits_{j=1}^{k} a_j w_{ij}}{\sum\limits_{j=1}^{k} w_{ij}}, \tag{1}$$

where weights w_{ij} are defined as

$$w_{ij} = \left(1 - \frac{d_{ij}}{\sum\limits_{j'=1}^{k} d_{ij'}}\right), \tag{2}$$

and d_{ij} are the distances between compound i and its k nearest neighbors. After each run, cross-validated R^2 (q^2) is calculated.

$$q^2 = 1 - \frac{\sum (y_i - \hat{y}_i)^2}{\sum (y_i - \bar{y})^2}, \tag{3}$$

where y_i, and $\bar{y}$ are the actual and average values of activity. The summation in (3) is performed over all compounds.

In summary, the kNN QSAR algorithm generates both an optimum k value and an optimal nvar subset of descriptors, which afford a QSAR model with the highest value of q^2. Figure 5-1 shows the overall flowchart of the current implementation of the kNN method.
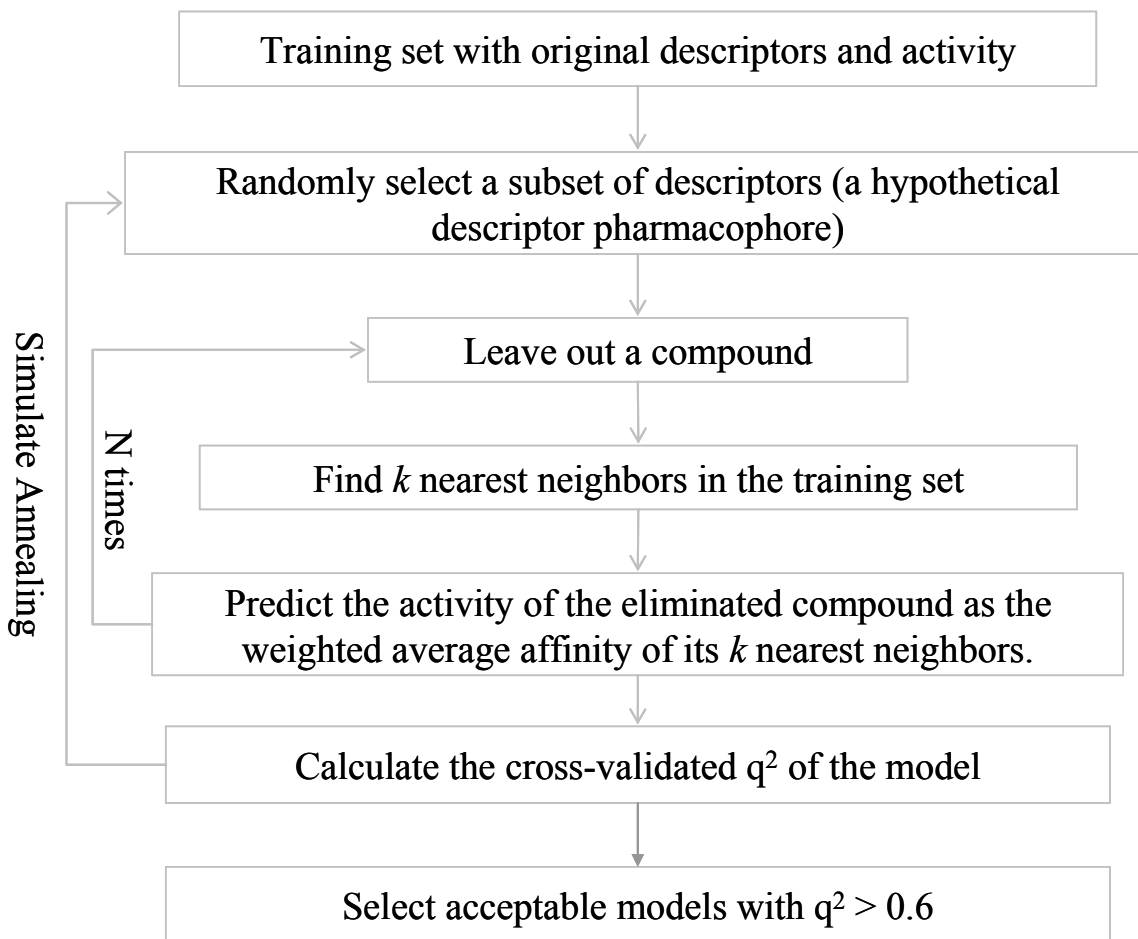
Figure 5-1. Flowchart of the kNN method.

5.3.4 Robustness and predictive power of QSAR Models (Y-Randomization Test)

The robustness of the models was examined by comparing them to those obtained when using randomized activity of the training set (this procedure is commonly referred to as the Y-randomization test). Briefly, we repeated the QSAR calculations with the randomized activities of the training sets. We also compared the q^2 values in the process of the iteration procedure of the simulating annealing for actual and random activities of training sets to see if there was any significant difference. This randomization was repeated five times for each splitting. This technique is widely used to ensure the robustness of a QSAR model.[34] It is

79

expected that the resulting QSAR models should generally have low training set fitness q^2 and low test set R^2. It is likely that sometimes, though infrequently, high training set statistics may be obtained due to a chance correlation or structural redundancy of the training set.[35] If all QSAR models obtained in the **Y**-randomization test exhibit relatively high training set statistics and test set R^2 values, it implies that an acceptable QSAR model cannot be obtained for the given dataset by the current modeling method. This test was applied to all data splits considered in this study.

To estimate the predictive power of a QSAR model, the following criteria were used:[16] (i) correlation coefficient R between the predicted and observed activities; (ii) coefficients of determination (predicted versus observed activities R_0^2, and observed versus predicted activities $R_0'^2$); (iii) slopes k and k' of regression lines (predicted versus observed activities, and observed versus predicted activities) through the origin. We conclude that a QSAR model has an acceptable predictive power if the following conditions are satisfied:[16]

$$q^2 > 0.5; \tag{4}$$

$$R^2 > 0.6; \tag{5}$$

$$\frac{(R^2 - R_0^2)}{R^2} < 0.1 \text{ or } \frac{(R^2 - R_0'^2)}{R^2} < 0.1; \tag{6}$$

$$0.85 \leq k \leq 1.15 \text{ or } 0.85 \leq k' \leq 1.15. \tag{7}$$

Earlier, we suggested[16] that preferably both values of R_0^2 and $R_0'^2$ must satisfy condition (6). This condition appears to be too strong; thus, herein we employed a less stringent condition: we have required that the difference between R_0^2 and $R_0'^2$ should not be too high as follows:

$$|R_0^2 - R_0'^2| < 0.3. \tag{8}$$

5.3.5   Applicability Domain of kNN QSAR Models.

Formally, a QSAR model can predict the target property for any compound for which chemical descriptors can be calculated. Since the training set models are developed in the kNN QSAR approach by interpolating activities of the nearest neighbor compounds,[10] a special applicability domain (i.e., similarity threshold) should be introduced to avoid making predictions for compounds that differ substantially from the training set molecules.[35]

To measure similarity, each compound is represented by a point in the M-dimensional descriptor space (where M is the total number of descriptors in the descriptor pharmacophore) with the coordinates X_{i1}, X_{i2}, ..., X_{iM}, where X_is are the values of individual descriptors. The molecular similarity between any two molecules is characterized by the Euclidean distance between their representative points. Compounds with the smallest distance between one another are considered to have the highest similarity. The distances (similarity) of compounds in our training set are compiled to produce an applicability domain threshold, D_T, calculated as follows:

$$D = <d> + Z\sigma \qquad (9)$$

where $<d>$ is the average of Euclidean distances between k nearest neighbors of all points of the training set used in model derivation, σ is the standard deviation of these distances, and Z is the empirical parameter to control the significance level.

Based on successful results from previous studies, we set the default value of this parameter to 0.5, which formally places the boundary for which compounds will be predicted at one-half of the standard deviation (assuming a Boltzmann distribution of distances between k nearest neighbor compounds in the training set). Thus, if the distance of the

external compound from at least one of its nearest neighbors in the training set exceeds this threshold, the prediction is considered unreliable.

5.3.6 Database Mining

A commercially available chemical database, Chemical Diversity (ChemDiv[17]), which is a small compound collection database containing ca. 500,000 compounds, was screened. MZ descriptors were generated for each compound in the database and linearly normalized based on the maximum and minimum values of each descriptor in the training set.[14]

The ten best kNN models were then used to predict activity for the database compounds that were within the applicability domain for that model. The results for each individual prediction exercise were then combined, and the mean predicted activity was calculated for each compound that was within the applicability domain of multiple models. The percentage of models that predicted each compound in the database and the standard deviation of those predictions were also recorded for each compound. We hypothesized that the higher the percentage of models with a stringent applicability domain that predict a compound's activity, the more likely the compound actually possesses the predicted activity. This postulate may also apply to the standard deviation of the predictions made for a single compound. The smaller the prediction variance across all models, the more confidence we have that the predicted biological activity for that compound is accurate. For these reasons, we selected a subset of compounds as hits that were predicted by at least 50% of the models and exhibited a small standard deviation across all models. We also performed an additional estimate as to whether the hits resulting from database mining using variable selection models possessed the features essential (i.e., common) for all PBTs. This additional precaution was considered

essential because variable selection procedure by default eliminates features (descriptors) that have the same values for all modeled compounds.

5.4 RESULTS AND DISCUSSION

5.4.1 QSAR models and Their Robustness

In the kNN QSAR method, *nvar* can be set to any value that is less than the total number of descriptors. Since the optimal number for *nvar* is not known a priori, multiple models must be generated to examine the relationship between q^2 and *nvar*. As previously discussed, the robustness of a QSAR model should be established by comparing results for the actual data set with those for data sets with randomized activity values. Thus, 10, 20, 30, 40 and 50 descriptor models were generated. Figure 5-2 shows a plot of q^2 vs *nvar* for the actual and random data sets obtained with kNN calculations. Every q^2 value is the average of 10 independent computations. Overall, we obtained consistently much higher q^2 values for the actual data set compared to those from Y-randomization. The q^2 values for the real data set were in the range 0.60 to 0.70 compared to -0.10 to 0.10 for the random data sets.
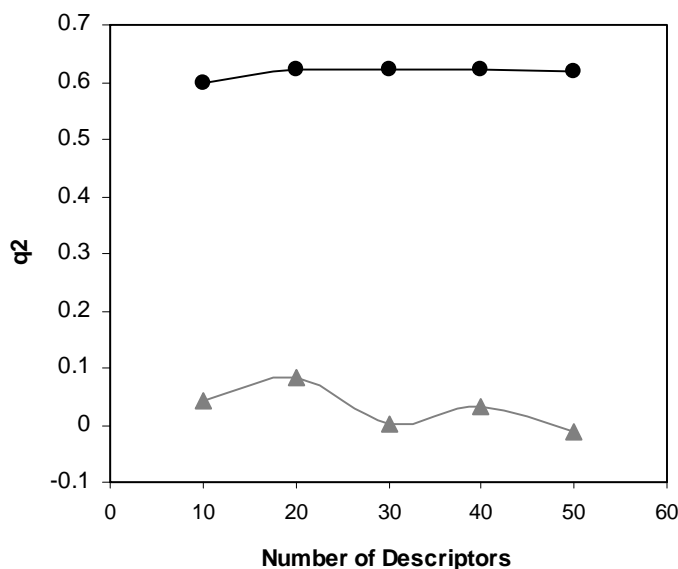
Figure 5-2. Plots of q^2 versus the number of descriptors selected for the best kNN QSAR models for 52 PBTs. The results for both actual and random (with shuffled activity values) data sets are shown. Every q^2 value is the average of 10 independent calculations. Circles represent the actual data set, and triangles represent the random data set.

5.4.2 kNN QSAR Model Validation

Generally, we accept models with q^2 values for the training set greater than 0.5 and R^2 values for predicted vs actual activities of the test set compounds greater than 0.6.[16] Table 5-4 presents the ten best models obtained from multiple kNN analyses. In order to obtain statistical significance, the original 52-compound dataset was divided into 50 training and test sets. Multiple variable selection models with the highest q^2 values (greater than 0.5) were collected. However, as indicated in one of our earlier studies,[16] no correlation was found between q^2 and R^2, also shown in Figure 5-3, demonstrating that q^2 alone does not serve as an estimate of the predictive power of kNN models. On the basis of our criteria, acceptable models with both high statistical significance ($q^2 > 0.5$) and predictive power ($R^2 > 0.6$) represented only a fraction of all models with $q^2 > 0.5$ (Figure 3). So the

aforementioned conditions (Equations 4–8) become very important. Based on all of these

criteria, the best models were obtained for the test sets including 14 and 18 compounds, with

the optimal number of descriptors as 15 and 20, respectively (Table 5-4). Figure 5-4 shows

actual vs. calculated activity correlations for the training and test sets with $q^2 = 0.59$ and $R^2 = 0.81$ respectively. Two outlying points {compound **20** and **54** antofine)] were poorly

predicted. The latter point represents antofine, a positional isomer of tylophorine isolated

from Asclepiadaceae by Dr. T. S. Wu[36] in Taiwan; its structure is shown in Table 5-3. It was

used as a reference compound when we screened PBTs. A possible explanation for this

observation is that this compound lacks the chemical structure descriptors that are most

meaningful and statistically significant in terms of correlation with biological activity: a *N*-

hydrophilic substituent and free rotating C-9 methylene bond, which were proven to be

required for PBT analog activity in our preliminary study. Mechanism of action studies for

antofine and PBTs are still ongoing and it remains possible that they have different modes of

action. In regard to compound **20**, its terminal Cl group may cause some solubility or cell

membrane transportation problem that would result in diminished activity in our cell-based
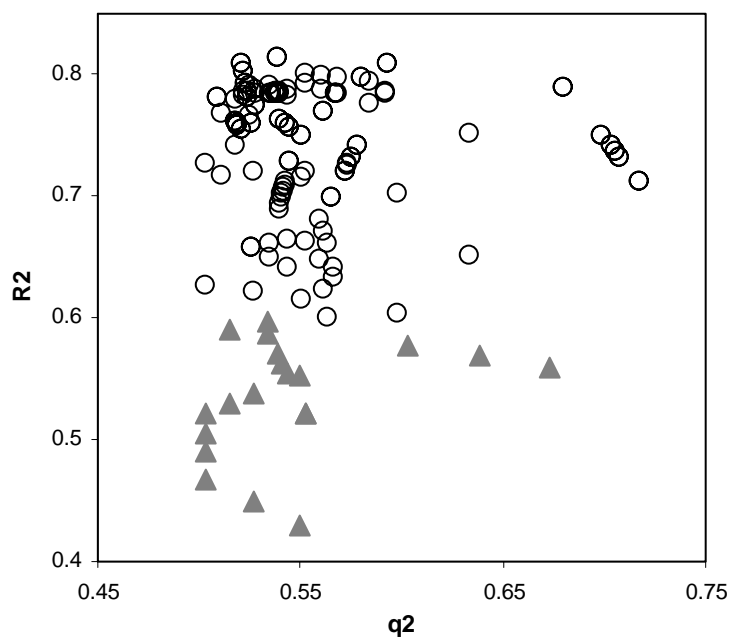
assay.

Figure 5-3. R^2 versus q^2 for all selected models with $q^2>0.5$. Triangles for models with $R^2<0.6$ and open circles for models with $R^2>0.6$
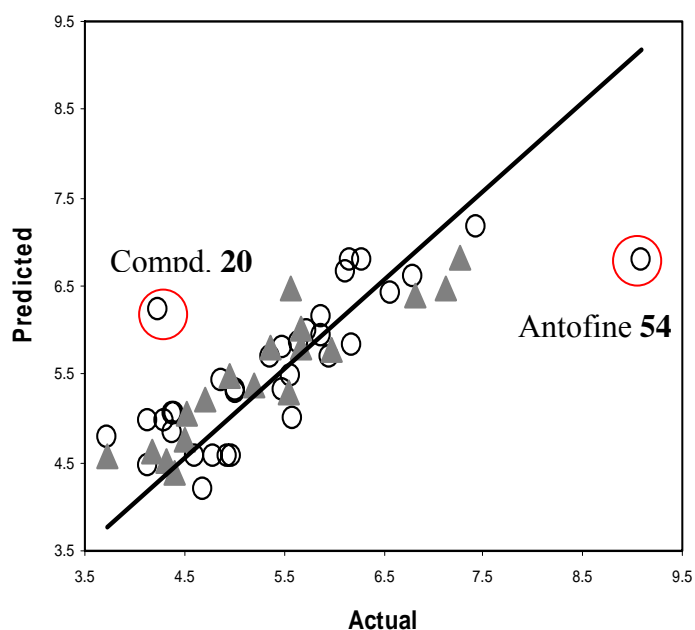

Figure 5-4. Plot of Actual versus Predicted activity for one of the best 10 models. This model has 18 compounds in the test set, and correspondingly, 34 in the training set. Twenty descriptors have been selected for the calculation. $q^2=0.59$ and $R^2=0.81$

5.4.3 Interpreting predictive QSAR models

Upon the frequency analysis of selected descriptors, a number of MolConnZ descriptors were identified suggesting that they played critical roles in relating chemical structures to their antitumor activity. These descriptors include molecular connectivity descriptors such as Chi indices, hydrogen bond counts and E-state descriptors, atom type E-state descriptors, shape indices, etc. These results are consistent with our preliminary SAR observations, as described in the Introduction to this chapter. Based on the MolConnZ manual and personal communication with Dr. Lowell Hall, one of the principle MolConnZ developers, these selected descriptors have been grouped into the following classes: 1) The high frequency of the Chi indices, including dXvp7, dXvp10, nXp6, Xvp7, etc., suggests the importance of those structure features such as size, branching, and cyclicity. Our previous SAR study showed that both para-positioned functional groups and three intra-atomic distances are very important to the antitumor activity. These features define the relative spatial dispositions of three significant atoms: the oxygen of C-9 chain terminal, the nitrogen atom, and a methoxy oxygen on the phenanthrene ring. 2) Hydrogen bond donors/acceptors counts and E-states descriptors, such as nHBint9, SHBd, Hmax, Hmin, indicate the importance of polar hydrogen atoms and hydrogen bond interactions during binding. This observation agrees with the finding that the presence of a hydrogen bond acceptor/donor group at the C-9 chain terminus appears essential for cytotoxic activity and analogs containing terminal carboxylic acid or hydroxymethyl groups are more favorable than those with methyl esters. 3) The appearance of atom type counts and E-states descriptors (SssCH2, nsssCH, and SsOH) demonstrated a high importance of electron accessibility for those atoms. Our studies indeed found that an

N-hydrophilic substituent at the C-9 position is essential for enhanced cytotoxicity and should be linked through a methylene rather than a carbonyl group. 4) Several steric crowding related descriptors (n2Pag12 and Tm) occurred many times in our models. This point is reflected in our finding that a methoxy substituent best fits both the steric and electronic requirements at the C-6 position. 5) Several Kappa and complexity indices (ka1, ka2, tets1, tets2, graphcomplexity, etc.) were found in many models, suggesting that shape related features are important for the cytotoxicity in our PBTs. It was noted that a planar phenanthrene system is required, although not sufficient, for the cytotoxic activity. Also adding a methylenedioxy ring at the 2, 3 positions of the planar phenanthrene system can dramatically enhance the cytotoxic activity and leads to the most potent derivatives. 6) Last, not least, descriptors such as nCl and SsCl indicate the importance of a Cl atom to the activity. Several structures with Cl (e.g., compounds **64** and **68**) showed high activity (EC_{50} as low as 1.8 μM) when their activities were not hindered by solubility in the biological assay.

5.4.4 Database mining with predictive QSAR models

ChemDiv., a small compound collection of ca. 500,000 compounds, was screened with our ten best QSAR models within a defined applicability domain, and predicted activities were averaged to yield consensus values. Thirty-four consensus hits were identified with moderate to high predicted activities. Among them, some compounds shared very similar core chemical structures, while some were very different. Eventually, ten structurally diverse hits (**59-68**, Table 5-5) with moderate to high predicted activity were chosen, purchased and screened using the same cell line and assay method as for the PBT screening. The chemical structures and experimental biological data are shown in Table 5-5. Eight (**59, 61-62, 64-68**)

of the ten compounds were confirmed to be active against the A549 lung cancer cell line, and compound **68** (ChemDiv #: K915-0700) showed the best activity with an EC_{50} of 1.8 μM, comparable to the active PBTs. This hit (**68**) has similar activity, but a novel core structure different from either known PBTs or anticancer drugs. Since all compounds in the ChemDiv database were synthesized automatically by combinatorial chemistry and no biological data were annotated, our screening provides the first associated anticancer activity for these novel structures.

Although the prediction accuracy for the screening hits was lower than for the original congeneric (core structure similar) compound set (see explanation in the next paragraph), the high experimental hit rate and capability of detecting novel active structures from a large chemical database confirm this method as a very useful and powerful tool in drug lead identification.

5.4.5 Prediction of Anticancer Activity for an External Data Set

As a reliable and truly predictive QSAR model, it is necessary to demonstrate that the training set models can accurately predict activities of new compounds in external test sets. To this end, the kNN QSAR models validated with the test sets were used to predict the activity of four new compounds (Table 5-5), which were not available prior to our QSAR studies of the 52-compound PBT dataset. Concurrently, the eight active hits (Table 5-6) from ChemDiv, which had moderate to high predicted activities, were also used to evaluate the accuracy of prediction using our models in a quantitative manner.

All of the external compounds displayed moderate to high predicted activity that ranged between 0.15 and 72.4 μM (Tables 5-5 & -6), while the original training set compounds (Tables 5-1, -2 & -3) featured EC_{50} activity values that ranged between 0.08 and 80 μM log

EC$_{50}$ units. Tables 5-5 & -6 list the averaged predicted activity values for the external data set obtained from the best kNN models. We intentionally selected a series of compounds that have a wide range of predicted activity, paralleling those used in the training and test sets during the model building. This choice will help us to confirm the predictive power of our models in a wider applicability domain. The obtained correlation coefficient R^2 was as high as 0.57 (Figure 5-5). It was interesting to analyze the performance of QSAR models with respect to the congeneric (core structure similar) compounds and novel (core structure different) compounds. With the four congeneric PBTs, the difference in absolute value between the predicted activity and experimental was less than 0.2 for compounds **55**, **56** and **58** and 0.6 for compound **57**. For the eight structurally diverse hits set (Table 5-6), the models performed slightly worse than for the congeneric compounds. Two reasons can be suggested and discussed as follows. 1) The congeneric and the novel hit compounds have high structural dissimilarity. The models are based on the structure-activity data of the training set (congeneric), so the selected descriptors are not sufficient to reliably and accurately predict the activity of external diverse (novel) structures. This problem always exists in statistical modeling, and the final result could be improved by using more descriptors. 2) Since this is a whole cell based assay, activity may be hindered by poor physicochemical properties (solubility, cell membrane transportation, stability, etc.) or metabolic problems, which lead to lower actual activity than predicted in most of the cases. (Compound **68** was an exception; the actual activity was higher than the predicted activity.) Fortunately, the high correlation coefficient (R^2=0.57) demonstrates that our QSAR models are still very robust and predictive for most of both congeneric and novel compound structures and could be used to diversify the chemical repertoire of anticancer agents.
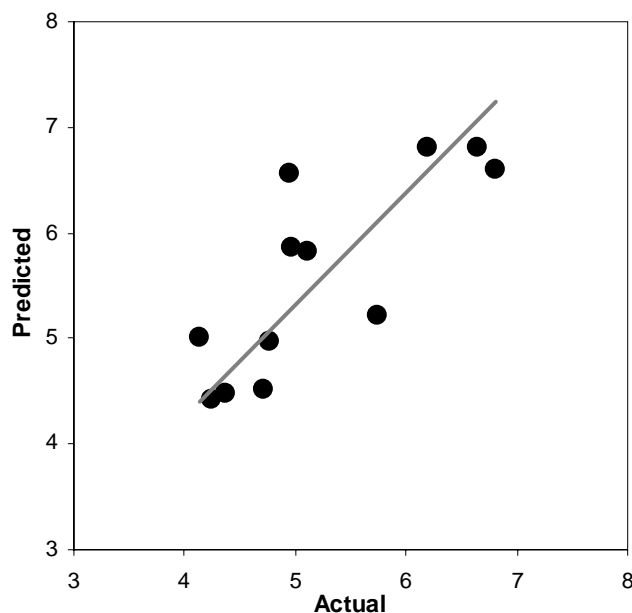
Figure 5-5. Plot of actual versus predicted activity for the screened and the designed compounds. Compounds **60** and **63** were inactive experimentally, so 12 out of 14 compounds were included with consensus prediction based on the 10 best models. $R^2 = 0.57$.
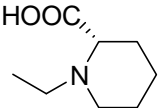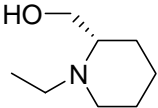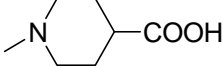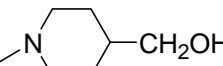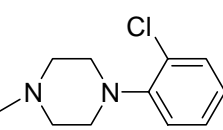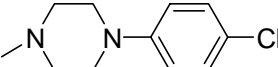
5.5   CONCLUSIONS

Since 1971, our Natural Products Lab at UNC-CH has discovered more than 1,000 new bioactive natural products and their synthetic derivatives. Among them are many anticancer compounds, 100 of which have been chosen by the National Cancer Institute for evaluation. As part of these studies in plant-derived antitumor agents, we initiated the design and synthesis of new tylophorine analogs, because of their profound anticancer activity. These PBTs were newly discovered and developed in our laboratory. The structure of this compound class is still being optimized and a mechanism of action study is in progress. Herein, we report our recent lead optimization using QSAR analysis and database mining. We developed and thoroughly validated QSAR models for a series of PBT derivatives. In
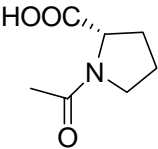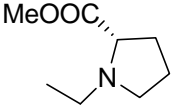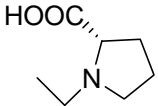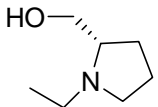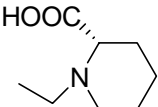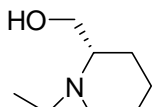
agreement with our expectation, the result showed that this approach could efficiently and successfully generate multiple models with high internal and external accuracy, and these models have been further exploited in database mining for new lead structures. Their high predictive ability allowed the successful virtual screening of a large chemical database with an exceptional high hit rate (80%). Those hits (**68**) lacking a phenanthrine ring but having high activity (EC_{50}=1.8 uM) may in fact lead to a novel structural class of anticancer agents. We believe that this approach should facilitate the design of new natural product analogs as well as the search for new structures with anticancer activity from large chemical databases. On the basis of the current QSAR results and earlier practical SAR trend analysis, a more detailed "pharmacophore" model may be constructed for guiding the further design of new analogs in the future.

Table 5-1. Structure and cytotoxic activity of PBTs (**3-40**) used in model building.
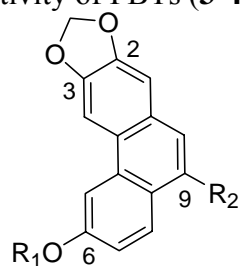
Compound	R_1	R_2	EC$_{50}$ (μM)[a,b]
3	-CH$_3$	-CONH(CH$_2$)$_4$COOH	73.3
4	-CH$_3$	-CH$_2$NH(CH$_2$)$_4$COOMe	25.3
5	-CH$_3$	-CH$_2$NH(CH$_2$)$_4$COOH	1.3
6	-CH$_3$	-CH$_2$NH(CH$_2$)$_4$CH$_2$OH	0.27
7	-CH$_3$	-CONH(CH$_2$)$_5$COOH	27
8	-CH$_3$	- CH$_2$NH(CH$_2$)$_5$COOMe	18
9	-CH$_3$	- CH$_2$NH(CH$_2$)$_5$COOH	0.8
10	-CH$_3$	- CH$_2$NH(CH$_2$)$_5$CH$_2$OH	0.2
11	-CH$_3$		5.3
12	-CH$_3$		73.8
13	-CH$_3$		2.1
14	-CH$_3$		0.7

15	-CH$_3$	(1-ethylpiperidine-2-carboxylic acid, HOOC)	0.5
16	-CH$_3$	(1-ethyl-2-(hydroxymethyl)piperidine, HO)	0.16
17	-CH$_3$	(1-methylpiperidine-4-carboxylic acid, —COOH)	0.23
18	-CH$_3$	(1-methyl-4-(hydroxymethyl)piperidine, —CH$_2$OH)	0.08
19	-CH$_3$	(1-methyl-4-(2-chlorophenyl)piperazine, Cl)	33.8
20	-CH$_3$	(1-methyl-4-(4-chlorophenyl)piperazine, Cl)	65.2
21	-CH$_3$	- CH$_2$NH(CH$_2$)$_{10}$COOH	3.2
22	-CH$_3$	- CH$_2$NH(CH$_2$)$_{10}$CH$_2$OH	2.6
23	-CH$_2$C$_6$H$_5$	-CONH(CH$_2$)$_5$COOMe	41.2
24	-CH$_2$C$_6$H$_5$	-CONH(CH$_2$)$_5$COOH	41.2
25	-CH$_2$C$_6$H$_5$	-CH$_2$NH(CH$_2$)$_5$COOH	1.6

26	-CH$_2$C$_6$H$_5$	-CH$_2$NH(CH$_2$)$_5$CH$_2$OH	1.1
27	-CH$_2$C$_6$H$_5$	-CH$_2$NH(CH$_2$)$_4$COOMe	17.0
28	-CH$_2$C$_6$H$_5$	-CH$_2$NH(CH$_2$)$_4$COOH	2.2
29	-CH$_2$C$_6$H$_5$		42.6
30	-CH$_2$C$_6$H$_5$		32.1
31	-CH$_2$C$_6$H$_5$		4.4
32	-CH$_2$C$_6$H$_5$		1.8
33	-CH$_2$C$_6$H$_5$		3.2
34	-CH$_2$C$_6$H$_5$		1.3
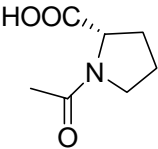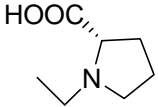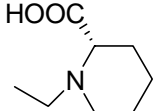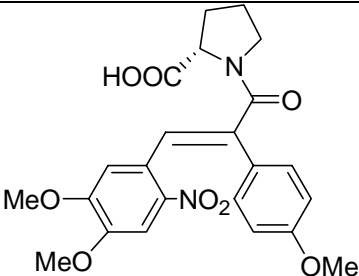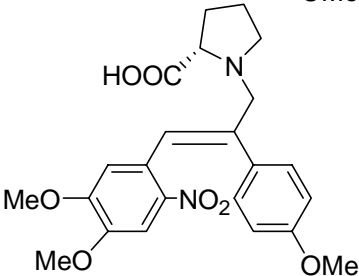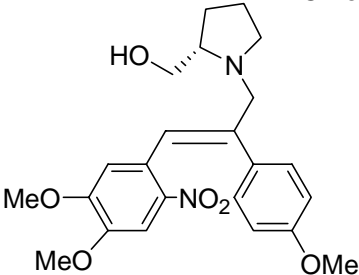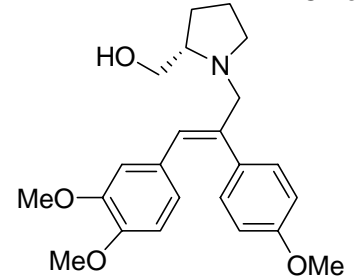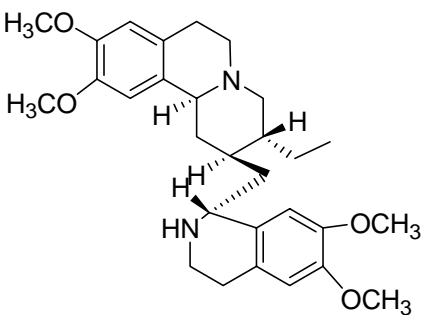
35	-CH$_2$C$_6$H$_5$	-CONH(CH$_2$)$_5$COOMe	41.2
36	-CH$_2$C$_6$H$_5$	-CONH(CH$_2$)$_5$COOH	41.2
37	-CH$_2$C$_6$H$_5$	-CH$_2$NH(CH$_2$)$_5$COOH	1.6
38	-H		39.7
39	-H		41.2
40	-H		39.7

Table 5-2. Structure and cytotoxic activity of PBTs (**41-48**) used in model building.
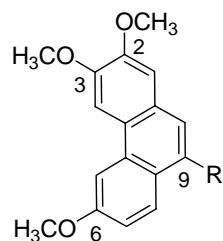
Compound	R	EC_{50} (µM)
41	-NH(CH$_2$)$_{10}$COOH	13.0
42	-NH(CH$_2$)$_{10}$CH$_2$OH	3.6
43	-CH$_2$NH(CH$_2$)$_5$COOH	9.7
44	-CH$_2$NH(CH$_2$)$_5$CH$_2$OH	2.7
45		9.7
46		6.3
47		19.2
48		2.4

Table 5-3. Structure and cytotoxic activity of PBTs (**49-54**) used in model building.

Compound	Structure	EC$_{50}$ (μM)
49		80
50		45.2
51		11.7
52		52.2
53		0.02

54
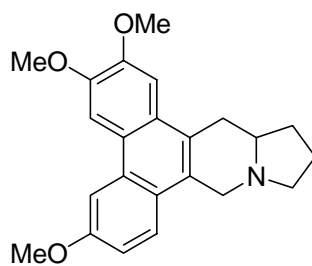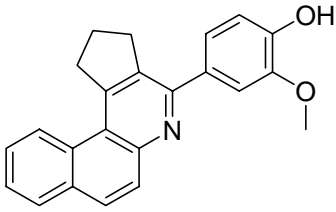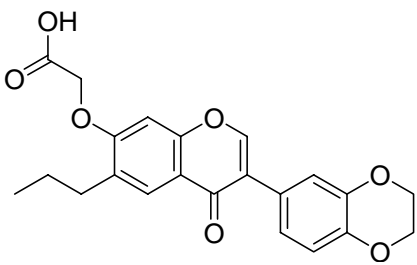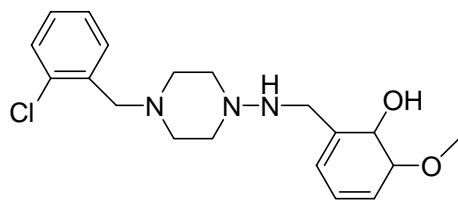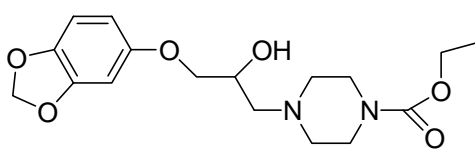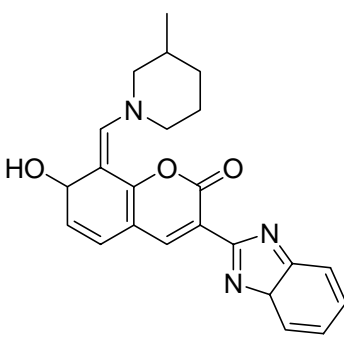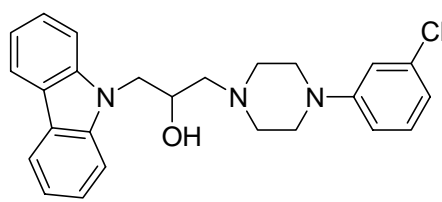
0.008

Table 5-4. Ten best kNN QSAR models.

Models	Test Sets	Training Sets	Number of Descriptors	q^2	R^2
1	8	44	15	0.52	0.75
2	11	41	20	0.53	0.8
3	12	40	10	0.72	0.71
4	12	40	15	0.72	0.72
5	14	38	10	0.56	0.77
6	14	38	20	0.51	0.81
7	14	38	15	0.58	0.81
8	14	38	15	0.54	0.79
9	18	34	20	0.59	0.81
10	20	32	15	0.55	0.73

Table 5-5. Structure and cytotoxic activity for compounds (**59-68**) from ChemDiv.

No	Structure	ChemDiv ID #	Actual Activity $EC_{50, uM}$	Actual Activity $-logEC_{50}$	Predicted Activity $-logEC_{50}$
59		1661-1313	10.9	4.959164	5.8601
60		2188-3298	N/A	N/A	4.993
61		3253-1073	19.3	4.714376	4.521778
62		3346-2033	42.6	4.370451	4.4711
63		3570-0022	N/A	N/A	5.7561
64		4106-0061	7.9	5.104735	5.8307
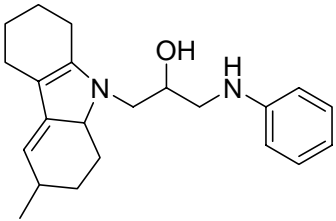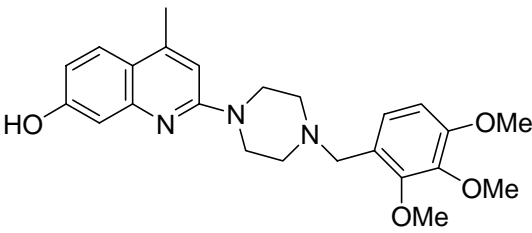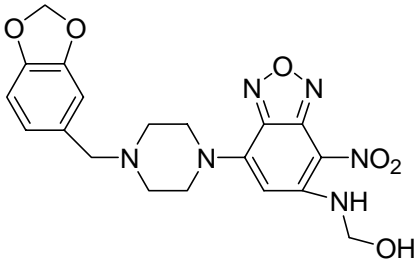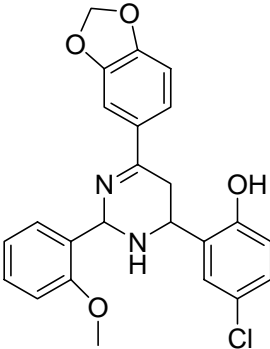
65		6658-0014	11.1	4.955545	6.5566
66		C614-0150	17.3	4.763018	4.969401
67		K901-0689	72.4	4.140272	5.0105
68		K915-0700	1.8	5.737391	5.210599

Table 5-6. Structure and cytotoxic activity for PBTs (**55-58**) in external set.
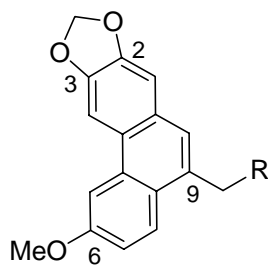
Compound	R	Actual Activity (EC_{50}, uM)	Actual Activity ($-\log EC_{50}$)	Predicted Activity ($-\log EC_{50}$)
55		0.22	6.645422	6.807934
56		0.63	6.197556	6.808
57		57.1	4.243534	4.416317
58		0.15	6.816241	6.604551

5.6   REFERENCES

1) Dietrich, S. W.; Dreyer, N. D.; Hansch, C.; Bentley, D. L. Confidence-interval estimators for parameters associated with quantitative structure-activity-relationships. *J. Med. Chem.* **1980**, *23*, 1201-1205.

2) Hadjipavloulitina, D.; Hansch, C. Quantitative structure-activity-relationships of the benzodiazepines - A review and reevaluation. *Chem. Rev.* **1994**, *94*, 1483-1505.

3) Hansch, C.; Muir, R. M.; Fujita, T.; Maloney, P. P.; Geiger, E.; Streich, M. The correlation of biological activity of plant growth regulators and chloromycetin derivatives with Hammett constants and partition coefficients. *J. Am. Chem. Soc.* **1963**, *85*, 2817-2824.

4) Hansch, C.; Kurup, A.; Garg, R.; Gao, H. Chem-bioinformatics and QSAR: a review of QSAR lacking positive hydrophobic terms. *Chem. Rev.* **2001**, *101*, 619-672.

5) Hansch, C.; Leo, A.; Mekapati, S. B.; Kurup, A. Qsar and Adme. *Bioorg. Med. Chem.* **2004**, *12*, 3391-3400.

6) Klein, T. E.; Huang, C.; Ferrin, T. E.; Langridge, R.; Hansch, C. Computer-assisted drug receptor mapping analysis. *ACS Symposium Series* **1986**, *306*, 147-158.

7) Kubinyi, H. Quantitative relationships between chemical-structure and biological-cctivity. *Chemie in Unserer Zeit* **1986**, *20*, 191-202.

8) Kubinyi, H. QSAR and 3D QSAR in drug design .1. Methodology. *Drug Discovery Today* **1997**, *2*, 457

9) Kurup, A.; Mekapati, S. B.; Garg, R.; Hansch, C. HIV-1 protease inhibitors: a comparative QSAR analysis. *Curr. Med. Chem.* **2003**, *10*, 1679-1688.

10) Zheng, W.; Tropsha, A. A novel variable selection QSAR approach based on the K-nearest neighbor principle. *J. Chem. Inf. Comput. Sci.* **2000**, *40*, 185-194.

11) Tropsha, A.; Cho, S. J.; Zheng, W. "New tricks for an old dog": development and application of novel QSAR methods for rational design of combinatorial chemical libraries and database mining. In *Rational Drug Design: Novel Methodology and Practical Applications*; ACS Symposium Series 719; Parrill, A. L., Reddy, M. R., Eds.; American Chemical Society: Washington, DC, **1999**. 198-211

12) Shen, M.; LeTiran, A.; Xiao, Y.; Golbraikh, A.; Kohn, H.; Tropsha, A. Quantitative structure-activity relationship analysis of functionalized amino acid anticonvulsant agents using k nearest neighbor and simulated annealing PLS methods. *J. Med. Chem.* **2002**, *45*, 2811-2823

13) Shen, M.; Beguin, C.; Golbraikh, A.; Stables, J; Kohn, H.; Tropsha, A. Application of predictive QSAR models to database mining: identification and experimental validation of novel anticonvulsant compounds. *J. Med. Chem.* **2004**, *47*, 2356-2364

14) Oloff, S.; Mailman, R; Tropsha, A. Application of validated QSAR Models of D1 dopaminergic antagonists for database mining. *J. Med. Chem.* **2005**, *48*, 7322-7332

15) EduSoft, LLC. MolconnZ, version 4.05; http://www.eslc.vabiotech.com/ [4.05], 2003.

16) Golbraikh, A.; Tropsha, A. Beware of q2! *J. Mol. Graphics Modell.* **2002**, *20*, 269-276.

17) ChemDiv. http://www.chemdiv.com . 2005.

18) Rubinstein, L. V.; Shoemaker, R. H.; Paull, K. D.; Simon, R. M.; Tosini, S.; Skehan, P.; Scudiero, D. A.; Monks, M. R. Comparison of in vitro anticancer-drug-screening data generated with a tetrazolium assay versus a protein assay against a diverse panel of human tumor cell lines. *J. Natl. Cancer Inst.* **1990**, *82*, 1113-1118.

19) Available from Tripos Inc. Sybyl User's Manual, version 7.8; Tripos, Inc.: St. Louis, MO, 2002.

20) Kier, L. B.; Hall, L. H. *Molecular Connectivity in Chemistry and Drug Research*; Academic Press: New York, **1976**.

21) Basak, S. C.; Mills, D. Prediction of mutagenicity utilizing a hierarchical QSAR approach. *SAR QSAR Environ. Res.* **2001,** 1*2,* 481-496.

22) Benigni, R.; Giuliani, A.; Franke, R.; Gruska, A. Quantitative structure-activity relationships of mutagenic and carcinogenic aromatic amines. *Chem. Rev.* **2000,** *100,* 3697-3714.

23) Cronin, M. T.; Dearden, J. C.; Duffy, J. C.; Edwards, R.; Manga, N.; Worth, A. P.; Worgan, A. D. The importance of hydrophobicity and electrophilicity descriptors in mechanistically-based QSARs for toxicological endpoints. *SAR QSAR Environ. Res.* **2002,** 1*3,* 167-176.

24) Fan, Y.; Shi, L. M.; Kohn, K. W.; Pommier, Y.; Weinstein, J. N. Quantitative structure-antitumor activity relationships of camptothecin analogues: cluster analysis and genetic algorithm-based studies. *J. Med. Chem.* **2001,** *44*, 3254-3263.

25) Girones, X.; Gallegos, A.; Carbo-Dorca, R. Modeling antimalarial activity: application of kinetic energy density quantum similarity measures as descriptors in QSAR. *J. Chem. Inf. Comput. Sci.* **2000,** *40*, 1400-1407.

26) Moss, G. P.; Dearden, J. C.; Patel, H.; Cronin, M. T. Quantitative structure-permeability relationships (QSPRs) for percutaneous absorption. *Toxicol. In Vitro.* **2002,** *16*, 299-317.

27) Randic, M.; Basak, S. C. Construction of high-quality structure-property-activity regressions: the boiling points of sulfides. *J. Chem. Inf. Comput. Sci.* **2000,** *40*, 899-905.

28) Suzuki, T.; Ide, K.; Ishida, M.; Shapiro, S. Classification of environmental estrogens by physicochemical properties using principal component analysis and hierarchical cluster analysis. *J. Chem. Inf. Comput. Sci.* **2001,** *41*, 718-726.

29) Trohalaki, S.; Gifford, E.; Pachter, R. Improved QSARs for predictive toxicology of halogenated hydrocarbons. *Comput. Chem.* **2000,** *24*, 421-427.

30) Wang, X.; Yin, C.; Wang, L. Structure-activity relationships and response-surface analysis of nitroaromatics toxicity to the yeast (*Saccharomyces cerevisiae*). *Chemosphere.* **2002,** *46*, 1045-1051.

31) Kubinyi, H.; Hamprecht, F. A.; Mietzner, T. Three-dimensional quantitative similarity-activity relationships (3D QSiAR) from SEAL similarity matrices. *J. Med. Chem.* **1998,** *41*, 2553-2564.

32) Golbraikh, A.; Tropsha, A. Predictive QSAR modeling based on diversity sampling of experimental datasets for the training and test set selection. *J. Comput. Aided Mol. Des.* **2002,** *16*, 357-369.

33) Sharaf, M. A.; Illman, D. L.; Kowalski, B. R. *Chemometrics*; John Wiley & Sons: New York, **1986**.

34) Wold, S. a. E. L. Statistical Validation of QSAR Results. In *Chemometrics Methods in Molecular Design*; van de Waterbeemd, H., Ed.; VCH: Weinheim, Germany, **1995**; pp 309-318.

35) Tropsha, A.; Gramatica, P.; Gombar, V. K. The importance of being earnest: validation is the absolute essential for successful application and interpretation of QSPR models. *QSAR Comb. Sci.* **2003**, *22*, 69-77.

36) Wu, P. L.; Rao K. V.; Su, C.-H.; Kuoh, C.-S.; Wu, T.-S. Phenanthroindolizidine alkaloids and their cytotoxicity from the leaves of *Ficus septica*. *Heterocycles* **2002**, 57, 2401-2408.

CHAPTER VI. ADME EVALUATION AND MODE OF ACTION STUDY

ADME EVALUATION

6.1   INTRODUCTION

Compound toxicity plays a key role in determining success in drug development,[*] and 50% of drug failures are attributed to ADME-Tox issues. Thus, it is critical to accurately predict these properties earlier in the investigation of a lead to assure appropriate selection in the drug development process. New prediction techniques and technologies are making it possible to more quickly eliminate compounds that are most likely to exhibit ADME or toxicity problems, and provide ways for researchers to still arrive at correct conclusions, but in less time. The more attractive compounds can then be put on the development fast track, saving time and money. Therefore, an ADME prediction program (http://preadme.bmdrc.org), which uses an artificial neural network with back-propagation method, was used to predict blood brain barrier (BBB) permeability, human intestinal absorption (HIA) and protein binding percentage of PBTs that hold promise for improving the selection of potent, on-target leads with fewer negative side-effects.

---

[*] As we mentioned earlier, in the early 1960s drug development of tylocrebrine was terminated due to its significant CNS toxicity manifested as disorientation and ataxia[1].

6.2 METHODOLOGY

6.2.1 Prediction of CNS Toxicity

An ADME prediction model (http://preadme.bmdrc.org), which uses an artificial neural network with back-propagation method, was used to predict the BBB permeability of selected compounds in comparison with their parent *tylophora* alkaloids. This model contains over 15,000 CNS active compounds and 50,000 CNS inactive compounds, and each molecule is describable by 7 1D descriptors and 166 2D descriptors. This model was validated by a database of 275 known CNS active compounds. The accuracy of the prediction was 92%. Therefore, it is a reliable filter to screen potential candidate compounds for CNS toxicity.[2]

6.2.2 Prediction of Human Intestinal Absorption[3-4] and Plasma Protein Binding[5]

An ADME prediction model (the same as above) was also used to predict the human intestinal absorption and plasma protein binding of selected compounds in comparison with their parent *tylophora* alkaloids.

6.2.3 Results and Discussion

The predicted ADME values of four PBTs (**1-4**) and three parent *tylophora* alkloids are shown in Table 6-1. Preliminary data indicated that all PBT compounds should be well absorbed in the human intestine (HIA ≥92.5%). In addition, the four PBTs showed lower predicted brain/blood concentration ratios ($C_{brain}/C_{blood} = 1$) than the tylophora alkloids, indicating that less PBT compound would penetrate the blood brain barrier (BBB) and, thus, the probability of CNS toxicity would be low. In contrast, the high predicted ratio (8.3) of tylocrebrine indicated a high probability of compound BBB entry, which would readily

explain its clinical CNS toxicity. In addition, the PBTs were predicted to have higher protein

bound constants (76%-90%) than the *tylophora* alkaloids (74%-78%). This parameter is a

favorable pharmacokinetic property for drug development. In summary, PBTs have better

predicted ADME profiles than *tylophora* alkaloids in our preADME screen.
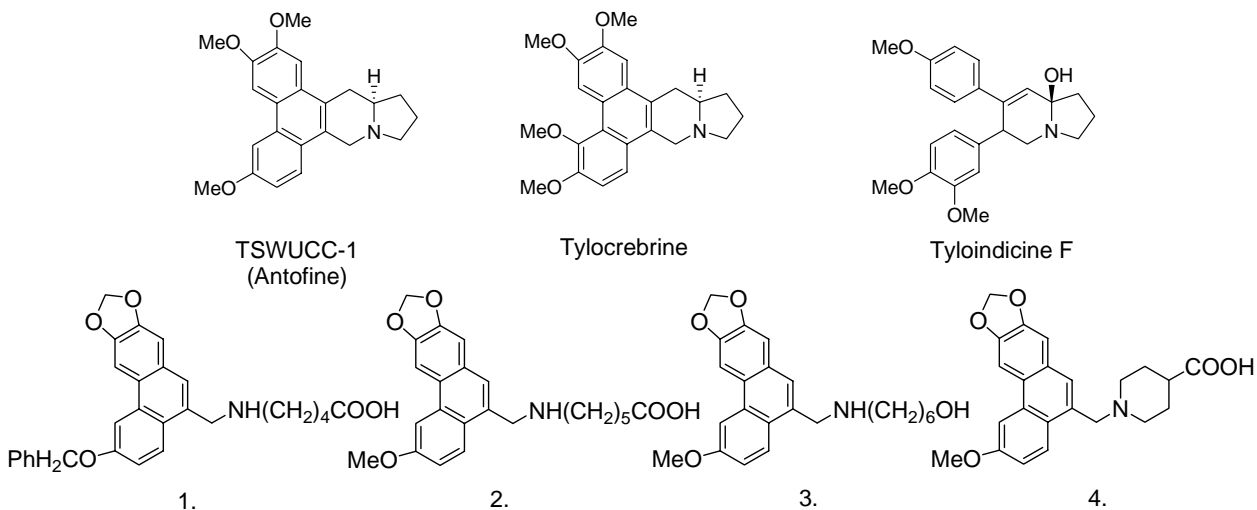
Figure 6-1. Structure of tylophora alkloids and PBTs (**1-4**) selected for ADME prediction.

Table 6-1. ADME predictions of human intestinal absorption, blood brain barrier penetration, and protein binding of PBT compounds vs *tylophora* alkaloids.

Compound	BBB permeability (C_{brain}/C_{blood})	HIA (%)	Plasma Protein Binding (%)
***Tylophora* Alkaloids**			
Antofine	11.7	94.2	74.9
Tyloindicine F	4.5	91.7	77.9
Tylocrebrine	8.3	93.9	74.0
PBTs			
1.	0.61	93.6	85.7
2.	1.0	93.8	89.8
3.	2.7	92.5	84.4
4.	1.6	93.5	75.7

MODE OF ACTION STUDY

6.3   INTRODUCTION

Prior evaluation of (+)-(S)-tylophorine and its analogs in the antitumor screen at the National Cancer Institute showed a uniform and potent inhibitory effect on cancer cell growth ($GI_{50} \approx 10^{-8}$ M) in all 60 cell lines with notable selectivity toward several refractory cell lines including melanoma and lung tumor cell lines.[6] Earlier studies in the 1960s demonstrated that the mechanism of antitumor activity of tylophorine alkaloids was to irreversibly inhibit protein synthesis at the elongation stage of translation.[7-11] However, comprehensive evaluation of antitumor potential has not been reported, and the mechanisms of cell growth inhibition are largely unknown. In the 1990s, several key regulators of signaling transduction were reported as the biological targets of tylophorine alkaloids including thymidylate synthase (TS)[12,13] and dihydrofolate reductase.[14] In addition, these compounds were also found to induce cell apoptosis.[15] Most recently, Gao et al.[16] demonstrated that the tylophorine analogs have significant inhibitory effects on NF-kB mediated transcription. These recent discoveries emphasize the great potential of developing tylophorine derivatives into a new antitumor drug class with a unique mode of action. In this study, we have reported the discovery of novel phenanthrene-based tylophorine (PBT) derivatives with profound inhibition against several human cancer cell lines. However, the biological target of this class of novel compounds has not been identified. Further screening against more cancer-related cell lines will facilitate our understanding of the specific targets of this new compound class and provide insight into definitive structure-activity relationships.

Selected interesting compounds were sent for additional screening at collaborative laboratories, including NCI-DTP, MD Anderson Cancer Center, Dr. M. Jarstfer's Laboratory at UNC-CH, and MDS Pharma Services -Taiwan Ltd. The major findings of these screens are given below.

6.4   NCI-DTP HUMAN TUMOR CELL LINES SCREENING ([17-19]):

The In Vitro Cell Line Screening Project (IVCLSP) is a dedicated service providing direct support to the DTP anticancer drug discovery program. This project utilizes 59 different human tumor cell lines, representing leukemia, melanoma and cancers of the lung, colon, brain, ovary, breast, prostate, and kidney. The aim is to prioritize synthetic compounds or natural product samples, which show selective growth inhibition or cell killing of particular tumor cell lines, for further evaluation. This screen is unique in that the complexity of a 59 cell line dose response produced by a given compound results in a biological response pattern that can be utilized in pattern recognition algorithms. Using these algorithms, it is possible to assign a putative mechanism of action to a test compound, or to determine that the response pattern is unique and not similar to that of any of the standard prototype compounds included in the NCI database. In addition, following characterization of various cellular molecular targets in the 59 cell lines, it may be possible to select compounds most likely to interact with a specific molecular target.

6.4.1 Methodology of the In Vitro Cancer Screen

The human tumor cell lines of the cancer screening panel are grown in RPMI 1640 medium containing 5% fetal bovine serum and 2 mM L-glutamine. For a typical screening experiment, cells are inoculated into 96 well microtiter plates in 100 µL at plating densities

ranging from 5,000 to 40,000 cells/well depending on the doubling time of individual cell lines. After cell inoculation, the microtiter plates are incubated at 37° C, 5 % CO2, 95 % air and 100 % relative humidity for 24 h prior to addition of experimental drugs.

After 24 h, two plates of each cell line are fixed *in situ* with TCA, to represent a measurement of the cell population for each cell line at the time of drug addition (Tz). Experimental drugs are solubilized in dimethyl sulfoxide at 400-fold the desired final maximum test concentration and stored frozen prior to use. At the time of drug addition, an aliquot of frozen concentrate is thawed and diluted to twice the desired final maximum test concentration with complete medium containing 50 µg/ml gentamicin. Four additional 10-fold or ½ log serial dilutions are made to provide a total of five drug concentrations plus control. Aliquots of 100 µl of these different drug dilutions are added to the appropriate microtiter wells already containing 100 µl of medium, resulting in the required final drug concentrations.

Following drug addition, the plates are incubated for an additional 48 h at 37°C, 5% CO2, 95% air, and 100% relative humidity. For adherent cells, the assay is terminated by the addition of cold TCA. Cells are fixed *in situ* by the gentle addition of 50 µl of cold 50% (w/v) TCA (final concentration, 10% TCA) and incubated for 60 minutes at 4°C. The supernatant is discarded, and the plates are washed five times with tap water and air dried. Sulforhodamine B (SRB) solution (100 µl) at 0.4 % (w/v) in 1 % acetic acid is added to each well, and plates are incubated for 10 minutes at room temperature. After staining, unbound dye is removed by washing five times with 1% acetic acid and the plates are air dried. Bound stain is subsequently solubilized with 10 mM trizma base, and the absorbance is read on an automated plate reader at a wavelength of 515 nm. For suspension cells, the

methodology is the same except that the assay is terminated by fixing settled cells at the bottom of the wells by gently adding 50 μl of 80 % TCA (final concentration, 16 % TCA). Using the seven absorbance measurements [time zero, (Tz), control growth, (C), and test growth in the presence of drug at the five concentration levels (Ti)], the percentage growth is calculated at each of the drug concentrations levels. Percentage growth inhibition is calculated as:

[(Ti-Tz)/(C-Tz)] x 100 for concentrations for which Ti$\geq$Tz

[(Ti-Tz)/Tz] x 100 for concentrations for which Ti<Tz.

Three dose response parameters are calculated for each experimental agent. Growth inhibition of 50% (GI_{50}) is calculated from [(Ti-Tz)/(C-Tz)] $\times$ 100 = 50, which is the drug concentration resulting in a 50% reduction in the net protein increase (as measured by SRB staining) in control cells during the drug incubation. The drug concentration resulting in total growth inhibition (TGI) is calculated from Ti = Tz. The LC_{50} (concentration of drug resulting in a 50% reduction in the measured protein at the end of the drug treatment as compared to that at the beginning) indicating a net loss of cells following treatment is calculated from [(Ti-Tz)/Tz] $\times$ 100 = -50. Values are calculated for each of these three parameters if the level of activity is reached; however, if the effect is not reached or is exceeded, the value for that parameter is expressed as greater or less than the maximum or minimum concentration tested.

6.4.2 Results and Discussion

Totally, 22 active compounds were sent to NCI-DTP and all were identified as new chemical entities with anticancer activity. The biological study is still ongoing.

6.5   MD ANDERSON CANCER CENTER:

As a primary assay to examine the effect of the compounds on cell growth, the metabolic activity of living cells treated with eight selected compounds (Figure 6.2) was measured by the MTT assay (see section 6.5.1). A panel of pancreatic cancer cells, namely BXPC-3, Panc-1, and Capan-2, as well as an immortalized cell line derived from normal pancreatic epithelium, E6E7, were tested in the assay. Among these cell lines, BXPC-3 was the most sensitive cell line to most compounds tested, while Capan-2 was the most resistant. The data are summarized in section 6.5.2 and Figures 6.3 – 6.8.

6.5.1   Methodology of MTT Assay

The MTT assay[20] was used to access the killing effect of the drugs. Cells were seeded into 96 well plates at a density of 6000 cells in 50 μl of media per well. The drug was dissolved in DMSO at a stock concentration of 0.01 M and then diluted in culture media to give different drug concentrations for testing in duplicates. The amount of DMSO was equalized for all of the wells and the total volume of media containing the drug was 50μl. After 72 hours of incubation at 37 °C in 5% CO_2, 25μl of MTT [3-(4,5-dimethylthiazol-2-yl)-2,5-diphenyl tetrazolium bromide] reagent was added to each well and incubated for two hours. Then 100 μl of cell lysis buffer was added and incubation was continued overnight. The plates were then read on a plate reader at OD 570. The cell killing efficiency was determined by plotting the percent of survival cells with different concentrations of the compounds in the same family, which were tested side-by-side. The MTT reading derived from the cells treated by DMSO only was set as 100%.

6.5.2 Results and Discussion

The following observations are of particular interest from the screening results. WLY-WP 5COOH displayed better killing in the pancreatic cancer cell line (panc-1) compared with the "normal" pancreatic line (E6E7), specifically at 10-20 µM (Figure 6.3). WLY-Waisp-OH showed a similar difference between pancreatic cancer and "normal" cells (Figure 6.4). These observations will be confirmed by using more pancreatic cancer cell lines and fine-tuning the doses used. WLY-WP5OH had outstanding general cytotoxicity (Figure 6.5), which will be useful information for future SAR study of this series. WLY-WHP-6COOH had a stronger cytotoxic effect against MCF-7 cells compared with MCF-10A, "normal" breast cells (Figure 6.6). This observation will also be confirmed later.

Compounds WLY-Wa4, WLY-WaispOH, WLY-WaLP6OH, and WLY-Wac6OH strongly inhibited cell survival and showed similar activity trends against four cell lines, E6E7, Panc-1, Capan-2, and CxPC-3 (Figures 6.7 and 6.8). While most cell lines exhibited significant sensitivity to these compounds, the Capan-2 cancer cell line was relatively resistant, with WaispOH having the strongest toxicity (Figure 6.8). However, lack of specificity is a major concern as the "normal cell" control E6E7 was quite sensitive to compound treatment (Figure 6.7). It remains possible that E6E7 does not represent the real situation in normal pancreas tissue and, therefore, is not the ideal control.

WLY-Wp5OH   WLY-Wp5COOH   WLY-Wp6COOH   WLY-WHp6COOH

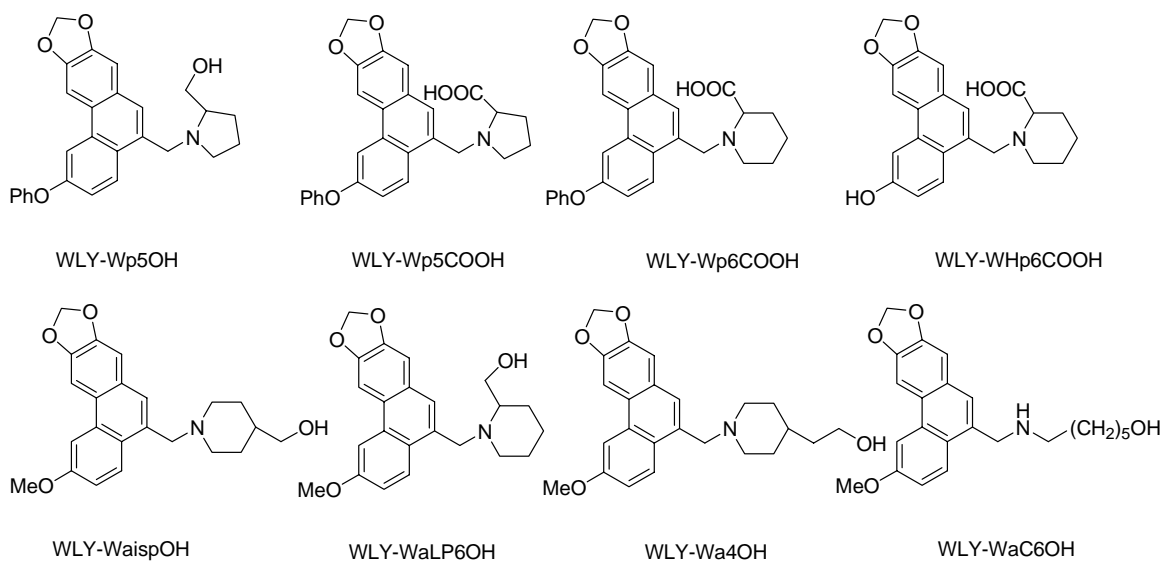WLY-WaispOH   WLY-WaLP6OH   WLY-Wa4OH   WLY-WaC6OH

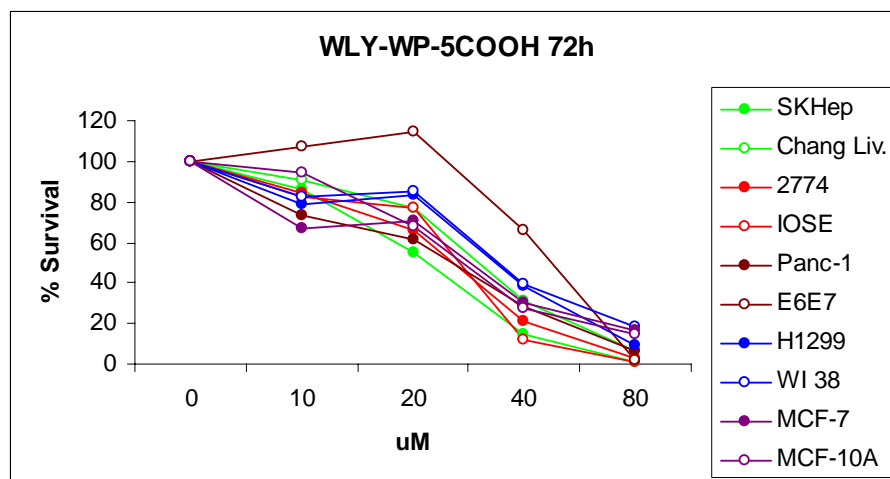Figure 6-2. Structure of WLY-series tested at MD Anderson Cancer Center

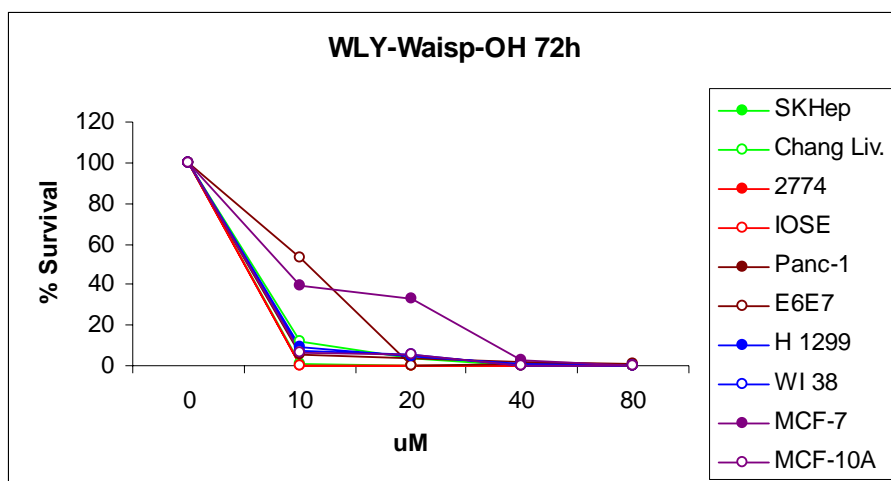Figure 6-3. MD Anderson Screening Data – Inhibition of Compound WP6COOH

Figure 6-4. MD Anderson Screening Data – Inhibition of Compound WaispOH
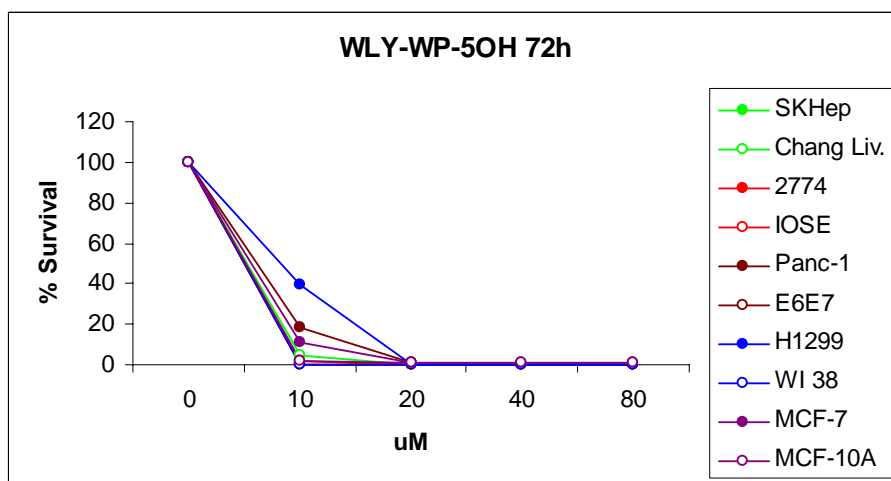

Figure 6-5. MD Anderson Screening Data – Inhibition of WP5OH
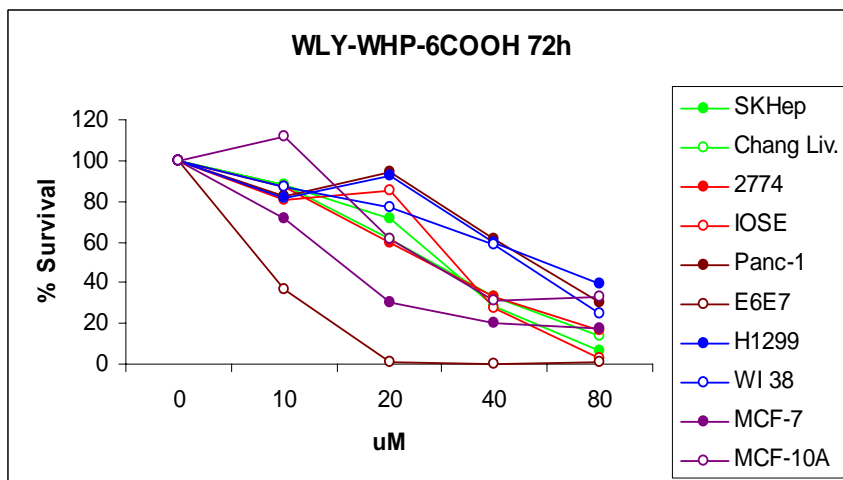

Figure 6-6. MD Anderson Screening Data – Inhibition of WHP6COOH
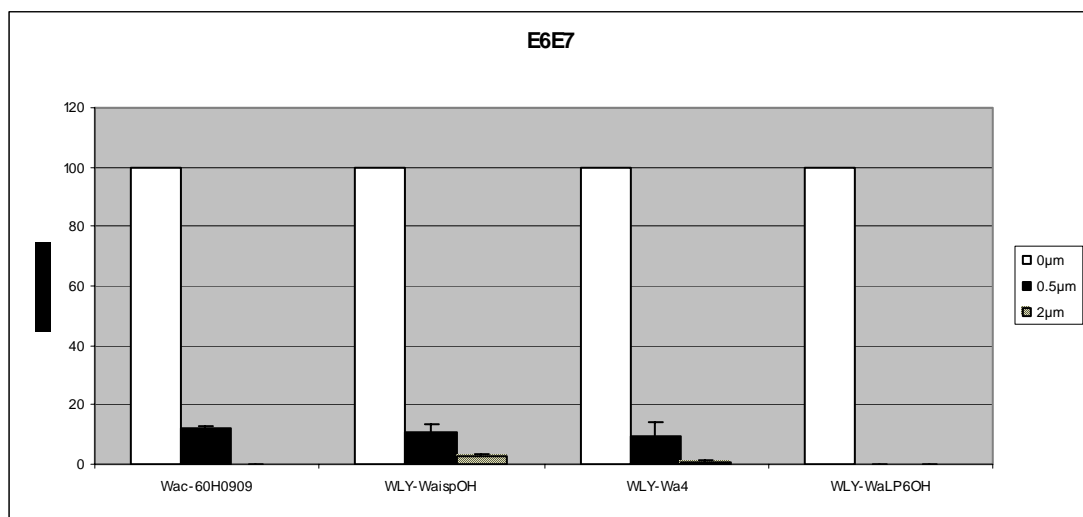
Figure 6-7. MD Anderson Screening Data – Inhibition of Compounds WaC6OH, WaispOH, Wa4OH and WaLP6OH at 0, 0.5, and 2 μM
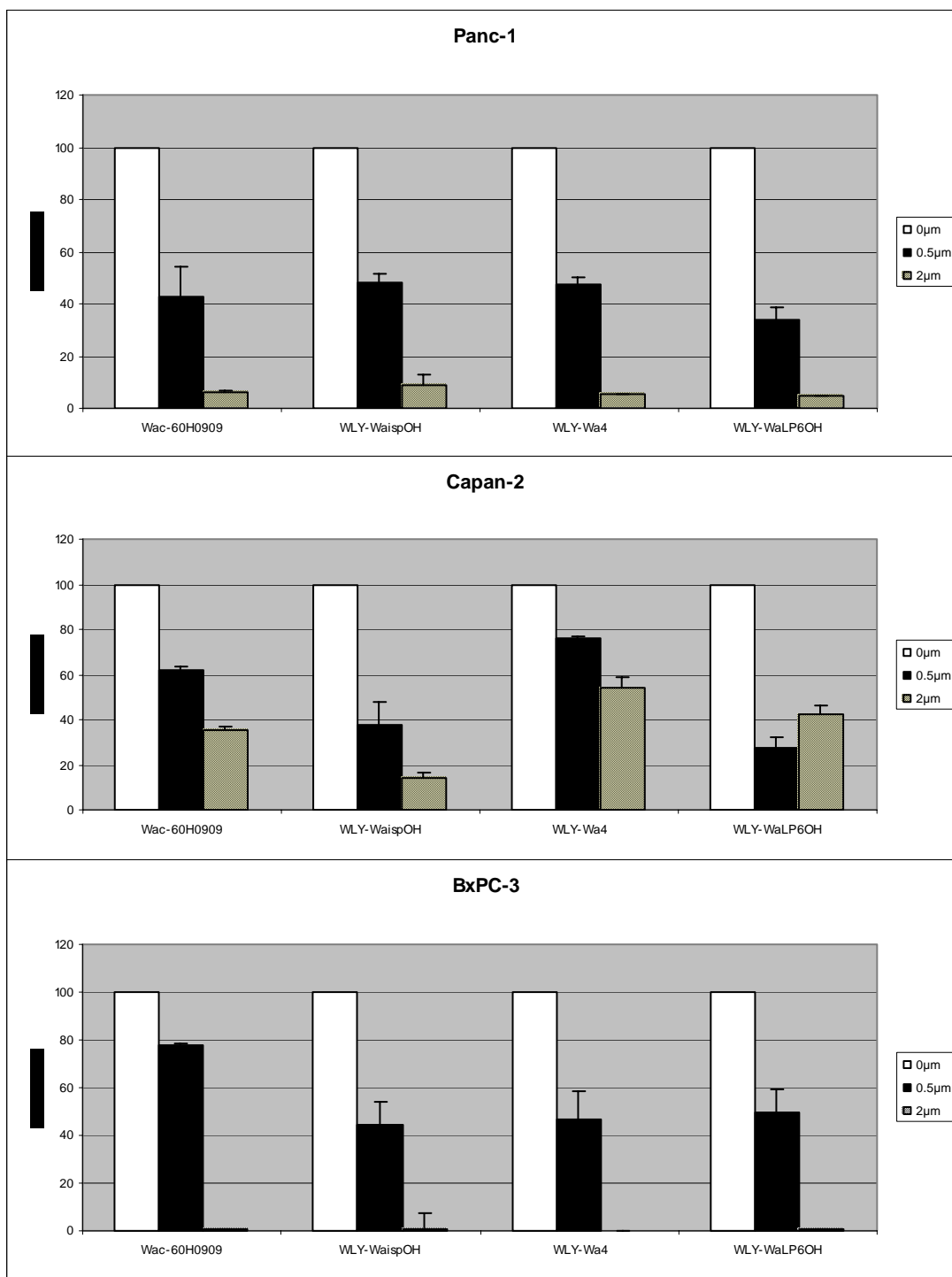
Figure 6-8. MD Anderson Screening Data – Inhibition of Compounds WaC6OH, WaispOH, Wa4OH and WaLP6OH at 0, 0.5, and 2 μM

6.6 ANTI-TELOMERASE ASSAY

Eukaryotic chromosomes end in DNA-protein complexes called telomeres, which function as protective caps that prevent nucleolytic degradation, end-to-end fusions, and aberrant recombination. In the absence of properly capped telomeres, cells are not able to divide thus either becoming senescent or undergoing apoptosis. Human telomeric DNA is composed of G-rich repeated sequences, (TTAGGG), which are not replicated efficiently by the normal DNA replication machinery because of the end-replication problem.[21] Instead, the G-rich strand of telomeric DNA is maintained by a RNA-dependent DNA polymerase called telomerase. Telomerase is a ribonucleoprotein complex that acts as a reverse transcriptase in the maintenance of chromosome ends, therefore preventing cell programmed death.[22] The minimally active human telomerase complex is composed of hTERT, a catalytic protein subunit, and hTR, a RNA subunit, which supply the template for telomeric DNA synthesis.[23-26] Telomerase activity is usually not present in most normal cells, but it is seen in cancerous and some precancerous cells. The maintenance of telomeric DNA is vital for tumor growth, and telomerase-mediated telomere extension is required for the growth of >90% of all cancers.[27] When telomerase is inhibited in positive cancer cell lines, telomere extension is disrupted leading to senescence or apoptosis.

Telomerase requires the proper association of hTERT and hTR to form an active complex. Dr. M. Jarstfer (UNC-CH) uses a telomerase assemblage assay to test if small molecules affect telomerase activity by preventing telomerase assemblage. Recombinant telomerase is assembled in rabbit reticulocyte lysates (RRL), followed by a direct assay for telomerase activity that follows extension of a telomeric primer using [α-^{32}P]-dGTP as one of the substrates.

6.6.1 Methods

In Vitro Transcription and Purification of hTR.[28] A total of 15 μg of phTR+HH was linearized by digestion with Fok-1 followed by extraction with phenol/chloroform/isoamyl alcohol, precipitation with ethanol, and resuspension in a suitable volume of TE (10 mM Tris-HCl, pH 7.5, and 1 mM EDTA). In vitro transcription was carried out at 37 °C for 18 h using the linearized DNA, 0.32 units/μL T7 RNA polymerase (Promega), 1× transcription-optimized buffer (Promega), 10 mM DTT, 0.8 units/μL RNasin (Fisher Scientific), 5 mM MgCl$_2$, and 1 mM each NTP. After transcription, the magnesium-inorganic diphosphate complexes were removed by centrifugation for 2 min at 22000g. Cleavage by the hammerhead ribozyme was initiated by the addition of MgCl$_2$ to a final concentration of 12 mM followed by incubation at 45 °C for 1 h. The entire reaction was then treated with 15 units of RQ1-DNase (Promega) for 20 min at 37 °C followed by extraction with phenol/chloroform/isoamyl alcohol and ethanol precipitation. The RNA was resuspended in a suitable volume of denaturing loading buffer (7 M urea/10% glycerol/1× TBE) and purified on a 4% denaturing polyacrylamide gel. The RNA was recovered using a modified version of the "crush and soak" method.[28] Briefly, the RNA was located in the gel by UV shadowing, cut out, crushed by passing through a sterile plastic syringe, and extracted into 2 vol of 1× TEN (10 mM Tris-HCl, pH 7.5, 1 mM EDTA, and 200 mM NaCl) at 4 °C for 16 h. After centrifugation, the supernatant was collected and a second extraction was performed with 2 vol of 1× TEN at room temperature for 1 h. The combined supernatants were filtered through a Whatman GF/C filter, precipitated with ethanol, and resuspended in a suitable volume of TE.

Synthesis of hTERT. hTERT was transcribed and translated using the TNT Coupled Reticulocyte Lysate Systems kit (Promega). A 400 µL reaction contained 8 µg of pET-28c-hTERT, and other components provided in the kit as described by the manufacturer. The reaction was incubated at 30 °C for 90 min, flash-frozen in a dry ice/ethanol bath, and stored at -80 °C.

Telomerase assemblage assay. Recombinant hTERT was transcribed and translated from pET28c-hTERT using the TNT® Coupled Reticulocyte Lysate Systems Kit (Promega) following the manufacture's instructions. Telomerase assemblage assays were performed by first combining 10 µL (~ 50 fmol) of hTERT from reticulocyte lysate reaction, 3.5 µL of 61 ng/µL of in vitro transcribed hTR, 0.6 µL of DMSO or different inhibitors diluted in DMSO and 0.9 µL of water. The reaction was allowed to incubate for 30 ºC for 90 min. It was then added to the 15 µL reaction, 0.4 µL of different inhibitors or DMSO and 0.6 µL of water, followed by 50 mM Tris-HCl, pH 8.0, 50 mM KCl, 1 mM $MgCl_2$, 5 mM β-mercaptoethanol, 1 mM spermidine, 1 µM human telomere primer (5'-TTAGGGTTAGGGTTAGGG), 0.5 mM dATP, 0.5 mM dTTP, 2.9 µM dGTP, 0.33 µM [χ-32P]-dGTP (3000 Ci/mmol, 10 µCi/µL; Perkin-Elmer) to reach a total volume of 25 µL. Inhibition studies were done using 50 µM final concentration of different inhibitors. Primer extension was carried out at 30º C for 90 min. After the addition of a 32P-labeled loading control (114 nucleotide, 5'-end labeled DNA oligonucleotide, 1000 cpm per reaction), the primer extension products were extracted with phenol/chloroform/isoamyl alcohol and ethanol precipitated in the presence of 0.6 M NH4OAc and 35 ng /µL glycogen. Products were precipitated at -80 ºC in 2.5 vol of absolute ethanol for 30 min followed by centrifugation at 22 000g at 4 ºC for 25 min and washing with 2 vol of 70% ethanol. Pellets were resuspended in a suitable volume of TE,

and ethanol precipitation was repeated to ensure the removal of all unincorporated [α-32P]-dGTP. The final pellets were dissolved in a formamide loading buffer containing 40% formamide, 10 mM Tris-HCl, pH 8.0, 10 mM EDTA, 0.05% xylene cyanol, and 0.05% bromophenol blue. The products were heated at 95 °C for 5 min and resolved on a prewarmed, 0.4 mm thick, 20 × 20 cm, 10% polyacrylamide/7 M urea/1× TBE gel. The gel was run at 800 V for 1 h in 1× TBE. After drying the gel and exposing it to a phosphorimager screen (Molecular Dynamics) overnight, telomerase activity was imaged using a phosphorimager (Molecular Dynamics Storm 860) and quantified with ImageQuant (version 5.2). The intensities of each band in each sample were summed and normalized to the loading control.

6.6.2 Results

We used the above-described telomerase assemblage assay to test if selected PBT compounds (**40-45**, Figure 6-9) could affect direct inhibition of the telomerase enzymatic activity. We used 50 µM of the selected compounds to get the percent activity in the telomerase assay as shown in Figure 6-10 and the results are illustrated graphically in Figure 6-11. Compounds **42, 43, 44**, and **45** showed almost complete inhibition. Further testing should be done using a post-assemblage assay to see if the compounds inhibit the assemblage of hTERT and hTR or if they inhibit telomerase by another mechanism.
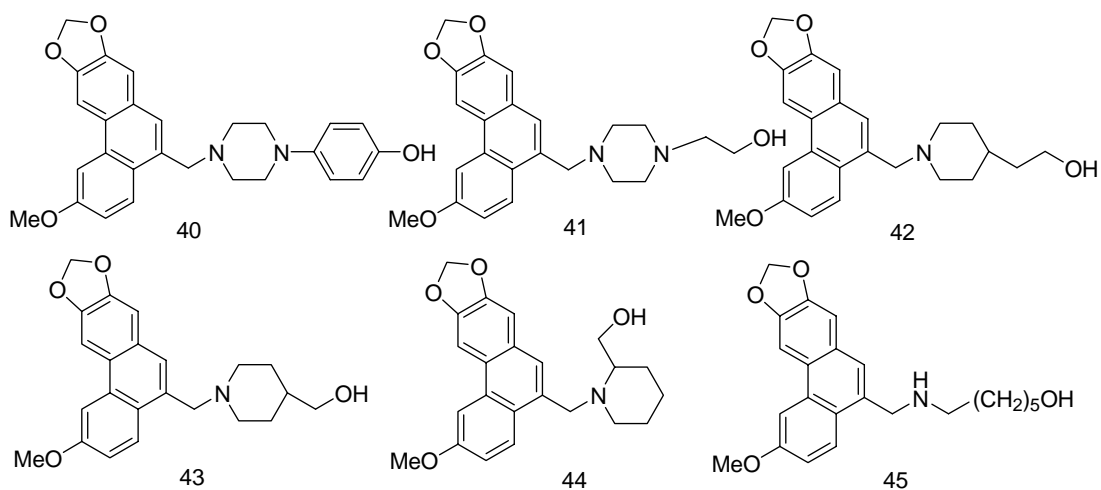
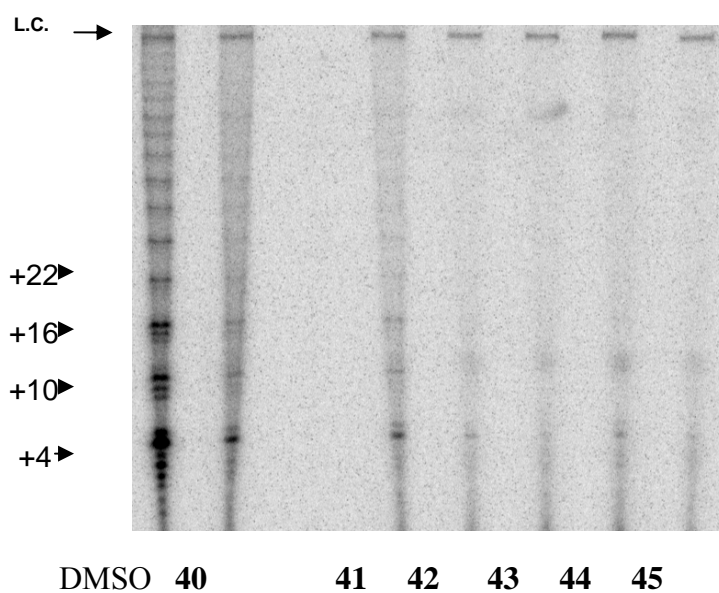Figure 6-9. Structures of compounds **40-45** screened in telomerase assay

Figure 6-10. Telomerase Assemblage Assay
[Telomerase inhibition was caused by different compounds. The 32P-labeled
loading control (L.C.) and the human telomere primer extension products (+4, +10,
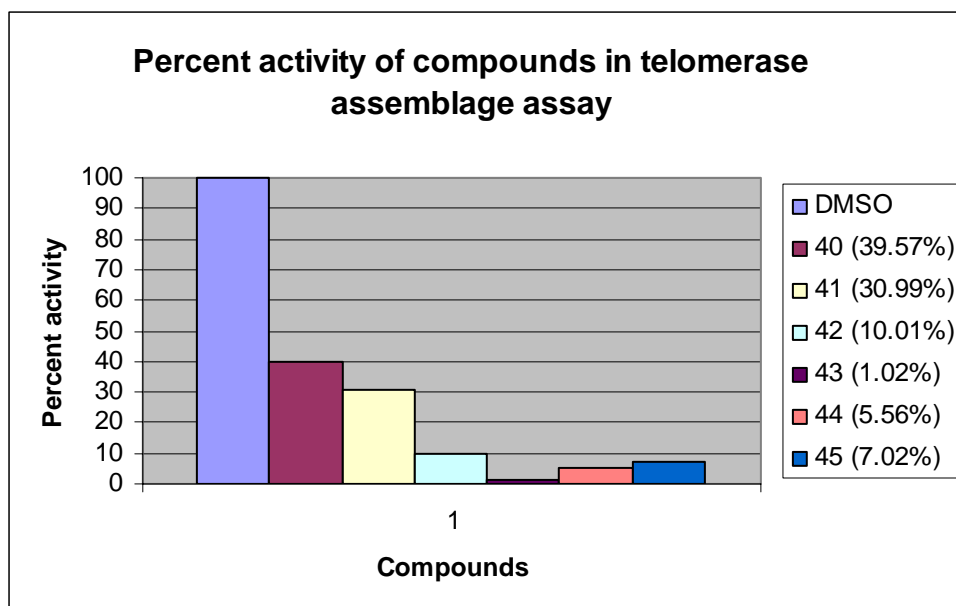+16, +22, etc. nucleotides added) are indicated.]

125

Figure 6-11. Telomerase activity inhibition by compounds **40-45**

6.7 *IN VIVO* STUDY

6.7.1 Objective

To evaluate possible anticancer activity of 4 PBTs, WLYWaispOH, WLY-Wac6OH, WLY-WaLP6OH and WLY-Wa4OH, in Tumor, Xenograft, Lung, A549 Cell in SCID mice [580900].
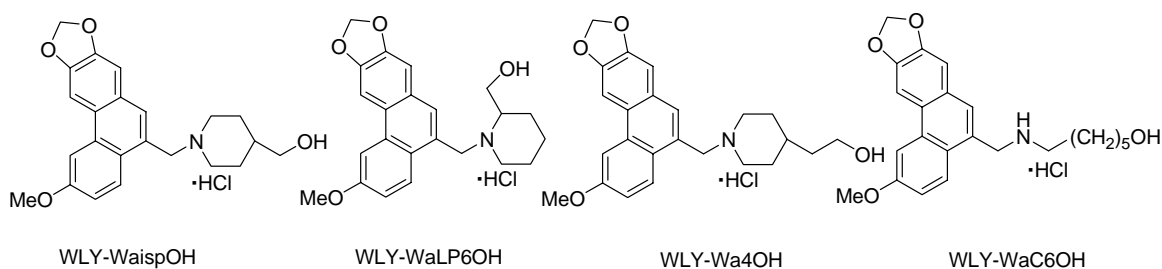

Figure 6-12. Structures of WLY-WaispOH, WLY-WaLP6OH, WLY-Wa4OH and WLY-WaC6OH used for in *vivo* screening

6.7.2 Methods

<u>Assay # 580900 Tumor, Xenograft, Lung, A549 Cell</u>

Severe Combined Immune Deficiency (SCID) male mice were used. Viable human lung tumor cells (A549) at a size of 1.5×10^7 cells in 0.2 ml were injected subcutaneously into the dorsal side of the test animals. When the tumor grew and reached ≥ 5 mm in diameter (designated as day 1), the tumor-bearing animals were divided into 14 groups (6 animals in each group) for antitumor studies.

For the inhibition of tumor growth, when the A549 tumor grew to reach ≥ 5 mm, WLY-WaispOH, WLYWac6OH, WLY-WaLP6OH and WLY-Wa4OH at 10, 3 and 1 mg/kg were administered at 4-day interval by intraperitoneal injection for a total of 6 doses using the dosing volume of 10 ml/kg.

Mitomycin at 2 mg/kg was given at 4-day interval for a total of 5 doses by IP injection. The animals were observed for signs of overt toxicity after dosing. Body weight and tumor size were measured and recorded every 4 days during the experiment period of 29 days.

Tumor weight (mg) was estimated according to the formula: length $\times$ (width)$^2 \times 0.5$ in mm^3, assuming its specific gravity to be 1. Tumor growth inhibition was calculated as T/C (treatment/control) by the following formula:

$$T/C = (T_n - T_1)/(C_n - C_1) \times 100\%$$

If $(T_n - T_1) < 0$, then

$$T/C = (T_n - T_1)/T_1 \times 100\%$$

C_1 (C_n): Tumor weight of day 1 (day n) in the control group

T_1 (T_n): Tumor weight of day 1 (day n) in the treated group

The result of T/C value ≤ 42% is considered significant antitumor activity.

6.7.3 Results and Discussion

In the xenograft model of human lung tumor cells (A549, ATCC CCL-185) in male SCID mice, WLY-WaispOH, WLY-Wac6OH, WLY-WaLP6OH and WLY-Wa4OH at 10, 3 and 1 mg/kg were administered by intraperitoneal (IP) injection at 4-day interval (q4d) for a total of 6 doses. The tumor size, body weight and signs of overt toxicity following test compound dosing were monitored and recorded for the duration of the experiment (29 days). Tumor growth inhibition was calculated as T/C (treatment/control) × 100%.

It appears that intraperitoneal administration of WLY-Wac6OH, WLY-WaLP6OH and WLY-Wa4OH at 10, 3 and 1 mg/kg q4d for a total of 6 doses did not cause any significant inhibition of tumor weight relative to the vehicle control during the experiment period of 29 days; WLY-WaispOH at 10 mg/kg, however, caused significant tumor inhibition on day 5 and moderate growth inhibition from day 9 to day 29 (the tumor growth data in terms of percent tumor weight relative to the vehicle control group are shown Figure 6-13).

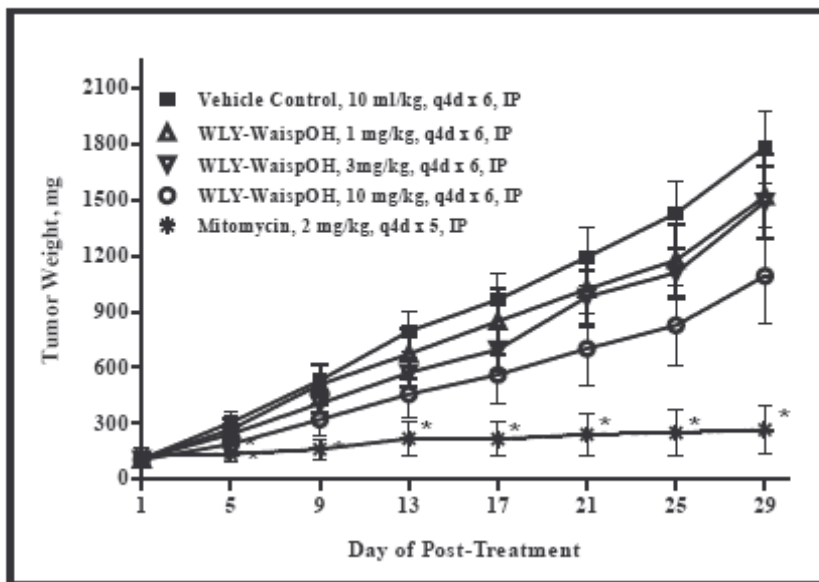Assay # 580900 Tumor, Xenograft, Lung, A549 Cell in SCID Mice

Figure 6-13. The tumor growth curves in SCID mice treated with WLY-WaispOH

Body weight and overt toxicity were monitored during the study. In comparison with the vehicle-treated control group, WLY-WaispOH, WLY-Wac6OH, WLY-WaLP6OH and WLY-Wa4OH at 10, 3 and 1 mg/kg were not associated with any changes in body weight and overt toxicity (Figure 6-14).
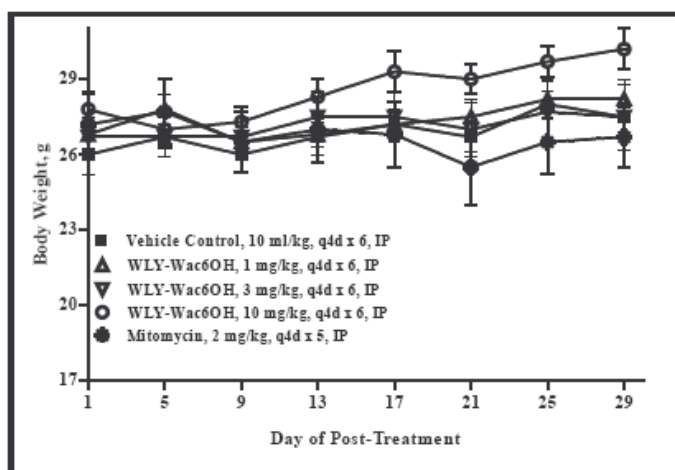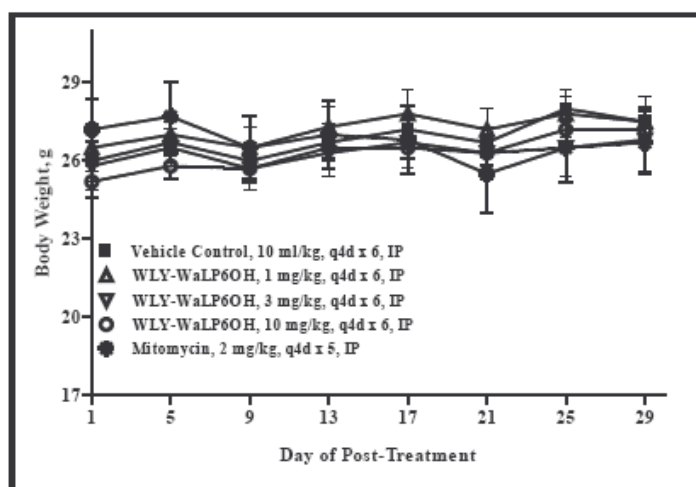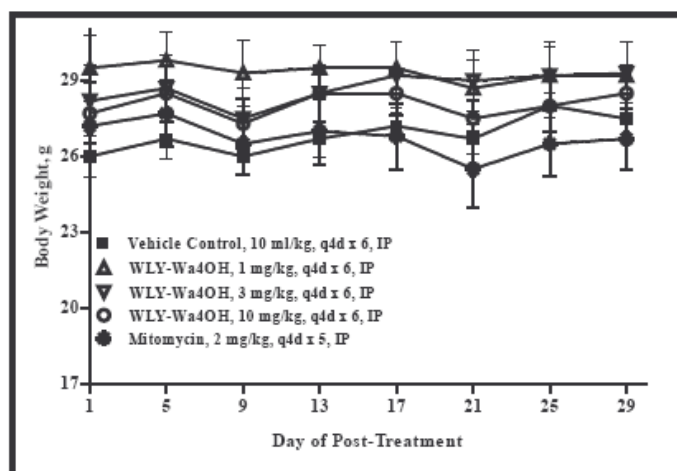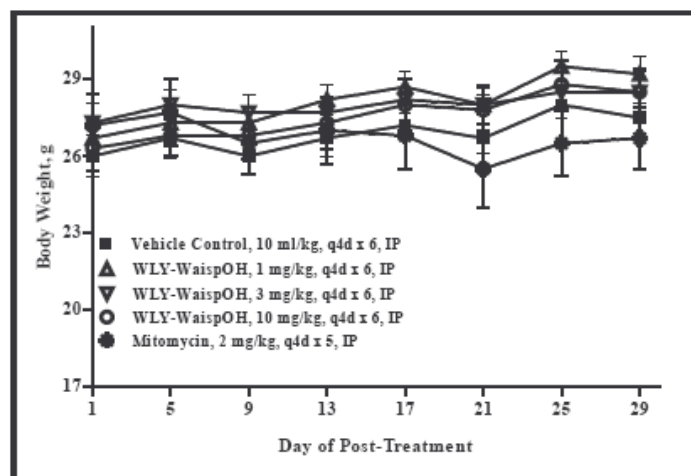
Figure 6-14. The body weight curves in SCID mice treated with
WLY-WaispOH, WLY-Wac6OH, WLY-WaLP6OH and WLY-Wa4OH

6.8 REFERENCES

1) The 60-cell line NCI test data, along with *in vivo* data can be accessed from the NSC numbers at the following Web site:
   http://dtp.nci.nih.gov/dtpstandard/dwindex/index.jsp

2) Ajay; Bemis, G. W.; Murcko, M. A. Designing libraries with CNS activity. *J. Med. Chem.* **1999**, *42*, 4942-4951.

3) Yazdanian, M.; Glynn, S. L.; Wright, J. L.; Hawi, A. Correlating partitioning and Caco-2 cell permeability of structurally diverse small molecular weight compounds. *Pharm. Res.* **1998**, *9*, 1490-1494.

4) Irvine, J. D.; Takahashi, L.; Lockhart, K. MDCK (Madin-Darby canine kidney) cells: a tool for membrane permeability screening. *J. Pharm. Sci.* **1999**, *88*, 28-33.

5) Saiakhov, R. D.; Stefan, L. R.; Klopman, G. Multiple computer-automated structure evaluation model of the plasma protein binding affinity of diverse drugs. *Perspect. Drug Discov. Des.* **2000**, *19*, 133-155

6) Bick, I. R. C.; Sinchai, W. In *The Alkaloids, Chemistry and Pharmacology*, Manske, R. H. F., Rodrigo, R. G. A, Eds.; Academic Press: New York, 1981; Vol 19, pp 193-220.

7) Donaldson, G. R.; Atkinson, M. R.; Murray, A. W. Inhibition of protein synthesis in Ehrlich ascites-tumour cells by the phenanthrene alkaloids tylophorine, tylocrebrine and cryptopleurine. *Biochem. Biophys. Res. Commun.* **1968**, *31*, 104-109.

8) Huang, M-T; Grollman, A. P. Mode of action of tylocrebrine: effects on protein and nucleic acid synthesis. *Mol. Pharmacol.* **1972**, *8*, 538-550.

9) Grant, P.; Sanchez, L.; Jimenez, A. Cryptopleurine resistance: genetic locus for a 40S ribosomal component in *Saccharomyces cerevisiae*. *J. Bacteriol.* **1974**, *10*, 1308-1314.

10) Gupta, R. S.; Krepensky, J. J.; Siminovitch, L. Structural determinants responsible for the biological activity of (-)-emetine, (-)-cryptopleurine, and (-)-tylocrebrine: structure-activity relationship among related compounds. *Mol. Pharmacol.* **1980**, *18*, 136-143.

11) Gupta R. S.; Siminovitch, L. Mutants of CHO cells resistant to the protein synthesis inhibitors, cryptopleurine and tylocrebrine: genetic and biochemical evidence for common site of action of emetine, cryptopleurine, tylocrebine, and tubulosine. *Biochemistry* **1997**, *16*, 3209-3214.

12) Rao, K. N.; Bhattachyarya, R. K.; Venkatachalam, S. R. Thymidylate synthase activity in leukocytes from patients with chronic myelocytic leukemia and acute lymphocytic leukemia and its inhibition by phenanthroindolizidine alkaloids pergularinine and tylophorinidine. *Cancer Lett.* **1998**, *128*, 183-188.

13) Rao, K. N.; Bhattachyarya, R. K.; Venkatachalam, S. R. Inhibition of thymidylate synthase and cell growth by the phenanthroindolizidine alkaloids pergularinine and tylophorinidine. *Chem. Biol. Interact.* **1997**, *106*, 201-212.

14) Rao, K. N.; Venkatachalam, S. R. Inhibition of dihydrofolate reductase and cell growth activity by the phenanthroindolizidine alkaloids pergularinine and tylophorinidine: the in vitro cytotoxicity of these plant alkaloids and their potential as antimicrobial and anticancer agents. *Toxicol. In Vitro* **2000**, *14*, 53-59.

15) Ganguly, T.; Khar, A. Induction of apoptosis in a human erythroleukemic cell line K562 by tylophora alkaloids involves release of cytochrome c and activation of caspase 3. *Phytomedicine* **2002**, *9*, 288-295.

16) Gao, W.; Lam, W.; Zhong, S.; Kaczmarek, C.; Baker, D. C.; Cheng, Y.-C. Novel mode of action of tylophorine analogs as antitumor compounds. *Cancer Res.* **2004**, *64*, 678-688.

17) Alley, M. C.; Scudiero, D. A.; Monks, P. A.; Hursey, M. L.; Czerwinski, M. J.; Fine, D. L.; Abbott, B. J.; Mayo, J. G.; Shoemaker, R. H.; Boyd, M. R. Feasibility of drug screening with panels of human tumor cell lines using a microculture tetrazolium assay. *Cancer Res.* **1988**, *48*, 589-601.

18) Grever, M. R.; Schepartz, S. A.; Chabner, B.A. *The National Cancer Institute: Cancer Drug Discovery and Development Program. Seminars in Oncology*, Vol. 19, No. 6, pp 622-638, 1992.

19) Boyd, M. R.; Paull, K. D. Some practical considerations and applications of the National Cancer Institute in vitro anticancer drug discovery screen. *Drug Develop. Res.* **1995**, *34*, 91-109.

20) Hansen, M. B.; Nielsen, S. E.; Berg, K. Re-examination and further development of a precise and rapid dye method for measuring cell growth/cell kill. *J. Immunol. Methods* **1989**, *119*, 203-210

21) Harrington, L. Biochemical aspects of telomerase function. *Cancer Lett.* **2003**, *194*, 139-154.

22) Keppler, B. R.; Jarstfer, M. B. Inhibition of telomerase activity by preventing proper assemblage. *Biochemistry* **2004**, *43*, 334-343.

23) Meyerson, M.; Counter, C. M.; Eaton, E. N.; Ellisen, L. W.; Steiner, P.; Caddle, S. D.; Ziaugra, L.; Beijersbergen, R. L.; Davidoff, M. J.; Liu, Q.; Bacchetti, S.; Haber, D. A.; Weinberg, R. A. HEST2, the putative human telomerase catalytic subunit

gene, is up-regulated in tumor cells and during immortalization. *Cell* **1997**, *90*, 785-795

24) Nakamura, T. M.; Morin, G. B.; Chapman, K. B.; Weinrich, S. L.; Andrews, W. H.; Lingner, J.; Harley, C. B.; Cech, T. R. Telomerase catalytic subunit homologs from fission yeast and human. *Science* **1997**, *277*, 955-959.

25) Feng, J.; Funk, W. D.; Wang, S. S.; Weinrich, S. L.; Avilion, A. A.; Chiu, C. P.; Adams, R. R.; Chang, E.; Allsopp, R. C.; Yu, J.; et al. The RNA component of human telomerase. *Science* **1995**, *269*, 1236-1241.

26) Kelleher, C.; Teixeira, M.T.; Forstemann, K.; Lingner, J. Telomerase: biochemical considerations for enzyme and substrate. *Trends Biochem Sci* **2002**, *27*, 572-579.

27) Cong, Y. S.; Wright, W. E.; Shay, J. W. Human telomerase and its regulation. *Microbiol. Mol. Biol. Rev.* **2002**, *66*, 407-425.

28) Maxam, A.M.; Gilbert, W. A new method for sequencing DNA. *Proc. Natl. Acad. Sci. U.S.A.* **1977**, *74*, 560-564.

CHAPTER VII. CONCLUSIONS AND FUTURE STUDIES

7.1 STRUCTURE ACTIVITY RELATIONSHIP

In this study, we have designed and synthesized new water-soluble phenanthrene-based tylophorine derivatives (PBTs) as potential antitumor agents. These compounds contain a core phenanthrene structure and can be synthesized efficiently in excellent yield. To obtain structure-activity relationship (SAR) information, we carried out chemical modification on nine different positions of the compound skeleton (Figure 7-1).
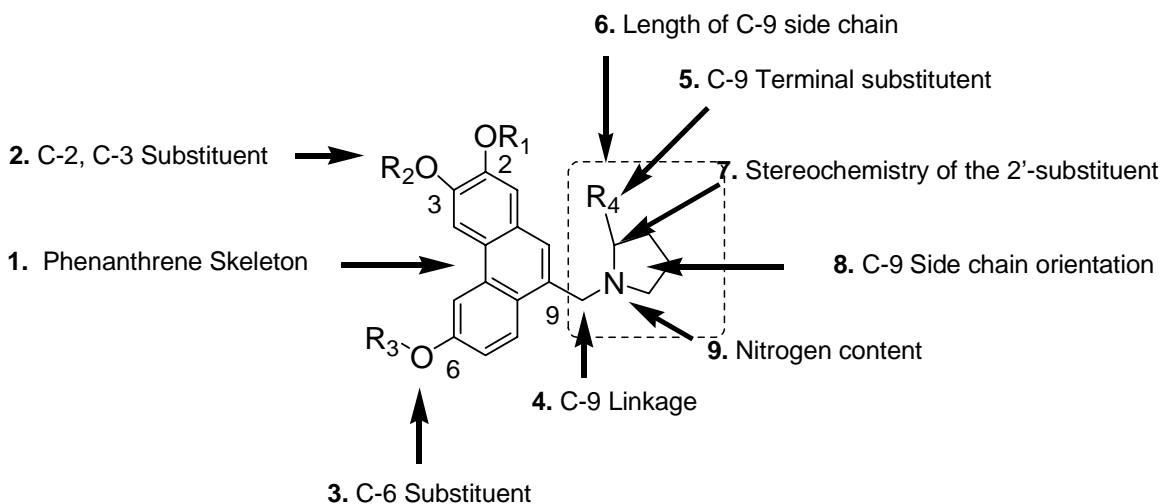

Figure 7-1. SAR Study of PBTs

A total of more than 70 PBTs were synthesized and evaluated for cytotoxic activity against the A549 human cancer cell line. Among them, *N*-(2,3-methylenedioxy-6-methoxy-phenanthr-9-ylmethyl)-L-4-piperidinemethanol (**1**), *N*-(2,3-methylenedioxy-6-methoxy-

phenanthr-9-ylmethyl)-L-2-piperidinemethanol (**2**), *N*-(2,3-methylenedioxy-6-methoxy-phenanthr-9-ylmethyl)-4-piperidineethanol (**3**) and *N*-(2,3-methylenedioxy-6-methoxy-phenanthr-9-ylmethyl)-6-aminohexanol (**4**) (Figure 7-2) showed the highest potency with EC_{50} values of 0.08, 0.16, 0.15 and 0.2 µM, respectively, which are comparable to those of currently used antitumor drugs.
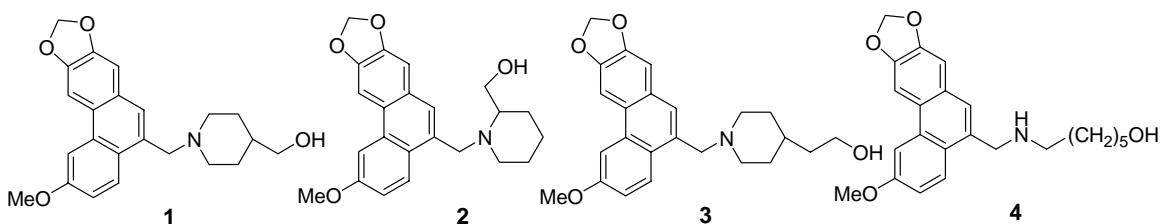

Figure 7-2. Structures of promising PBTs developed in the NPL

These four compounds incorporated all of the favorable modifications identified to date in the preliminary SAR study. The favorable modifications for these novel PBTs are as follows (Table 7-1). 1) A planar phenanthrene system is required, but not sufficient for cytotoxic activity. 2) An *N*-hydrophilic substituent at the C-9 position is essential for enhanced cytotoxicity and should be linked through a methylene rather than a carbonyl group. 3) This C-9 *N*-hydrophilic substituent is ideal for the introduction of a polar moiety. Analogs containing terminal carboxylic acid or hydroxymethyl groups are more favorable than those with methyl esters. 4) On the phenanthrene skeleton, a methoxy substituent best fits both the steric and electronic requirements at the C-6 position and is preferred over benzyloxy and hydroxy groups. 5) Adding a methylenedioxy ring at the 2, 3 position of the planar phenanthrene system can dramatically enhance the cytotoxic activity and led to the most potent derivatives.

135

Table 7-1. SAR of PBTs.

7.1.1 Position Number	7.1.2 SAR Result
1. Phenanthrene Skeleton	A planar phenanthrene system is required, but not sufficient for cytotoxic activity.
2. C-2, C-3 Substituent	Adding a methylenedioxy ring at the 2,3 position of the planar phenanthrene system enhanced the cytotoxic activity and led to the most potent derivatives.
3. C-6 Substituent	A methoxy substituent best fits both the steric and electronic requirements at the C-6 position and is preferred over benzyloxy and hydroxy groups.
4. C-9 Linkage	An N-hydrophilic substituent at the C-9 position is essential for the enhanced cytotoxicity and should be linked through a methylene rather than a carbonyl group.
5. C-9 Terminal Substitutent	C-9 N-hydrophilic substituent is ideal for the introduction of a polar moiety. Analogs containing terminal carboxylic acid or hydroxymethyl groups are more favorable than those with methyl esters.
6. Length of C-9 Side Chain	The distance between the nitrogen and terminal substituent affected the potency; 6 carbon length is

|	the most favorable for the activity.
7. Stereochemistry of the 2'-Substituent	2'*S*–substituted compounds showed equal or higher cytotoxicity than *R* isomers.
8. C-9 Side Chain Orientation	The terminal hydroxyl/carboxylic acid in a para position could favorably affect the activity compared with other orientations.
9. Nitrogen Content	The second nitrogen was tolerated; its presence slightly decreased activity.

In summary, the new PBT derivatives possess a novel structure and showed remarkable EC_{50} values in the sub-micromolar range, comparable with current front-line antineoplastic drugs such as etoposide. These derivatives are the first reported water soluble tylophorine derivatives with remarkable cytotoxic activity, in particular against multidrug-resistant cancer cell lines, suggesting a great potential of developing this compound class into antitumor agents to treat cancer (particularly for refractory cancer).

7.2 FUTURE STUDIES

7.2.1 Short total synthesis of phenanthroindolizidine alkaloids.
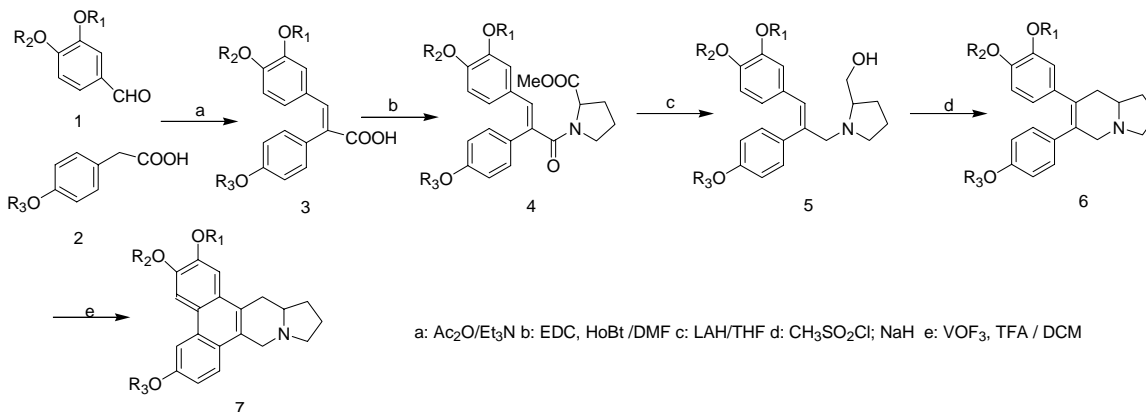
Scheme 7-1. Short total synthesis of antofine

a: Ac$_2$O/Et$_3$N b: EDC, HoBt /DMF c: LAH/THF d: CH$_3$SO$_2$Cl; NaH e: VOF$_3$, TFA / DCM
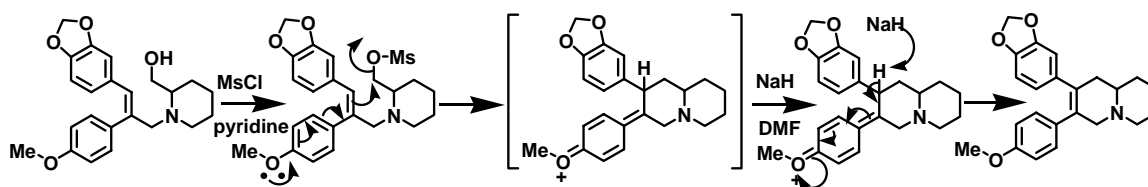

Scheme 7-2. Base-induced cyclization

Russel and Hunziker proposed a base-promoted ring closure in the total synthesis of septicine.[1] Using this methodology in step d of Scheme 7-1 allows a modified total synthesis of the phenanthroindolizidine ring. The target compound will be accessed in five steps, which should be the shortest synthetic route reported to date. This synthetic route avoids an unstable ketone intermediate by using an intramolecular based-induced cyclization of amino alcohols. In addition to the base-induced cyclization, a Lewis acid mediated Friedel-Crafts type cyclization was also reported (Scheme 7-2).[2] Several bases or Lewis acid will be examined for this step.

7.2.2 Parallel Synthesis of PBTs

A general method of rapidly preparing PBT analogs would be advantageous and merits

investigation for drug discovery. Meanwhile, parallel synthesis of small organic molecules

has emerged as an important technology, enabling chemists to synthesize numerous

pharmaceutically interesting compounds.[3] The relative ease of automation, along with a

multiple parallel synthesis strategy, has greatly supported the growing needs for identifying

novel biologically active lead compounds and accelerated structure-activity relationship

studies in drug discovery.

We will apply parallel synthesis of new PBTs using an active ester resin[4] procedure.

The synthetic route is described in Scheme 7-3.

Parallel Reaction Formate
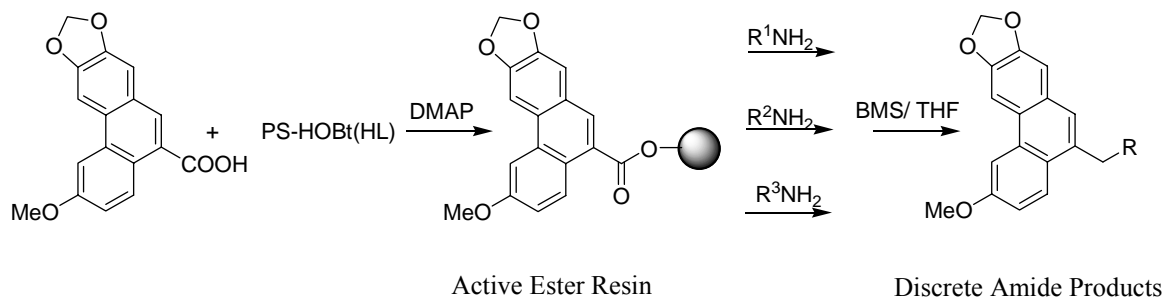
Scheme 7-3. Parallel synthesis of PBTs

General Procedure

Formation of active ester:

1.5 equiv of carboxylic acid, 4.5 equiv of DIC, 0.6 equiv of DMAP, and a 4:1

DCM/DMF solvent mixture at room temperature for 2–3 h. Order of addition proved to be

an important variable: DMAP and the carboxylic acid were mixed with PS-HOBt(HL),

followed by addition of DIC. The purpose of including DMF as a cosolvent is to improve the solubility of the carboxylic acid component. It is preferable to keep the DMF composition in the reaction mixture to a minimum (< 20%), since it compromises the level of active ester formation. If more DMF is required to dissolve the carboxylic acid, up to 50% DMF can be used; however, the loading level will be reduced.

Amide synthesis

To 1.5 equiv of PS-HOBt(HL) active ester resin was added a mixture of 0.7 equiv of amine and 1.0 equiv of DIEA in DCM or THF and the mixture was stirred at 25 °C for 3 h. The solution was filtered, and the resin rinsed with DCM or THF (3 ×). The combined filtrate was concentrated to afford the desired amide.

7.2.3 Making Organic/inorganic Salt

In the multi-cancer cell assay study, the corresponding HCl salt of the active free base showed better water solubility, while still retaining similar cytotoxic activity. Making organic/inorganic salt is a very useful way to improve a compound's pharmacological properties. Thus, we continue to prepare the pharmaceutically acceptable salts of active compounds. Pharmaceutically acceptable salts are salts that retain the desired biological activity of the parent compound and do not impart undesired toxicological effects. Examples of such salts are (a) acid addition salts formed with inorganic acids, such as hydrochloric acid, hydrobromic acid, sulfuric acid, phosphoric acid, nitric acid and the like; and salts formed with organic acids, such as acetic acid, oxalic acid, tartaric acid, succinic acid, maleic acid, fumaric acid, gluconic acid, citric acid, malic acid, ascorbic acid, benzoic acid, tannic acid, palmitic acid, alginic acid, polyglutamic acid, naphthalenesulfonic acid, methanesulfonic

acid, p-toluenesulfonic acid, naphthalenedisulfonic acid, polygalacturonic acid, and the like; and (b) salts formed from elemental anions such as chlorine, bromine, and iodine.

7.2.4 Design of Bioisosteric Skeleton Modification

Bioisosteric modification may profoundly affect pharmacological action, metabolism activity, and toxicity. This basic principle of analog design has been successfully applied in many natural product modifications. Therefore, we will apply this approach in new PBTs development. The general molecular formulas of new PBTs are shown in Figure 7-3 and these compounds should be efficiently synthesized by our general procedure in chapter III or parallel synthesis mentioned in section 7.2.2.
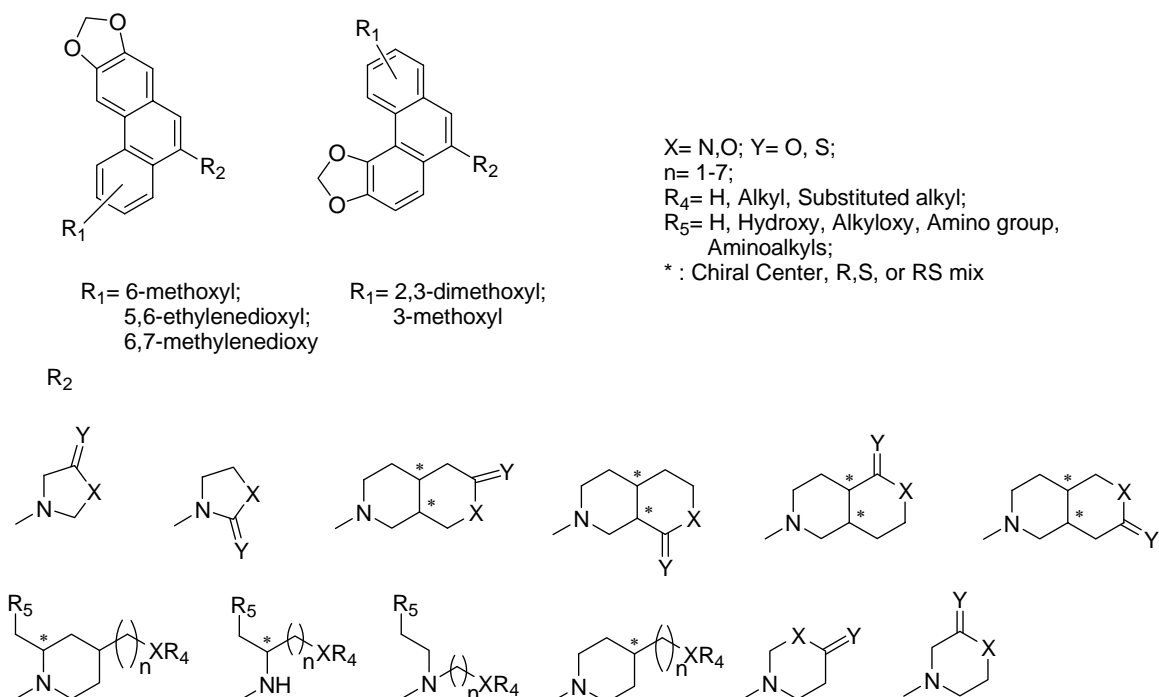

Figure 7-3. Structure Formulas of New PBTs

7.2.5 Mechanism of Action Study

The biological target of PBTs is still unknown and the mechanism of action of PBTs has not been elucidated. The preliminary results have shown that PBTs are a unique class of antitumor compounds that may have a mode of action different from known antitumor drugs. The active PBTs will be screened against several interesting cancer-related targets, such as NFκB, topoisomerase, etc. It would be helpful to assign a putative mechanism of action and identify a specific molecular target with which PBTs are most likely to interact. More cancer cell lines will be used to characterize selective growth inhibition or cell killing of particular tumor cell lines. The further screening of PBTs will facilitate the understanding of SAR and provide more rationale to design a more potent compound targeting wild/resistant cancer cells.

7.2.6 QSAR study and Database Mining

The approach applied herein to QSAR modeling of PBTs does not stop since more new PBTs will come into the database and more pharmacological datasets will be available for screening. Our approach places the emphasis of the entire QSAR modeling study on making reliable predictions of chemical structures expected to have the desired biological activity, rather than on respectable statistical characteristics of (training set) models. These predicted structures either are already available in existing chemical databases or are synthetically feasible (i.e., included in virtual combinatorial chemical libraries, which can also be mined with QSAR models). The focus of the modeling will be brought closer to the needs of medicinal chemists who both supply computational chemists with experimental structure-activity data and expect novel structures rather than equations and statistical parameters in

return. We believe that this approach will bring QSAR modeling in tune with the ultimate

needs of our interest in new plant-derived anti tumor agents.

7.3 REFERENCES

1) Russel, J. H.; Hunziker, H. Synthesis of septicine. *Tetrahedron Lett*. **1969**, *10*, 4035-4036.

2) Chandrasekhar, S.; Reddy, N. R.; Reddy, M. V.; Jagannadh, B.; Nagaraju, A.; Ravi Sankar, A.; Kunwar, A. C. Highly efficient synthesis of 3-alkyl/aryl-4-aryl-1,2,3,4-tetrahydroisoquinolines from N,N-dibenzylaminols. *Tetrahedron Lett*. **2002**, *43*, 1885-1888.

3) Balkenhohl, F.; Bussche-Hunnefeld, C.; Lansky, A.; Zechel, C. Combinatorial synthesis of small organic molecules. *Angew. Chem., Int. Ed. Engl.* **1996**, *35*, 2288-2337. (b) Baldwin, J. J.; Henderson, I. Recent advances in the generation of small-molecule combinatorial libraries: encoded split synthesis and solid-phase synthetic methodology *Med. Res. Rev.* **1996**, *16*, 391-405. (c) Thompson, L. A.; Ellman, J. A. Synthesis and applications of small molecule libraries. *Chem. Rev*. **1996**, *96*, 555-600. (d) Creswell, M. W.; Bolton, G. L.; Hodges, J. C.; Meppen, M. Combinatorial synthesis of dihydropyridone libraries and their derivatives. *Tetrahedron* **1998**, *54*, 3983-3998.

4) For the Resin Selection: www.argotech.com.